(2)

NAVAL POSTGRADUATE SCHOOL

Monterey, California

THESIS

A MULTI-FACETED ENGINEERING STUDY
OF AERODYNAMIC ERRORS OF THE SERVICE
AIRCRAFT INSTRUMENTATION PACKAGE (SAIP)

by

Joseph W. Rixey

September 1992

Thesis Advisor: O. Biblarz

REPORT DOCUMENTATION PAGE

1a. REPORT SECURITY CLASSIFICATION Unclassified	1b. RESTRICTIVE MARKINGS
2a. SECURITY CLASSIFICATION AUTHORITY	3. DISTRIBUTION/AVAILABILITY OF REPORT Approved for public release; distribution is unlimited.
2b. DECLASSIFICATION/DOWNGRADING SCHEDULE	
4. PERFORMING ORGANIZATION REPORT NUMBER(S)	5. MONITORING ORGANIZATION REPORT NUMBER(S)
6a. NAME OF PERFORMING ORGANIZATION Naval Postgraduate School 6b. OFFICE SYMBOL (*If applicable*) AA	7a. NAME OF MONITORING ORGANIZATION Naval Postgraduate School
6c. ADDRESS (*City, State, and ZIP Code*) Monterey, CA 93943-5000	7b. ADDRESS (*City, State, and ZIP Code*) Monterey, CA 93943-5000
8a. NAME OF FUNDING/SPONSORING ORGANIZATION 8b. OFFICE SYMBOL (*If applicable*)	9. PROCUREMENT INSTRUMENT IDENTIFICATION NUMBER
8c. ADDRESS (*City, State, and ZIP Code*)	10. SOURCE OF FUNDING NUMBERS Program Element No. / Project No. / Task No. / Work Unit Accession Number

11. TITLE (*Include Security Classification*)
A MULTI-FACETED ENGINEERING STUDY OF AERODYNAMIC ERRORS OF THE SERVICE AIRCRAFT INSTRUMENTATION PACKAGE (SAIP)

12. PERSONAL AUTHOR(S) Joseph W. Rixey

13a. TYPE OF REPORT	13b. TIME COVERED	14. DATE OF REPORT (*year, month, day*)	15. PAGE COUNT
Engineer's Thesis	From To	September 1992	120

16. SUPPLEMENTARY NOTATION
The views expressed in this thesis are those of the author and do not reflect the official policy or position of the Department of Defense or the U.S. Government.

17. COSATI CODES			18. SUBJECT TERMS (*continue on reverse if necessary and identify by block number*)
FIELD	GROUP	SUBGROUP	

19. ABSTRACT (*continue on reverse if necessary and identify by block number*)

The general objectives of this research are to investigate, identify, and quantify the aerodynamic sources of altitude determination errors of the U.S. Navy's Service Aircraft Instrumentation Package (SAIP) and to make recommendations to remedy these errors. This multi-faceted study includes aero-panel methods, computational fluid dynamics (CFD), wind tunnel testing, and flight test evaluations.
The Airflow Sensor Assembly (ASA), a device similar to a calibrated pitot static tube, was intended to meet the SAIP's required specifications for altitude determination. However, the ASA is housed in the five inch diameter body of the SAIP and mounted on a variety of host aircraft. The over-pressure generated by the SAIP body as well as the wing/pylon system engulf the static pressure ports creating altitude errors well out of performance limits. This over-pressure associated with these bodies was apparently not accounted for during design and acquisition and extensive modifications will be needed to offset or eliminate their effects.

20. DISTRIBUTION/AVAILABILITY OF ABSTRACT	21. ABSTRACT SECURITY CLASSIFICATION	
☒ UNCLASSIFIED/UNLIMITED ☐ SAME AS REPORT ☐ DTIC USERS	Uclassified	
22a. NAME OF RESPONSIBLE INDIVIDUAL O. Biblarz	22b. TELEPHONE (*Include Area code*) (408) 646-3096	22c. OFFICE SYMBOL AA/Bi

DD FORM 1473, 84 MAR — 83 APR edition may be used until exhausted; All other editions are obsolete

Approved for public release; distribution is unlimited.

A Multi-Faceted Engineering Study
of Aerodynamic Errors of the Service
Aircraft Instrumentation Package (SAIP)

by

Joseph W. Rixey
Lieutenant, United States Navy
B.S., United States Naval Academy, 1983
M.S., Naval Postgraduate School, 1992

Submitted in September 1992 in partial fulfillment
of the requirements for the degree of

AERONAUTICAL ENGINEER

from the

NAVAL POSTGRADUATE SCHOOL
September 1992

Author: _____
Joseph W. Rixey

Approved by: _____
O. Biblarz, Thesis Advisor

_____
G. V. Hobson, Second Reader

_____
D. J. Collins, Chairman
Department of Aeronautics and Astronautics

_____
Richard S. Elster, Dean of Instruction

ABSTRACT

The general objectives of this research are to investigate, identify, and quantify the aerodynamic sources of altitude determination errors of the U.S. Navy's Service Aircraft Instrumentation Package (SAIP) and to make recommendations to remedy these errors. This multi-faceted study includes aero-panel methods, computational fluid dynamics (CFD), wind tunnel testing, and flight test evaluations.

The Airflow Sensor Assembly (ASA), a device similar to a calibrated pitot static tube, was intended to meet the SAIP's required specifications for altitude determination. However, the ASA is housed in the five inch diameter body of the SAIP and mounted on a variety of host aircraft. The over-pressure generated by the SAIP body as well as the wing/pylon system engulf the static pressure ports creating altitude errors well out of performance limits. This over-pressure associated with these bodies was apparently not accounted for during design and acquisition and extensive modifications will be needed to offset or eliminate their effects.

TABLE OF CONTENTS

ACKNOWLEDGEMENTS

This project could not have been completed without the assistance of numerous individuals. I wish to thank Prof. Oscar Biblarz for his guidance and friendship, and for making this project a wonderful learning experience. As for the individuals at NAWCWPNS Point Mugu, I would like to single out Brian Frankhauser for personally keeping this project alive. I would like to also express deep gratitude to the following individuals: to Larry Gleason at NAWCWPNS China Lake, who's valuable time and expertise in panel methods was greatly appreciated; to Francis Richason and the gentlemen at NASA Ames for introducing and teaching me the intricacies of the PMARC code; to Prof. Rick Howard for his advice in wind tunnel testing; to Prof. Garth Hobson for his CFD expertise; and to Jack King for his help in the wind tunnel. Finally I would like to thank the Lord for his guidance, and to my wife and children I would like to express my love and appreciation for their steadfast support and patience.

I. INTRODUCTION

A. BACKGROUND

This thesis is the third in a series of investigations of the altitude determination deficiencies of the Service Aircraft Instrumentation Package (SAIP). The author of the first thesis [Ref. 1] developed the experimental techniques and identified an ambiguous grounding specification leading to a fault in the electronic circuitry located in the Air Data Unit (ADU). The second author [Ref. 2] determined that this grounding fault was not the sole cause of error, and that the principal source of altitude determination errors remained aerodynamic in nature. This thesis quantifies those aerodynamic errors using computational methods and further wind tunnel testing, and presents recommendations for system modifications in order to eliminate errors.

1. System Description

The Service Aircraft Instrumentation Package (SAIP) (Fig. 1, Ref. 3) is designed to provide independent, three-dimensional tracking information on aircraft operating within the Extended Area Test System (EATS) located at the Naval Air Warfare Center, Point Mugu, California (NAWCWPNS). Designed by the General Dynamics Electronic Division, this self-contained airborne positioning pod is configured to mount on

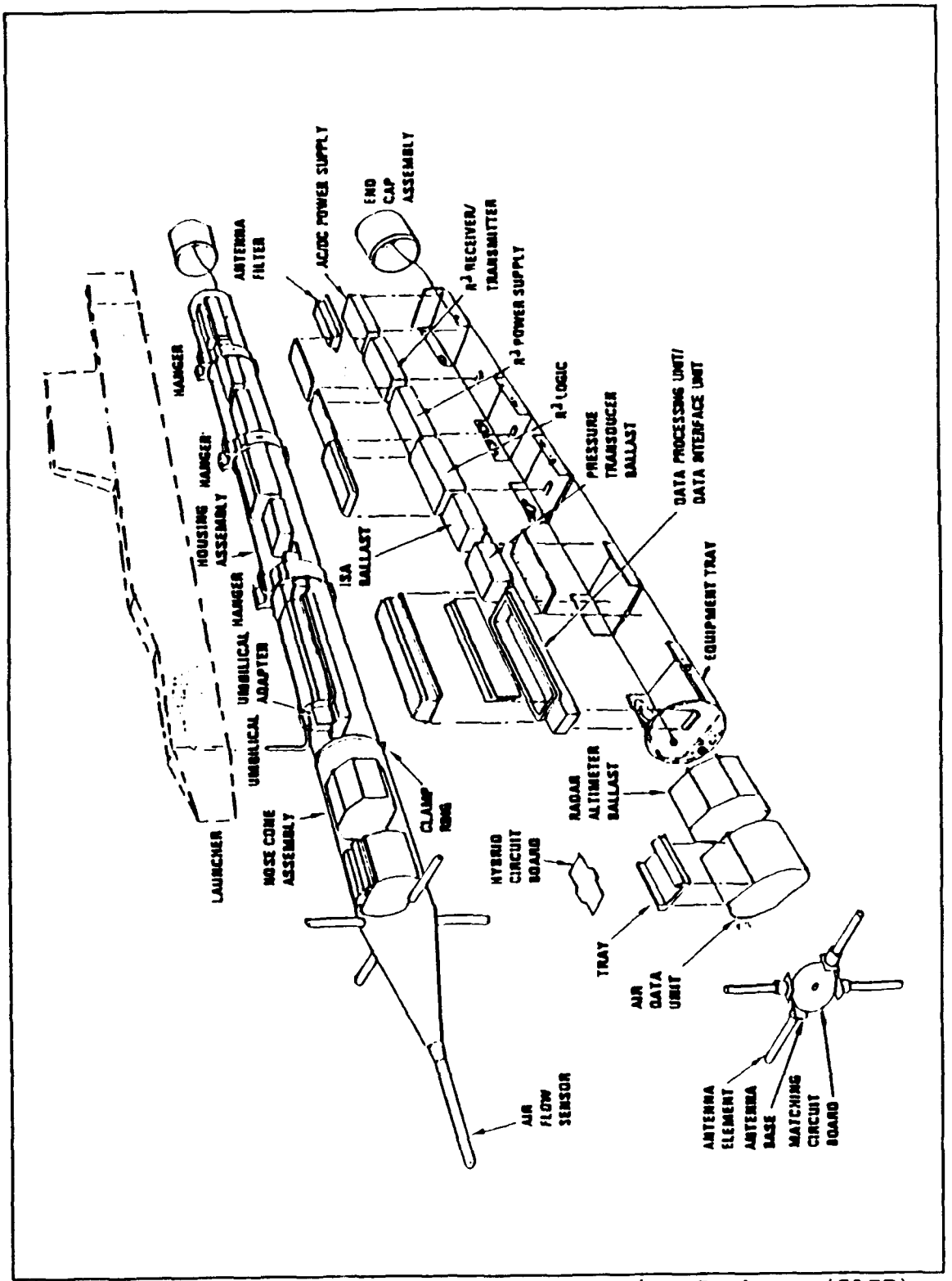

Figure 1. Service Aircraft Instrumentation Package (SAIP); [Ref. 3]

aircraft equipped with the LAU-7/A (series) launcher. The SAIP body consists of a five-inch diameter stainless-steel tube, which contains electronic subassemblies as shown in Figure 1. It requires only primary AC and DC power from the host aircraft and in return it is supposed to provide range, altitude, airspeed, attitude and weapon-system data. The SAIP communicates with the EATS through its antenna system which transmits and receives RF signals at 141 MHz.

The SAIP is required to operate throughout the entire aircraft flight regime, with aircraft lift devices and landing gear retracted and deployed, at all attitudes, and in subsonic and supersonic flight.

2. System Components

Two SAIP nose cones were presented to the Naval Postgraduate School for extensive study by NAWCWPNS in 1991. These are second-generation units which possess 12 static port locations, displaced by 30 degrees circumferentially about the Airflow Sensor Assembly. First generation pods possess only dual static port locations. This hardware modification was the first attempt to alleviate the altitude measurement inaccuracies found during early testing.

a. Nose Cone Assembly

The Nose Cone Assembly shown in Figure 2 houses the antenna subsystem, The Air Data Unit (ADU), the Air Flow

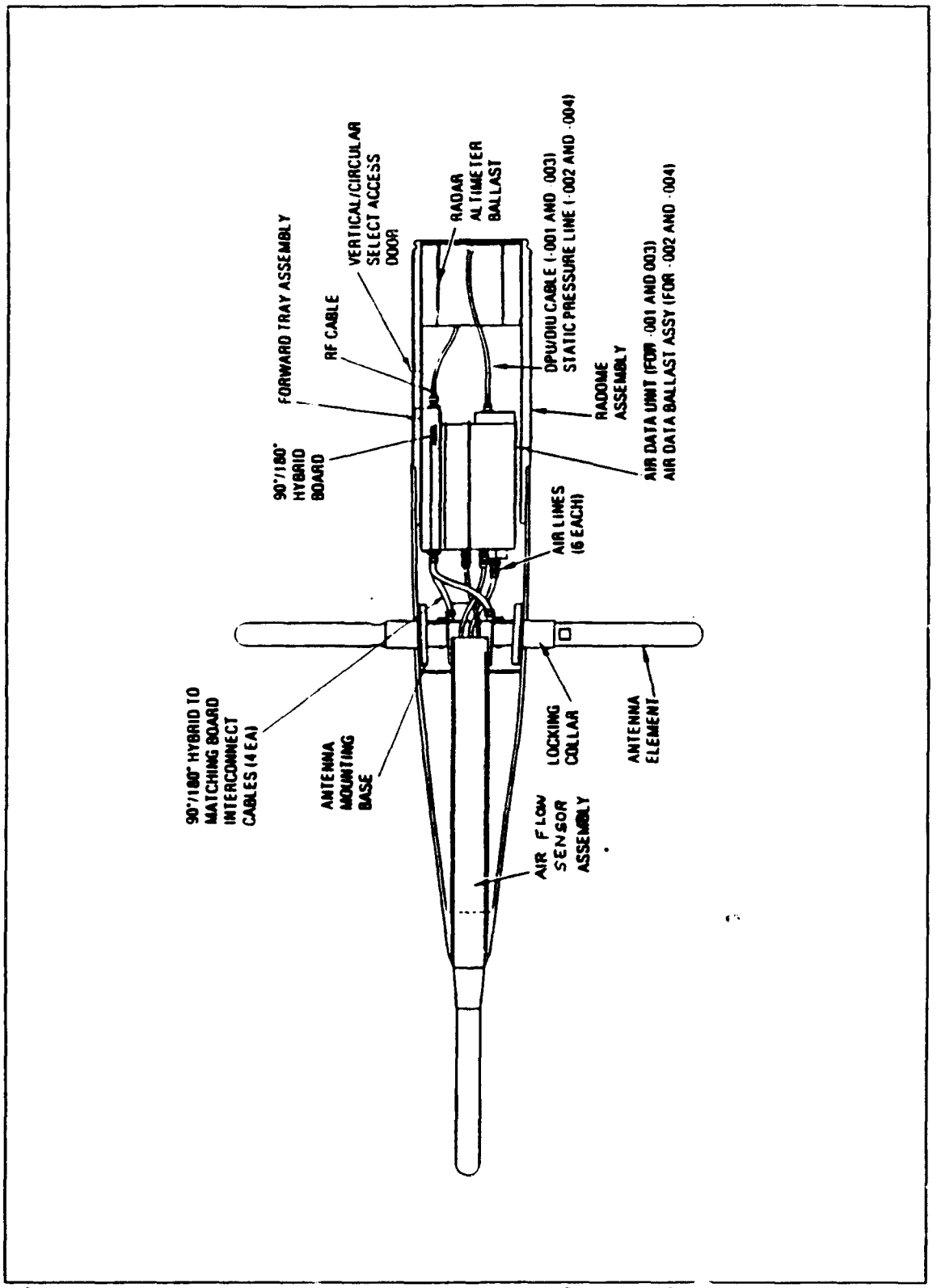

Figure 2. Nose Cone Assembly (NCA) [Ref. 3].

Sensor (ASA), the radar altimeter ballast and the antenna filter [Ref. 3:pp. 132-135].

b. Airflow Sensor Assembly

The Airflow Sensor Assembly (ASA) is the main focus of this study (Fig. 3). Manufactured by the Rosemount Corporation of Burnville, Minnesota, the ASA is tapped with pressure ports including two angle of attack ports (A1 and A2), two angle of sideslip ports (B1 and B2), a total pressure port (P3) and 12 static pressure ports (S) as shown in Figure 4. The static ports are located 3.5 inches aft of the forward tip. The ASA is placed in the airstream and is used as a pitot static tube, where raw data (local static pressure) is used to determine the barometric altitude. The ASA was wind tunnel tested and calibrated separate of the nose cone by Rosemount to meet the specifications required for altitude determination.

c. Air Data Unit

The function of the Air Data Unit (ADU) is to assimilate the six pressure parameters output from the ASA and provide the analog outputs required to compute altitude, indicated airspeed, true airspeed, Mach number, angle-of-attack and angle-of-sideslip. On fully operational SAIP's, these analog outputs are subsequently supplied to the DAT Processing Unit/Data Interface Unit (DPU/DIU) for digitizing and formatting for down-link communications [Ref.3:p. 134].

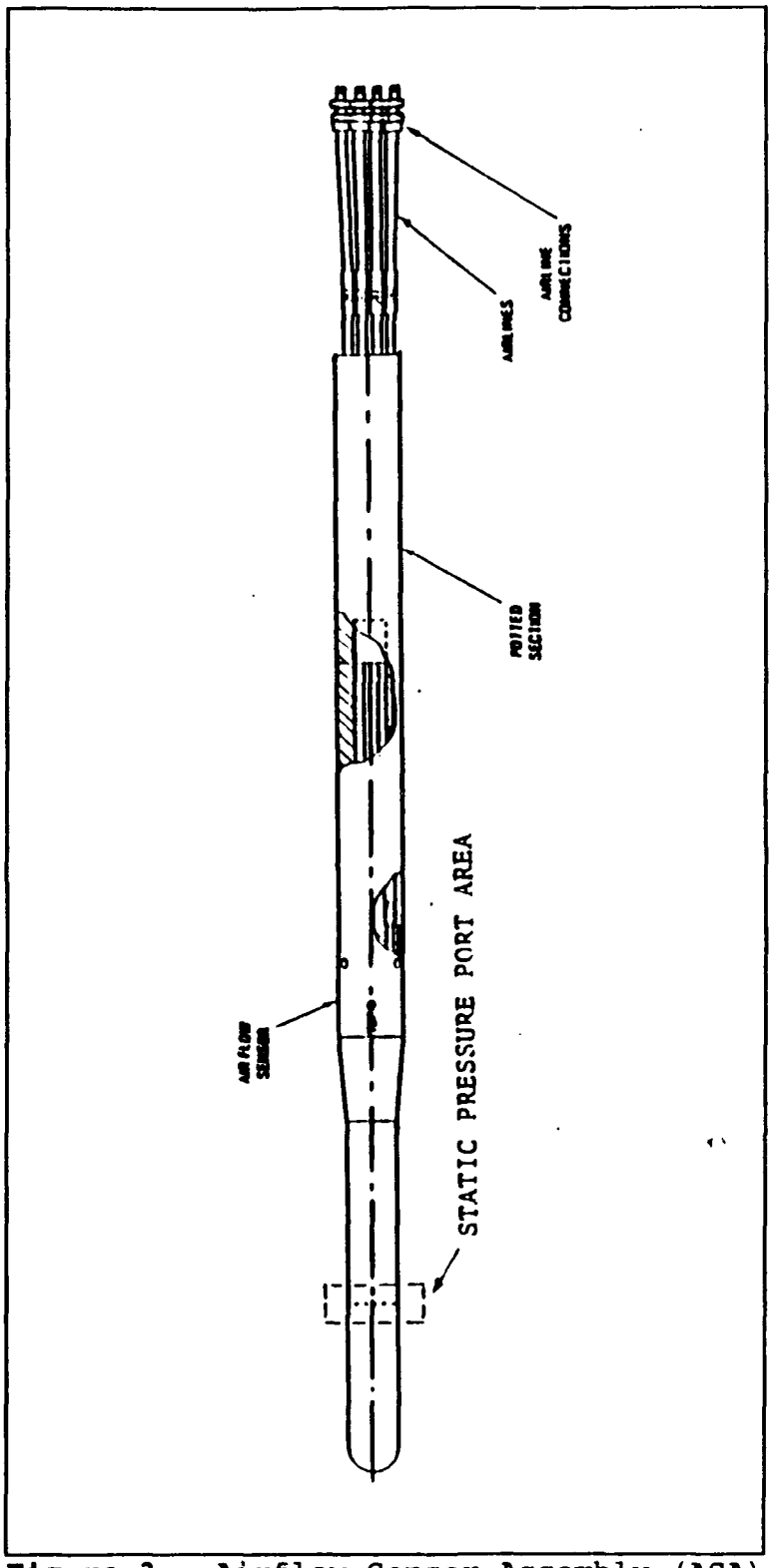

Figure 3. Airflow Sensor Assembly (ASA) [Ref. 3].

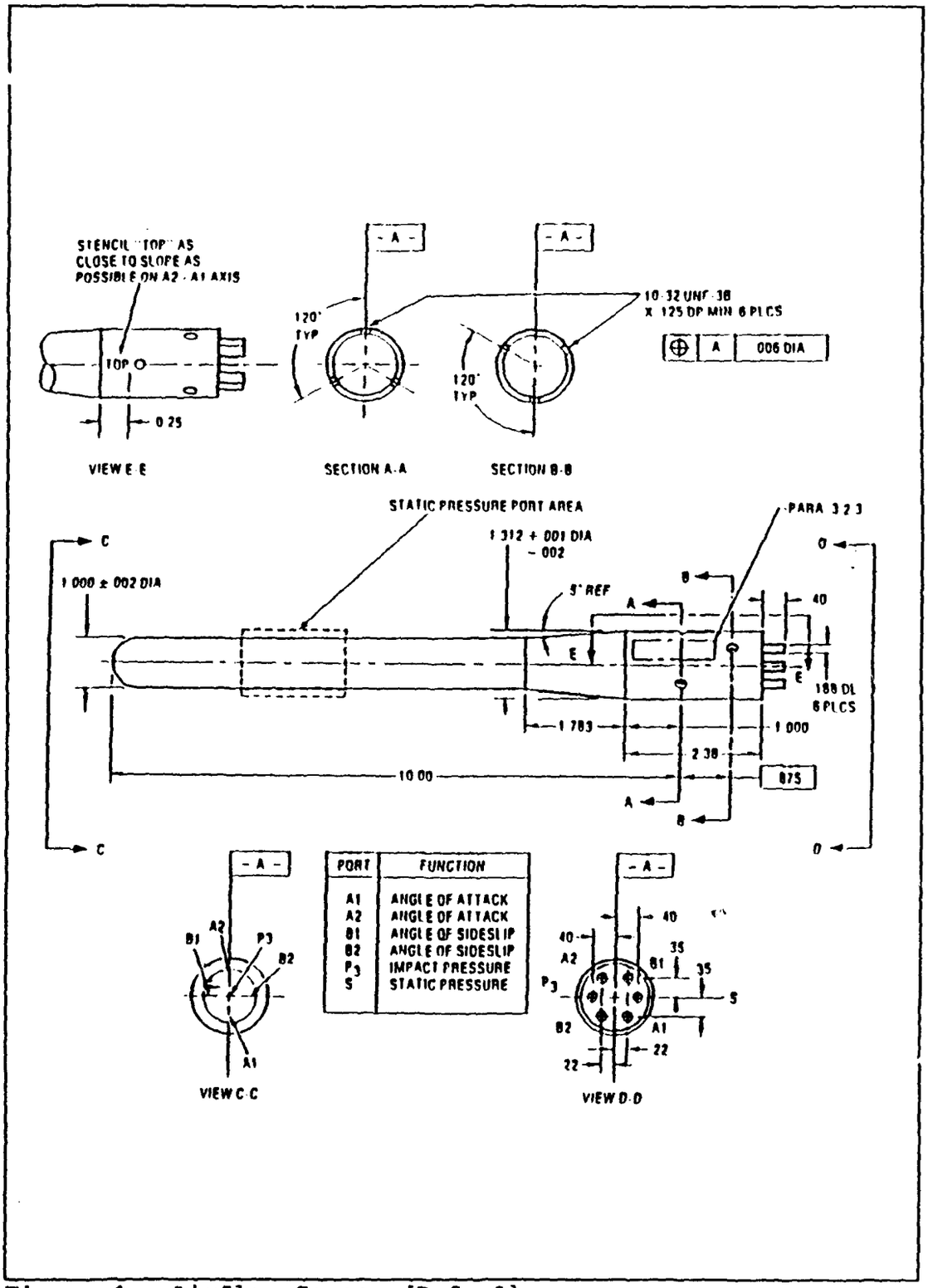

Figure 4. Airflow Sensor [Ref. 3].

3. System Performance

The SAIP functional specifications for altitude determination states:

> The altitude error in 50 percent of the track updates shall be less than the larger of 100 feet or three percent of the participant altitude [Ref. 3].

On 23 May 1989, an experiment (op #1218) was conducted at NAWCWPNS to determine the quality of the SAIP altitude measurements. Three aircraft carrying four SAIP modules were used. A-6 aircraft BH-57 had two SAIP modules, A-6 aircraft BH-55 had one SAIP, and A-7 aircraft BH-85 had one SAIP. Performance was so unacceptable that on 07 September 1989, another A-6 was configured with four SAIP modules and retested using more refined procedures and experimental techniques. Reference 1 presents in detail the system performance during these flight test. To briefly summarize these results, altitude errors were well in excess of specifications. The errors reached magnitudes of 500-600 ft at an altitude of 4,000 ft, to 900-1,000 ft at an altitude of 10,000 ft [Ref. 1:pp 4-5]. The magnitude of the errors displayed airspeed and altitude dependence, where higher aircraft speeds and elevations substantially increased altitude errors.

After the September 89 flight test, the Naval Postgraduate school was contacted and requested to study these phenomena and present recommendations on how to remedy the problem.

B. THESIS PURPOSE

1. To use computer modeling to calculate the pressure distribution over the body of the SAIP. This quantifies the pressures measured at the static pressure ports and determines where static pressure may best be measured.

2. To test the Airflow Sensor Assembly (ASA) in the wind tunnel in order to determine its performance void of the SAIP body.

3. To retest the SAIP based on more accurate wind tunnel correction factors. These correction factors are associated with wind tunnel flow blockage due to the body and test stand which were not thoroughly investigated in Reference 2.

4. To conduct extensive flow visualization studies of the ASA and SAIP to investigate the effects of flow separation at the hemispherical tip on static pressure measurements.

5. To quantify the errors associated with the host aircraft's pressure field. This is accomplished with powerful computational methods (VSAERO panel code) and further examination of the flight test data found in Reference 1.

6 To verify the computational results with flight test data and/or wind tunnel data in order to recommend proper modifications to improve altitude determination.

II. PANEL METHOD

A. PMARC/PMAPP

PMARC (Panel Method Ames Research Center) is a low-order potential-flow panel code (FORTRAN) currently being developed by the NASA Ames Research Center computational fluid dynamics engineers. It is used for modeling complex three-dimensional geometries and includes such features as internal flow modeling for ducts, simple jet plume modeling, and time-stepping wake modeling for the study of steady and unsteady motions. The code was written to be used on computers ranging from the Macintosh II workstation to the Cray Y-MP. PMARC is a non-proprietary code derived from another low-order panel code, VSAERO (Vortex Separation Aerodynamics Program). [Ref. 4:pp. 1-2]

The selection of PMARC as the computational method of choice was based on the nature of the problem (i.e., the SAIP configuration) and on an AIAA paper titled "Subsonic Panel Methods - A Comparison of Several Production Codes" [Ref. 5]. Inviscid flow was assumed to occur over the SAIP. The selection of a low-order singularity panel method was due to the trade-off between the limited increase in accuracy attainable with a high-order panel method compared to the significantly greater cost and execution time high-order panel

methods require. Also, PMARC is public domain software and very "user friendly".

PMAPP (Panel Method Aerodynamic Plotting Program) is a post-processor software package used to plot the three-dimensional aerodynamic flow output generated with PMARC. PMAPP outputs include data curves superimposed over 2-dimensional model geometry section cuts, contour plots, vector plots, 3-dimensional geometry plots, wire-frame geometry plots with wakes, aerodynamic surface data, streamline data, and off-body velocity data. PMAPP is designed to run on the VAX/MicroVAX with a VMS operating system. A proprietary Tektronix TCS code is necessary for data display. [Ref. 6:p. 1]

The PMARC and PMAPP codes are currently loaded on the Department of Aeronautics and Astronautics MicroVAX system located in the Advanced Computational Laboratory, Naval Postgraduate School, Monterey, California.

B. PARAMETER DEFINITIONS

1. Pressure Coefficient

The primary goal of this study is to determine the pressure found at the static ports. A distinct feature of the PMAPP code is the aerodynamic surface cut, which in addition to other parameters, can plot the pressure coefficient C_p along the length of the section chosen. Plots of C_p along the length of the SAIP would achieve this primary objective.

Therefore, it is necessary to define the pressure coefficient (C_p), for it will be used extensively throughout this study.

a. Incompressible Flow

The pressure coefficient is defined as

$$C_p = \frac{p-p_\infty}{q_\infty} = \frac{\Delta p}{q_\infty} \tag{1}$$

where the dynamic pressure is

$$q_\infty = \frac{1}{2}\rho_\infty V_\infty^2 \tag{2}$$

C_p is a dimensionless quantity used in all flight regimes from incompressible to hypersonic flow. It is a function of Mach number, Reynolds number, shape and orientation of the body and location on the body. At low Mach numbers (less than 0.3) the flow is considered incompressible and C_p is only a function of shape, orientation, location and Reynolds number. Wind tunnel test speeds at the Naval Postgraduate School are conducted at Mach numbers below 0.14, well within the incompressible regime.

b. Compressible Flow

The flight regime encountered by the SAIP will be predominantly compressible. PMARC uses the Prandtl-Glauert compressibility correction which is based on linearized perturbation theory. This is essentially a compressibility correction for a two-dimensional profile that is applied to the pressure coefficients. The geometry is not transformed

into compressibility coordinates [Ref. 4]. The Prandtl-Glauert rule is defined as

$$C_p = \frac{C_{p,0}}{\sqrt{1-M_\infty^2}} \qquad (3)$$

where $C_{p,0}$ is the incompressible pressure coefficient. The limitations to this correction factor are based on its derivation for two-dimensional thin airfoils and small angles of attack. Also, it applies to purely subsonic flight and gives erroneous results at Mach numbers greater than 0.7 (in the transonic regime) [Ref. 7].

2. Static Pressure

Static pressure is a measure of the purely random motion of molecules in the gas. The static pressure tap drilled perpendicular to the surface of the Airflow Sensor Assembly (ASA) measures the pressure due only to the random motion of the molecules in air. In this case, if the flow velocity over the static ports is equal to the free-stream velocity then $p_s = p_\infty$ and therefore, $C_p = 0$. The altitude determination of the SAIP is based purely on these static pressure readings. The 12 static pressure port measurements are averaged in a chamber and sent to the absolute pressure transducer, the output of which goes to the ADU. This information is digitized and sent to the EATS system which compares the barometric pressure readings to a standard atmospheric profile and computes the altitude. Therefore, if

C_p = 0 at the static pressure ports, then p_s will equal p_∞ and the correct altitude would have been determined.

3. Altitude Error Determination

It is difficult to design a unit for which C_p will equal zero over the static pressure ports. Altitude errors are expressed in terms of C_p in order to determine the magnitude of the altitude errors predicted by the PMARC code. Derivation of an algorithm for ΔZ begins with the hydrostatic equation and perfect gas law [Ref. 2]

$$\frac{dp}{p} = -g\,\frac{dZ}{RT} \tag{4}$$

where, for the atmosphere

$$T = T_o - \lambda Z \tag{5}$$

where λ = lapse rate = + 6.5 degrees C/km (from "U.S. Extension of the ICAO Standard Atmosphere," 1958). Substitution of (5) into (4) and integrating yields

$$\frac{p}{p_0} = \left[1 - \frac{\lambda Z}{T_o}\right]^{g/\lambda R} \tag{6}$$

Assuming small changes where $dp \cong \Delta p$ and substituting (6) into (4) yields

$$\Delta p = \frac{-gP_o\left[1 - \frac{\lambda Z}{T_o}\right]^{g/\lambda R}}{T_o R\left[1 - \frac{\lambda Z}{T_o}\right]} \cdot \Delta Z \tag{7}$$

$$= -\frac{gp_o}{RT_o}\left[1 - \frac{\lambda Z}{T_o}\right]^{4.26} \cdot \Delta Z \qquad (8)$$

Using the binomial approximation ($\lambda Z/T_o < 1$) where

$$\left[1 - \frac{\lambda Z}{T_o}\right]^{4.26} \approx 1 - 4.26\frac{\lambda Z}{T_o} \qquad (9)$$

Equation (8) becomes,

$$\Delta p \approx \left[-\frac{gp_o}{RT_o}\right]\left[1 - 4.26\frac{\lambda Z}{T_o}\right]\Delta Z \qquad (10)$$

Dividing both sides by q_∞,

$$\frac{\Delta p}{q_\infty} \approx -\frac{1}{q_\infty}\left[\frac{gp_o}{RT_o}\right]\left[1 - 4.26\frac{\lambda Z}{T_o}\right]\Delta Z \qquad (11)$$

and substituting C_p for $\Delta p/q_\infty$ yields

$$C_p \approx -\left[\frac{g\rho_o}{.5\rho_\infty V_\infty^2}\right]\left[1 - 4.26\frac{\lambda Z}{T_o}\right]\Delta Z \qquad (12)$$

Rearranging,

$$\Delta Z \approx \frac{-C_p}{\left[1 - 4.26\frac{\lambda Z}{T_o}\right]} \cdot \frac{V_\infty^2}{2g} \cdot \frac{\rho_\infty}{\rho_o} \qquad (13)$$

It can be shown that

$$\left[1 - 4.26\frac{\lambda Z}{T_o}\right]\left[\frac{\rho_o}{\rho_\infty}\right] \approx 1 \qquad (14)$$

for any value of Z and the corresponding density ratio. Therefore, Equation (13) becomes

$$\Delta Z \approx -\frac{C_p V_\infty^2}{2g} \approx -\frac{\gamma R T_\infty}{2g} C_p M_\infty^2 \qquad (15)$$

where $T_\infty = T_0 - \lambda Z$ as per Equation 5. This useful equation will be used extensively throughout this study to get a feel for the magnitude of the altitude errors associated with the computationally determined pressure coefficients.

C. PMARC Model of the SAIP

1. Modeling Techniques

The SAIP has been modelled using the PMARC code as shown in Figure 5 and 6. The axisymmetric shape (no antennas) represents the SAIP used during wind tunnel tests at the Naval Postgraduate School [Refs. 1 and 2]. Over 1200 panels were used in modeling the SAIP with higher resolution on the ASA. The lower left end of the SAIP in Figure 5 tapers to a cone because of the PMARC requirement of simulating wakes with panels downstream of the body which must separate from a smooth body as opposed to a blunt end. Wakes must be generated in order to attain any aerodynamic data. This region is located well aft of the area of interest so that its effects have no bearing on the solution and its shape is irrelevant.

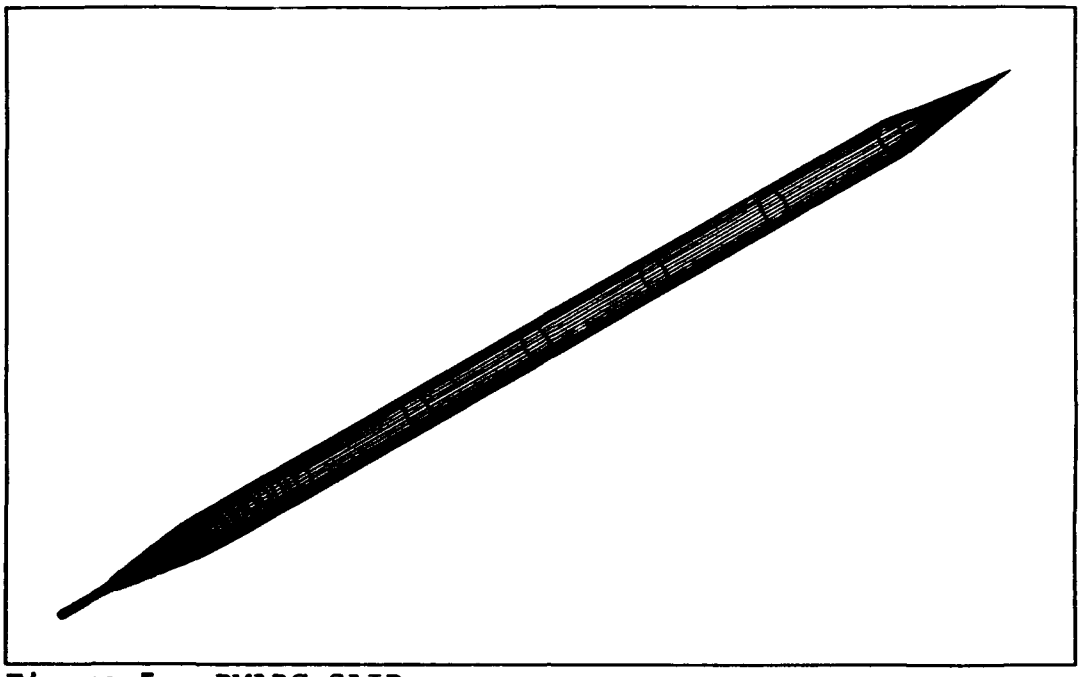

Figure 5. PMARC SAIP.

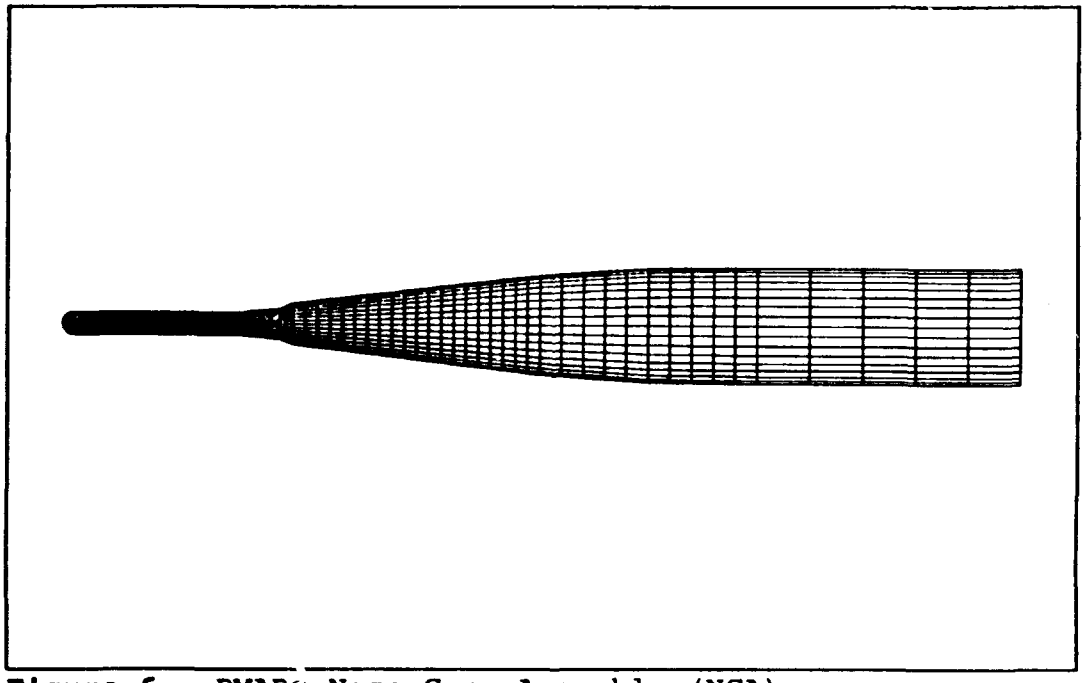

Figure 6. PMARC Nose Cone Assembly (NCA).

2. Results

Computational runs were made at Mach 0.13 and 0.6. Mach 0.13 corresponds to the velocities found in the NPS wind tunnel and Mach 0.6 corresponds to a median flight test speed. Figure 7 is an aerodynamic surface cut showing the C_p as a function of the length x from the nose for both Mach numbers. Figure 8 is this same profile zoomed in the region of the static ports for Mach 0.6.

a. C_p Magnitude

The static pressure ports are located 3.5 inches aft of the nose. The C_p found in this region, according to the PMARC code (Fig. 8) is approximately 0.02 for both Mach numbers. Using equation (15) this corresponds to an altitude error of 129.9 ft at Mach 0.6 at 10,000 ft altitude. Compared to the C_p of 0.1 predicted by Russell [Ref. 2] and to the altitude errors revealed during initial flight tests (900 ft at 10,000 ft altitude), this result is somewhat perplexing. Russell attributed his high values of C_p to the five-inch diameter body of the SAIP and verified his results in the NPS wind tunnel.

b. VSAERO Verification

In light of the above discrepancy, independent verification of the results from the PMARC code was necessary. VSAERO is used extensively at the Naval Air Warfare Center, China Lake, California to predict store separation

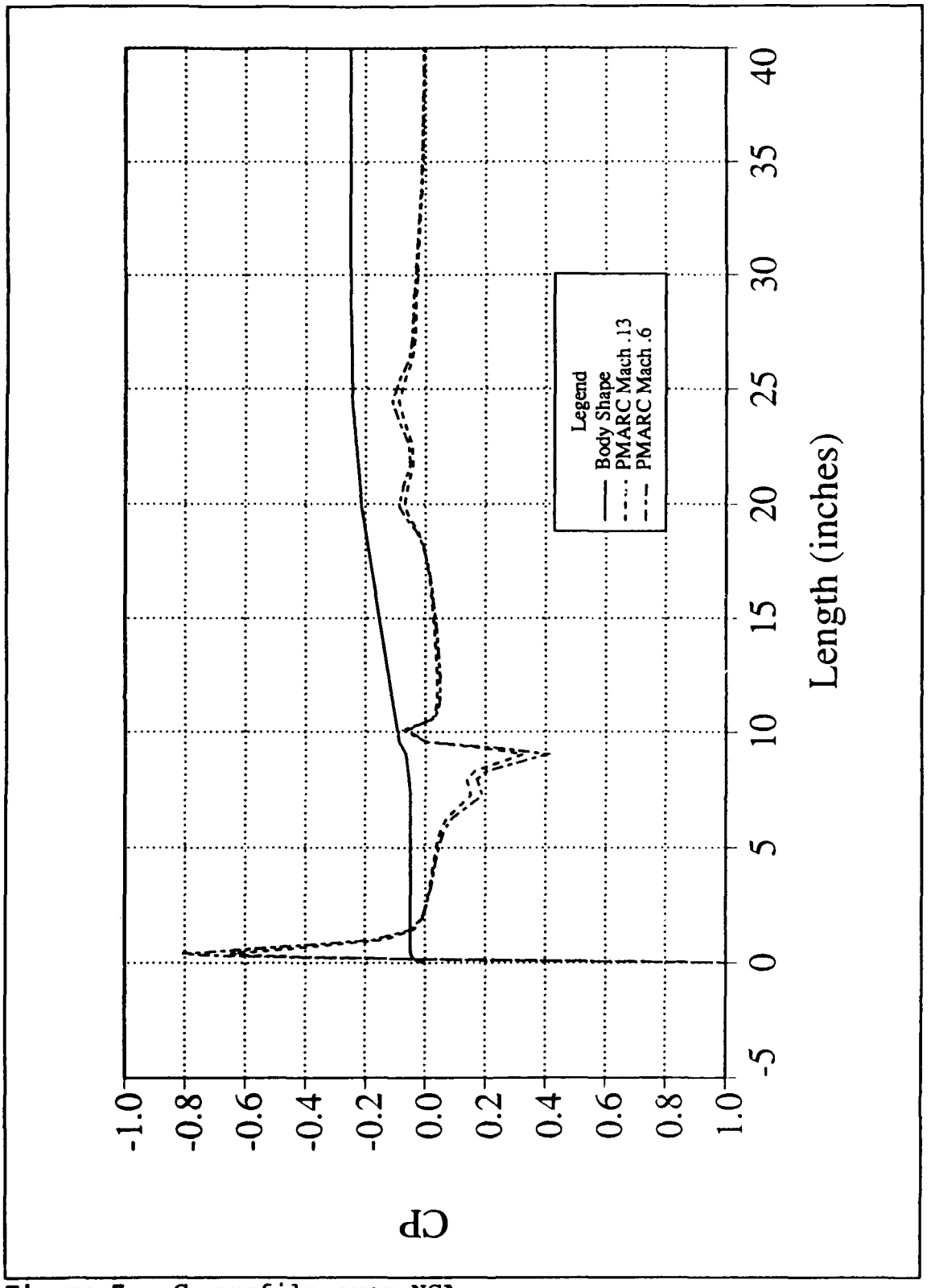

Figure 7. C_p profile over NCA.

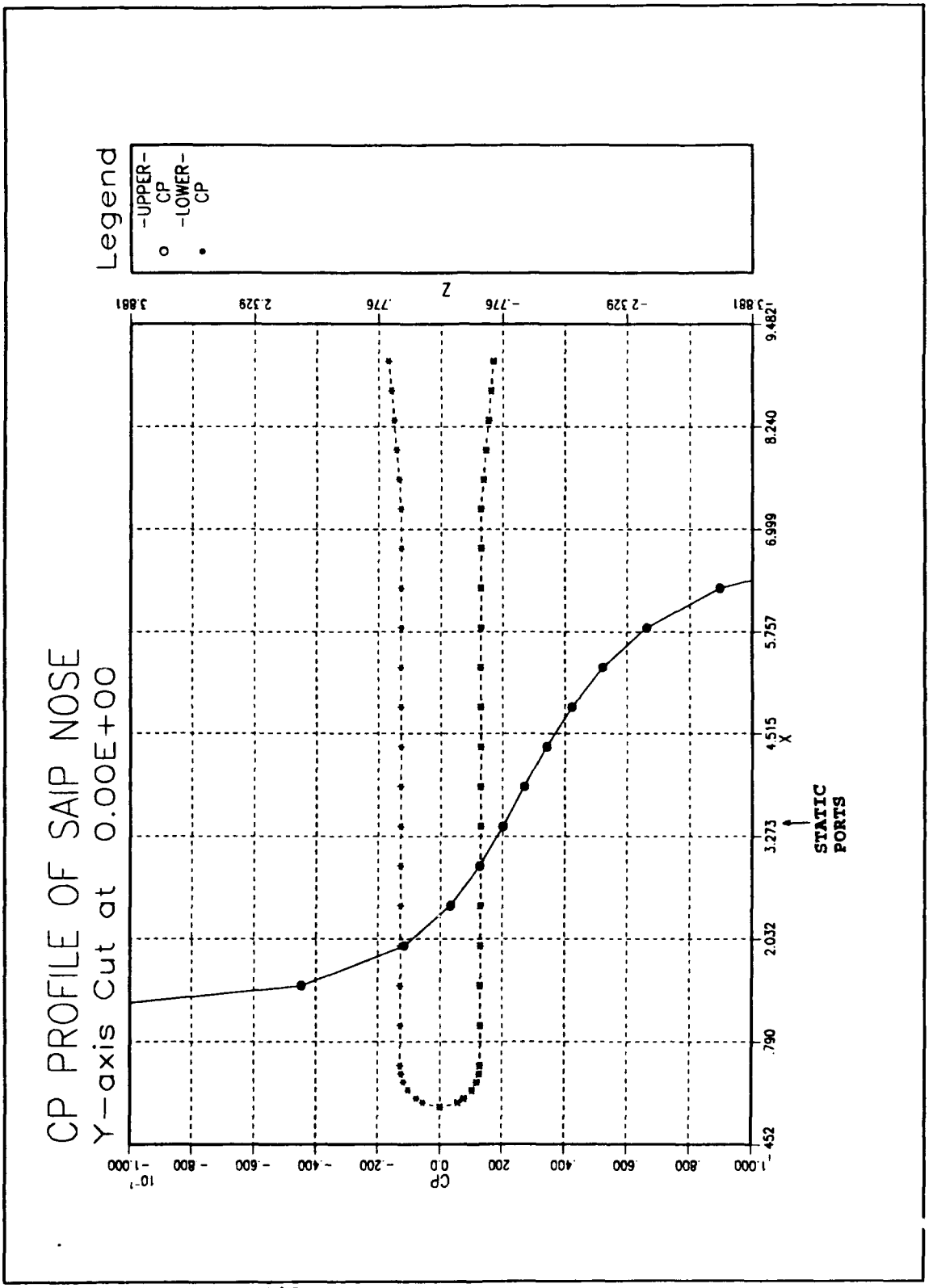

Figure 8. C_p profile over SAIP nose.

trajectories from aircraft. Larry Gleason, a China Lake computational fluid engineers, was contacted and asked to model the SAIP in order to provide verification of correct panel method techniques. Figure 9 is the C_p profile as predicted by the VSAERO code. The pressures found here compare identically with the PMARC code (PMARC is a derivative of VSAERO).

c. Nose and Body Effects

Another significant factor affecting the C_p profile is the shape of the curve over the front ten inches of the SAIP (Figs. 7 and 8). This shape gives rise to "nose" and "body" effects. Nose effects are caused by the rapid acceleration of the flow over the hemispherical nose from stagnation velocity to the velocities encountered over the static ports. Body effects are a result of over-pressures propagated forward due to the motion of the SAIP body in subsonic flight. For incompressible flow the pressure coefficient can be expressed as

$$C_p = 1 - [\frac{V}{V_\infty}]^2 \qquad \textbf{(16)}$$

The pressure coefficient ranges from C_p = 1.0 (stagnation region) to near free-stream conditions (i.e., C_p = 0) over the static ports. The body effects cause the over-pressure region five to 9 inches from the nose. Although the flow looks relatively near free-stream conditions near the static ports

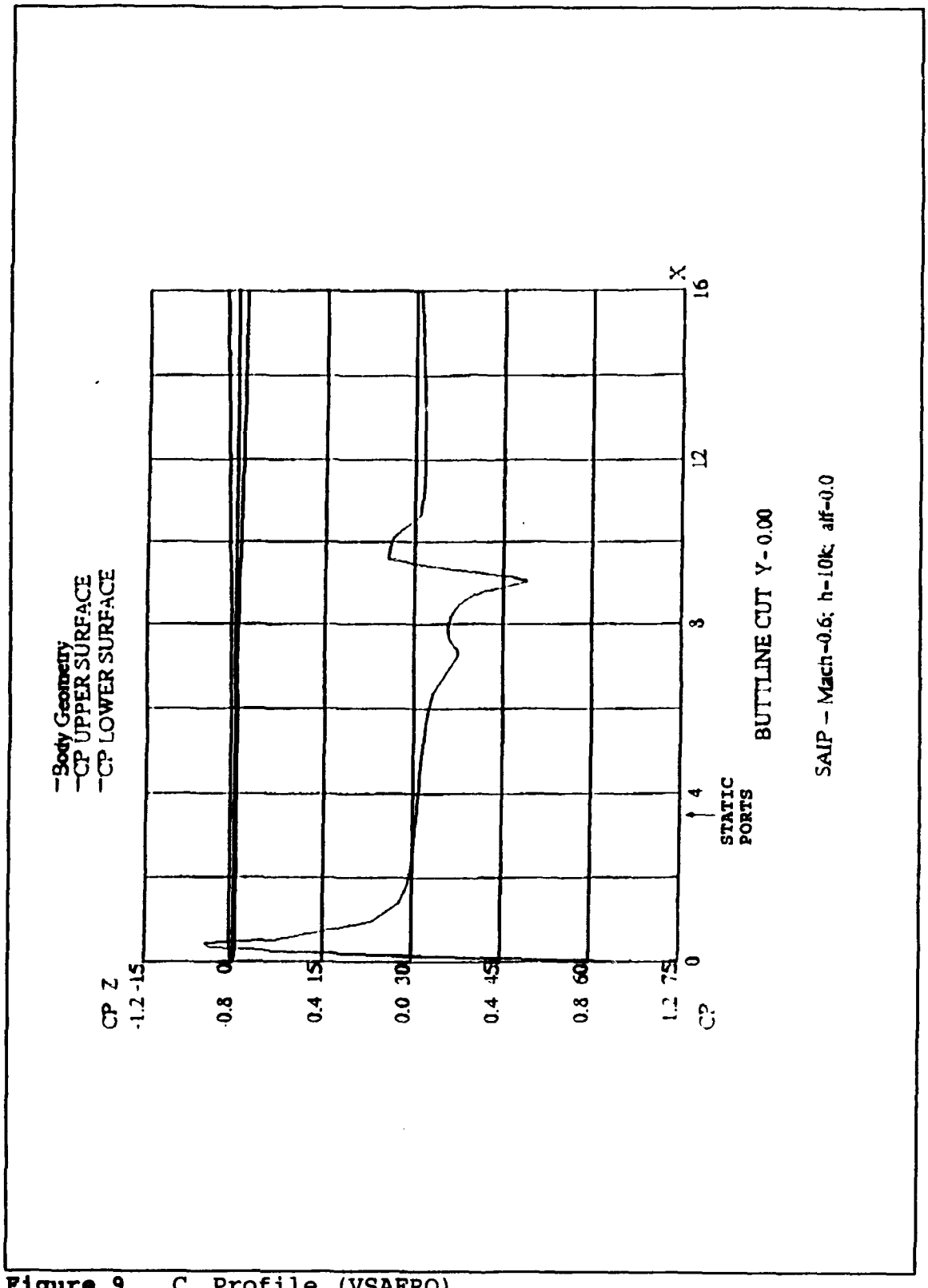

Figure 9. C_p Profile (VSAERO)

(Fig. 7) and conducive to accurate static pressure readings, this turns out not to be the case. Figure 8 shows the effects of the nose and body. In an ideal case, the C_p profile should be flat and have a magnitude of zero. However, the slope of the C_p distribution incurred near the static ports creates a pressure coefficient range from 0.0 at x = 2.0 inches to 0.05 at x = 5.5 inches. This corresponds to altitude errors of 0 ft to 324.7 ft (Mach 0.6, 10,000 ft altitude) respectively. These pressure coefficients are not of the magnitude found during flight tests, however, they do indicate a trouble spot. It must be emphasized that the PMARC data are a computational prediction of inviscid pressure coefficients. The value of the code is to predict magnitudes and analyzed trends. Because the static ports are located so close to the nose tip and also near a region of over-pressure, and because the pressure coefficient curve is a function of the PMARC code's accuracy, the curve over the static ports (Figs. 7 and 8) could be in reality displaced left or right.

Figure 10 shows empirical results found in the literature on the effects of the nose and stem on pitot static measurements as a function of static port location from the nose and stem respectively [Ref 8.:p. 351]. Ref. 8 recommends that static ports be located six to eight diameters aft of the nose and well forward of the stem. The static pressure ports of the SAIP are 3.5 diameters from the nose and eight diameters from the widening body.

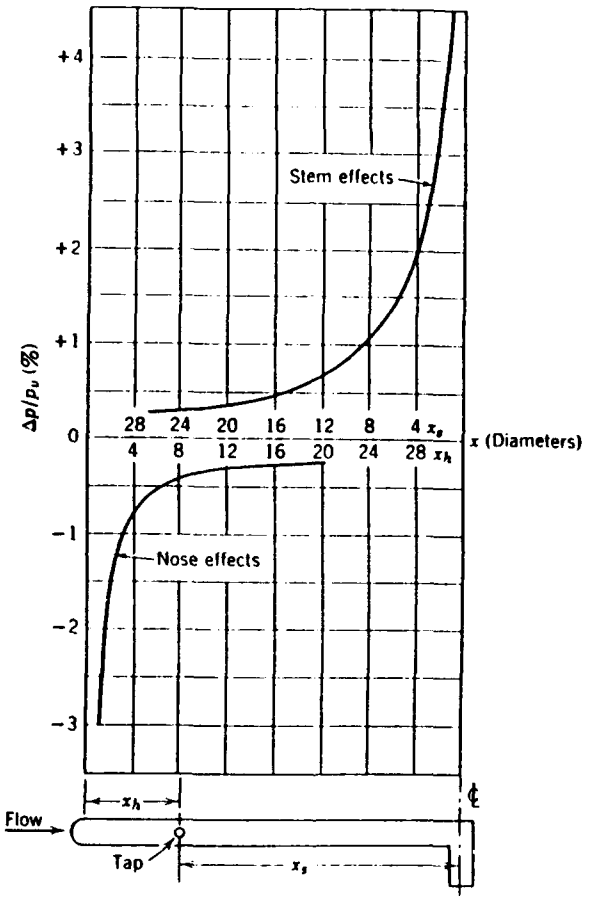

Figure 10. Static tube characteristics [Ref. 8].

d. Compressibility Effects

The compressibility effects predicted by PMARC are simply linear corrections applied to the pressure coefficient. This accounts for the higher spikes of the Mach 0.6 curve (Fig. 7) and the crossing of the curves at $C_p = 0$. PMARC predicts higher altitude errors due to compressibility. The significance of compressibility will covered more thoroughly in the Chapter V.

D. AIRFLOW SENSOR ASSEMBLY (ASA) MODEL

Rosemount wind tunnel tested the ASA to meet NAWCWPNS specifications. Wind tunnel tests of the ASA at NPS were also performed to verify its performance (Chapter IV). Therefore, a model of the ASA was generated with PMARC (Fig. 11) in order to compare code predictions with wind tunnel data. Figures 12 and 13 are plots of the C_p profile similar to those generated for the SAIP (the X axis is non-dimensionalized). The profile shows that the C_p over the static port is very close to zero and slightly negative. Also, the curve is relatively flat in the static port region. In fact, it will be shown in Chapter IV that the pressure coefficient measured by the ASA during NPS wind tunnel tests was extremely close to zero as anticipated. This profile reaffirms the hypothesis about "body" effects discussed earlier. Without the five inch body of the SAIP, over-pressures are not felt forward, and the curve flattens considerably.

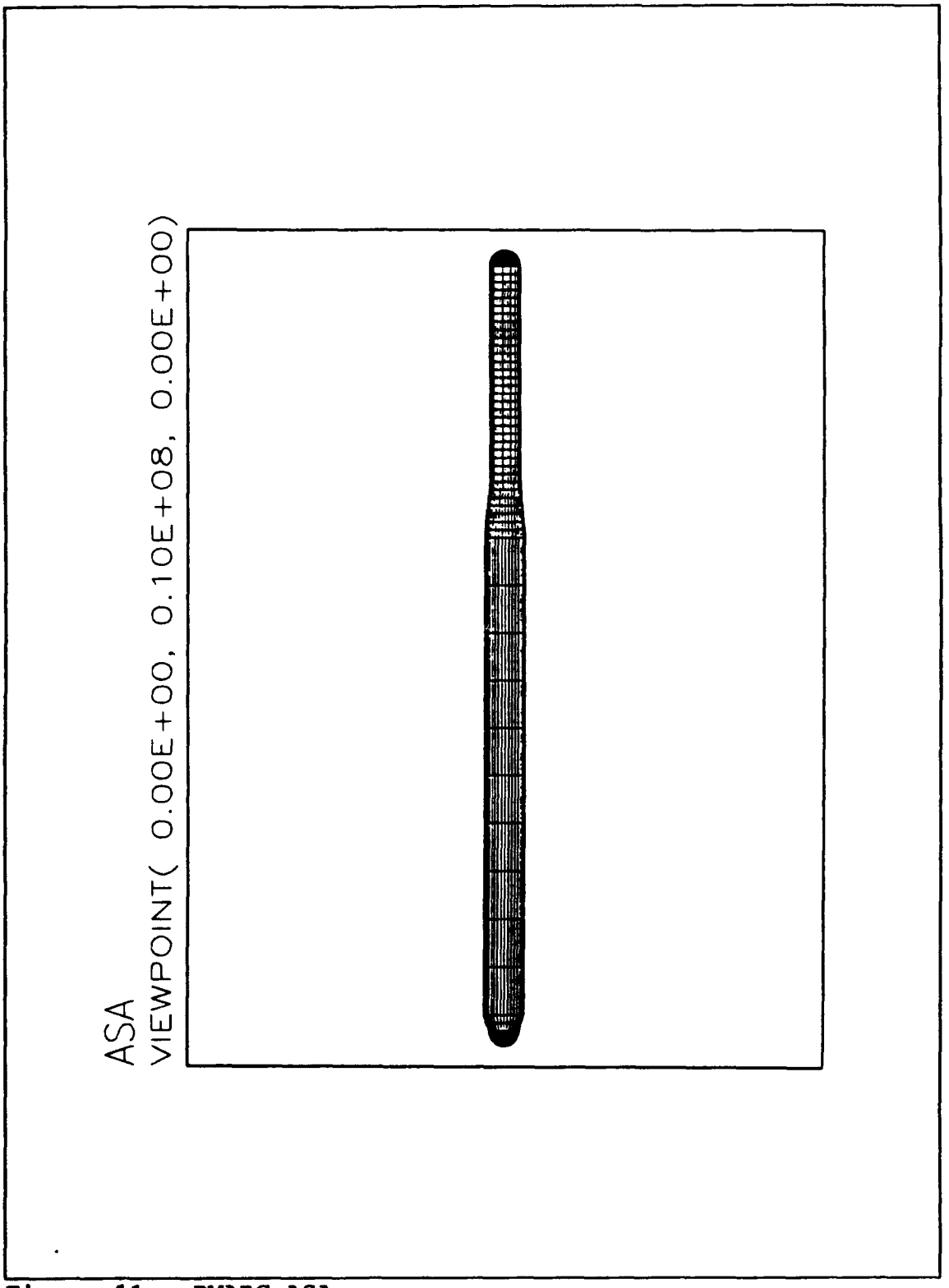

Figure 11. PMARC ASA.

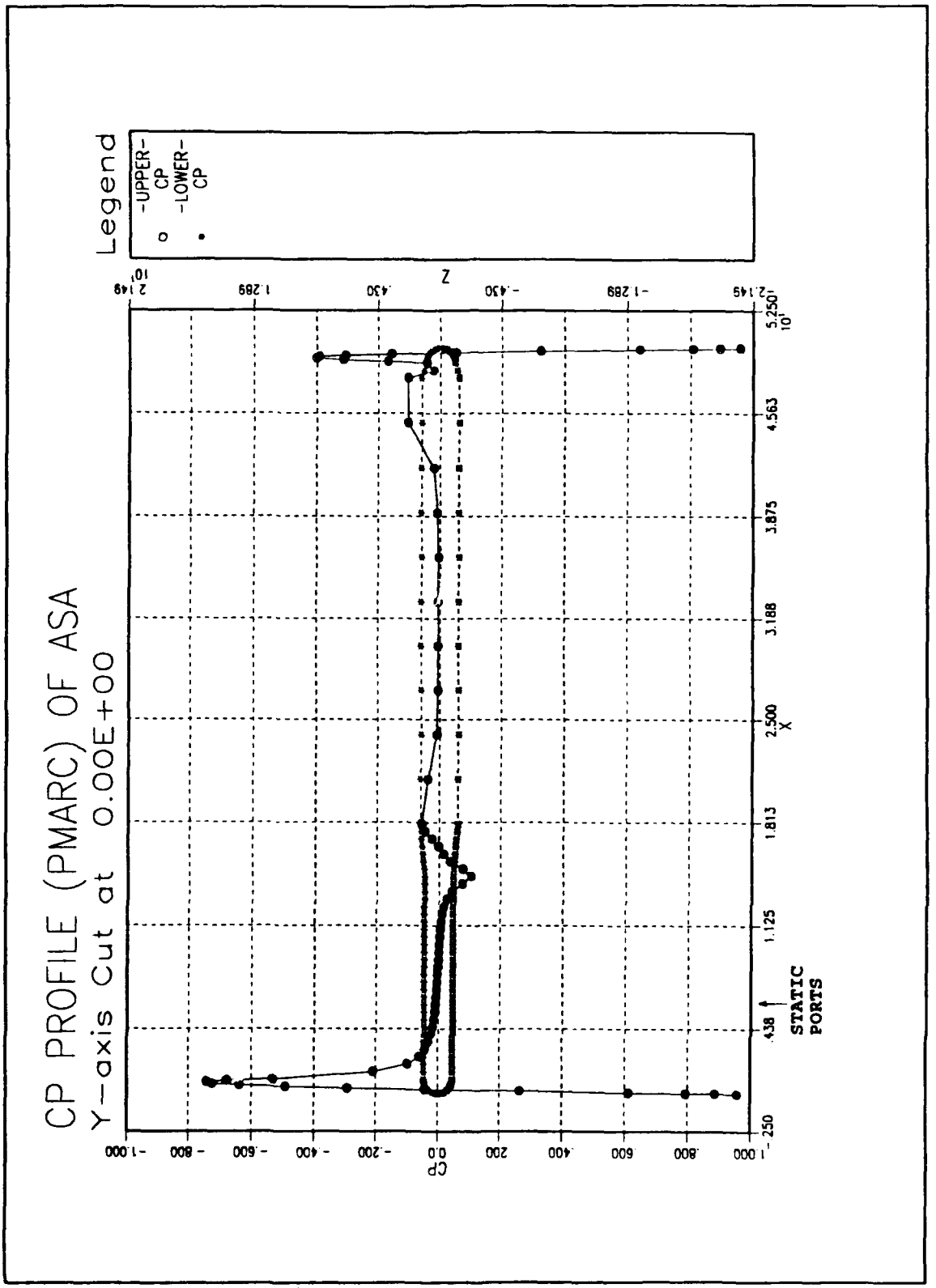

Figure 12. C_p profile over ASA (PMARC).

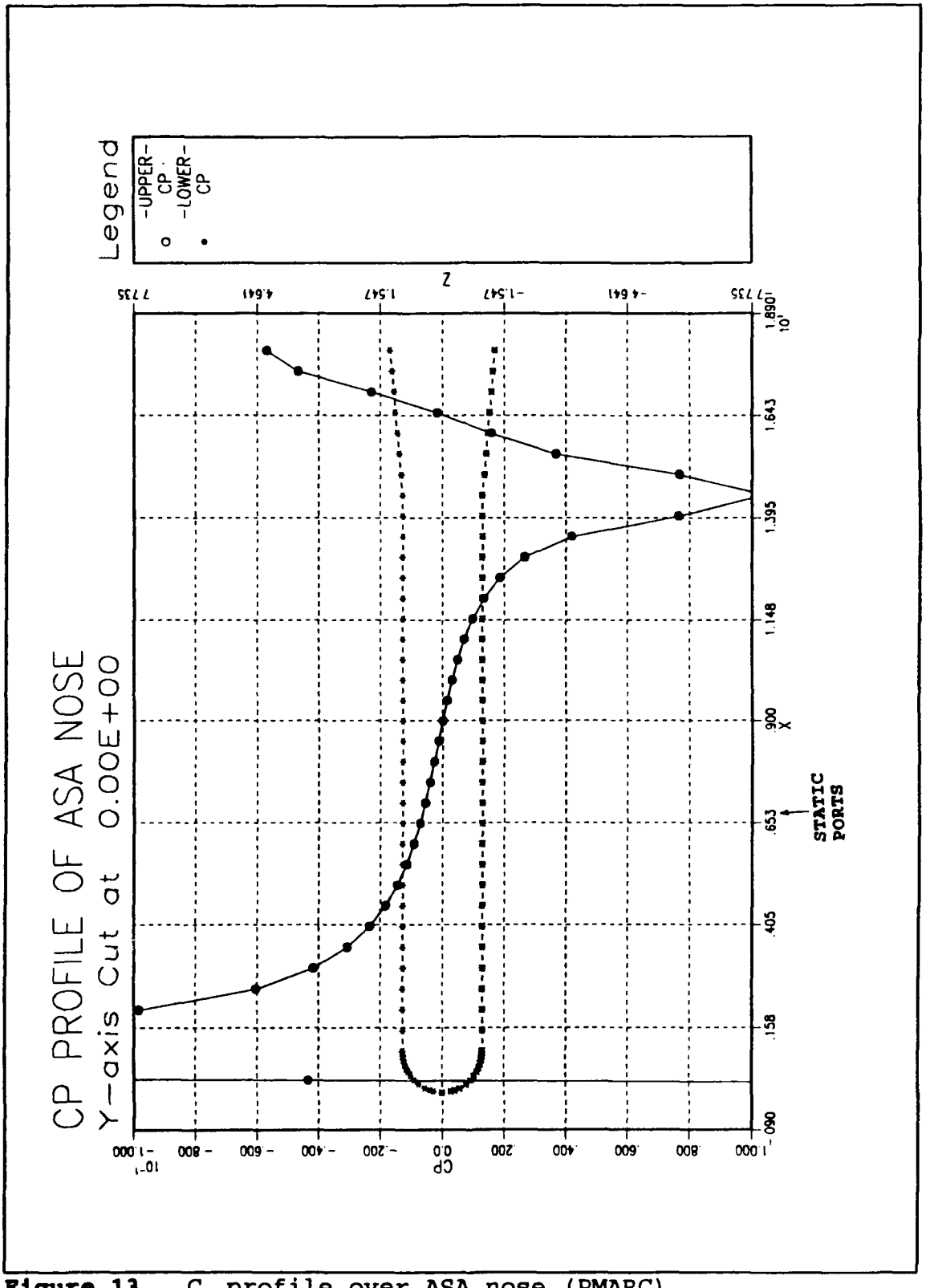

Figure 13. C_p profile over ASA nose (PMARC).

A constant diameter pitot tube was generated with PMARC for comparison (Fig. 14). The C_p profile versus length (diameter units) is shown in Figure 15. This pitot static tube has the same length as the ASA. If static ports were placed 3.5 diameters aft of the nose, a region of under-pressure would occur resulting in static pressure errors. This compares well with the effects shown in Figure 10. Rosemount eliminated this under-pressure by placing a slight flare 7.25 inches aft of the nose (Fig. 3) to create a slight over-pressure effect, dropping the C_p closer to zero at the static ports as shown in Figures 12 and 13. The ASA is essentially a finely calibrated pitot static system.

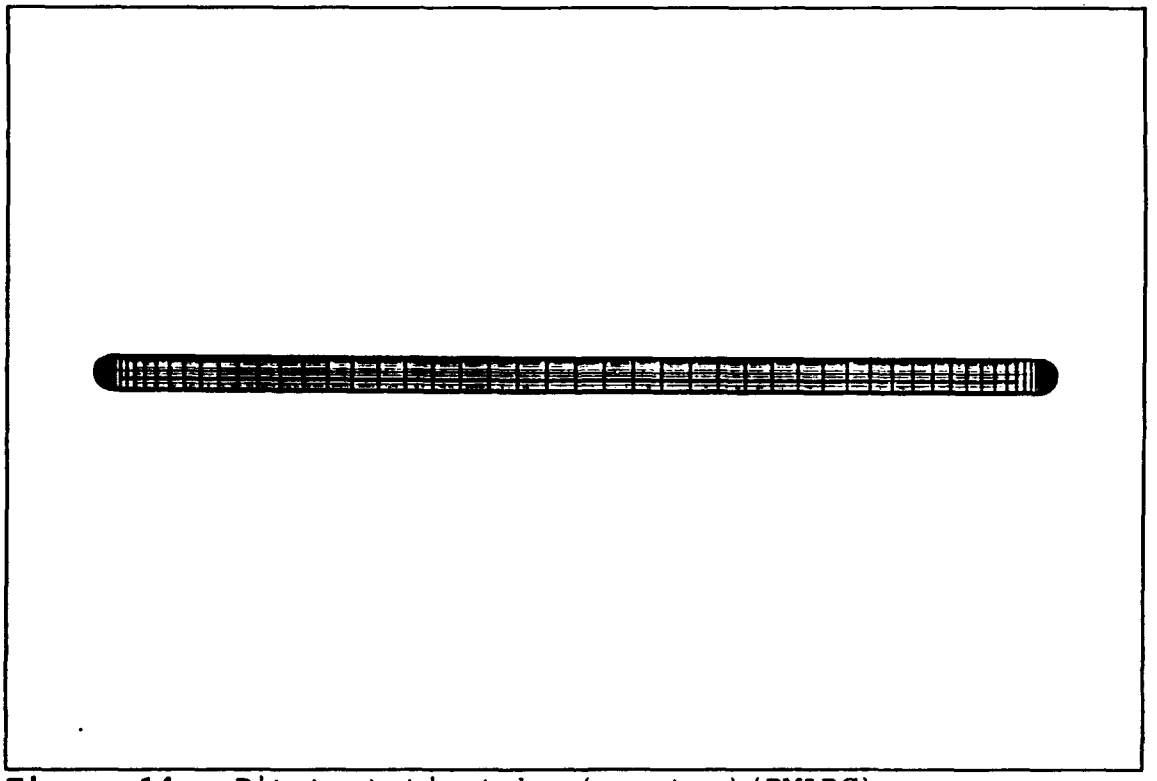

Figure 14. Pitot static tube (no stem)(PMARC).

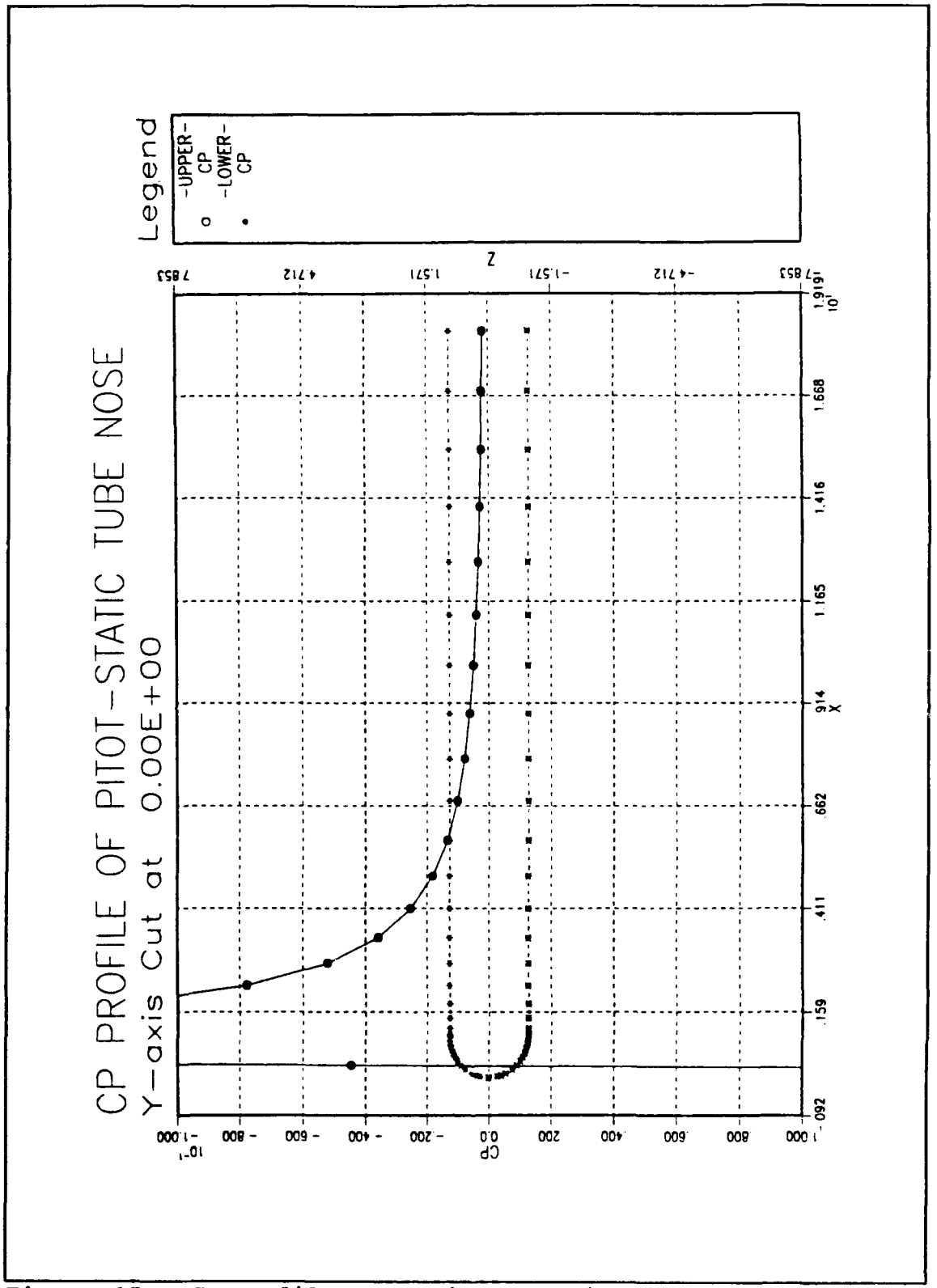

Figure 15. C_p profile over pitot static tube nose (PMARC).

E. MODEL OF SAIP WITH ELONGATED NOSE

It was postulated earlier that an elongated nose would solve system errors. Figure 16 is a PMARC model of the SAIP with a 10 inch extension of the one inch diameter nose. Figure 17 illustrates that end effects still dominate the first 3 inches of the nose, while body effects dominate the region 11 inches from the nose tip. However, the region from 3.5 to 10 inches aft of the nose tip presents a relatively accurate place to locate static ports. Here the curve flattens nicely and would present altitude readings within

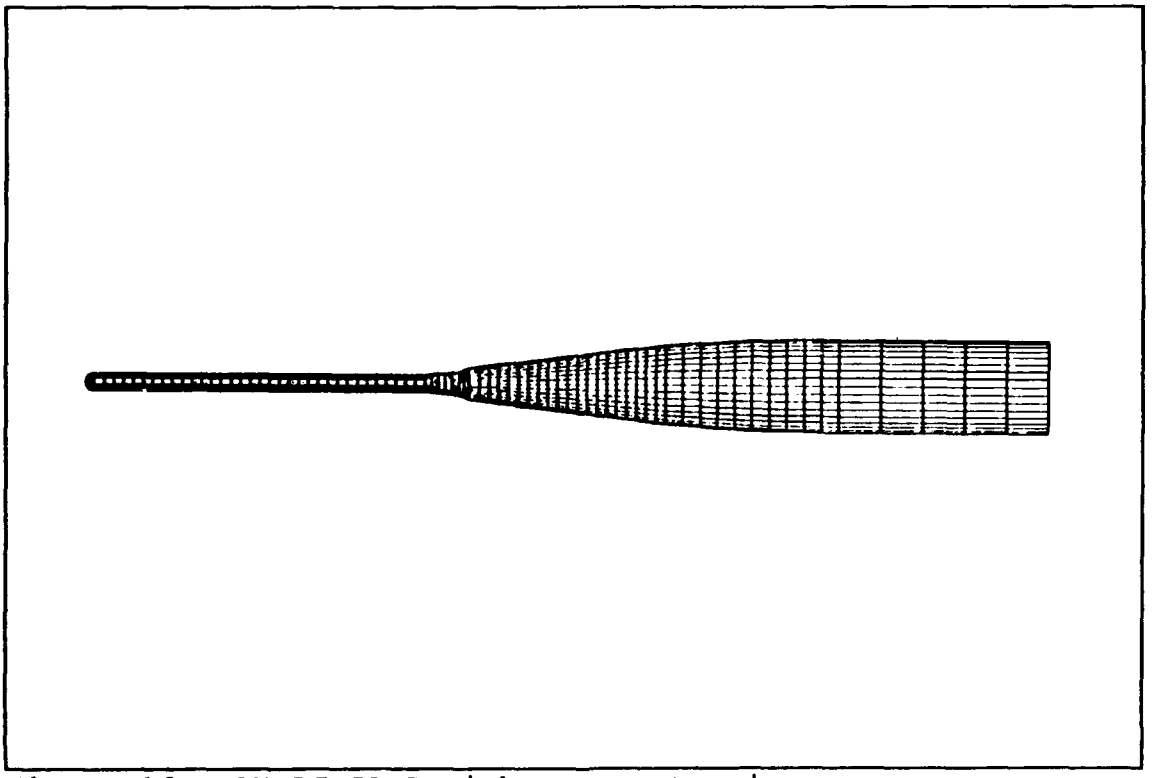

Figure 16. PMARC SAIP with nose extension.

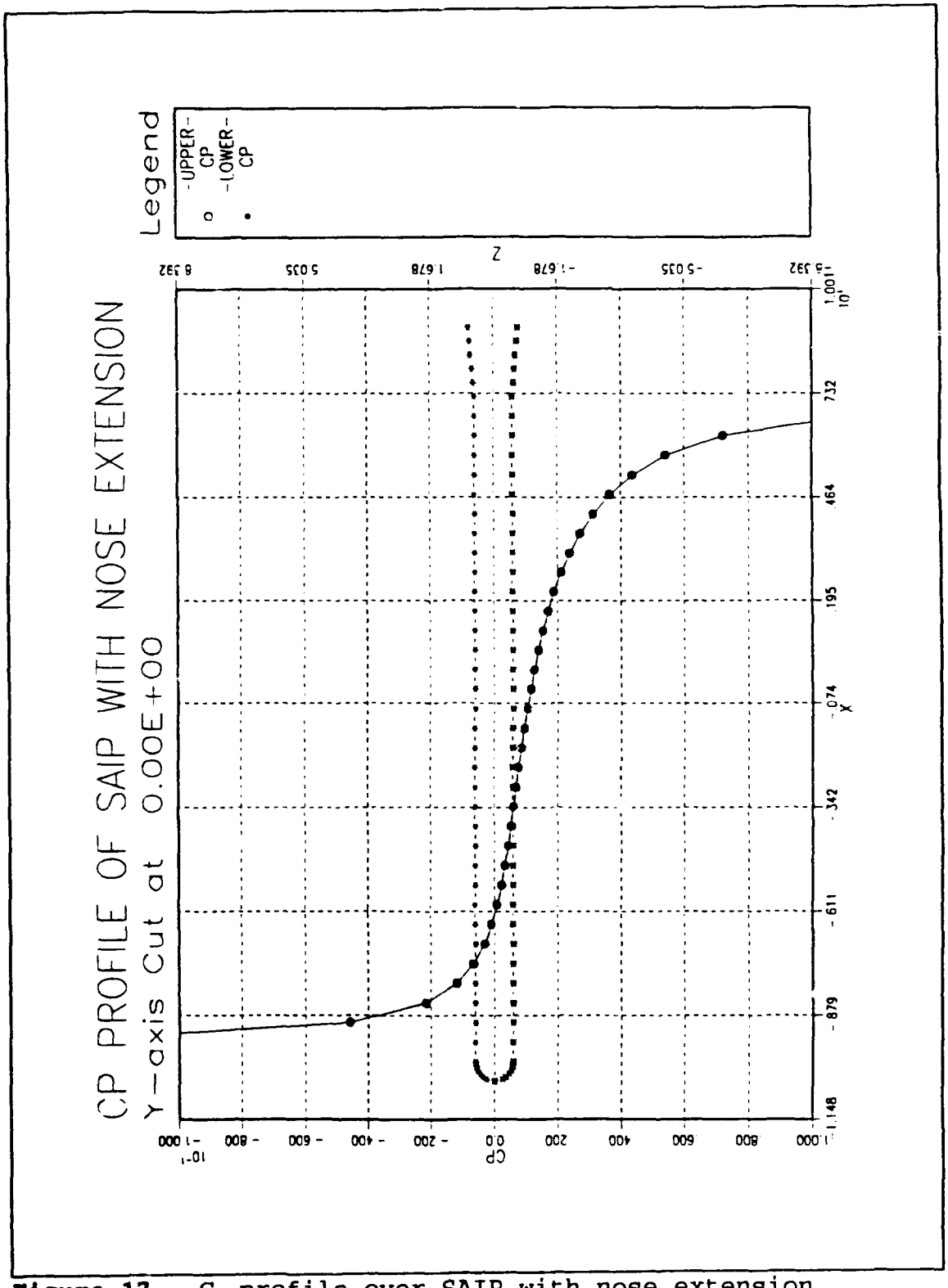

Figure 17. C_p profile over SAIP with nose extension (PMARC).

specifications, assuming no other pressure effects are felt (i.e., antennas, pylon, aircraft wing/body).

F. PANEL results

The PMARC code provides rapid and powerful results that supply a plethora of information. Despite this, all computation methods require verification with wind tunnel and/or flight test data in order to fully ascertain that accurate data are being computed. Unfortunately, the gulf between the PMARC code results and the data generated from the wind tunnel tests [Ref. 2] is too large. Russell measured C_p to be approximately 0.1 at zero degrees angle of attack. He also derived an algorithm that supported these results [Ref. 2:pp. 32]. However, a review of Russell's test procedures show a discrepancy with his wind tunnel pressure corrections due to flow blockage. The SAIP presents a large, varying cross-section even at small changes of angle of attack. Russell assumed this blockage to be a constant under-pressure in the test section associated with the empty NPS wind tunnel. This was felt to be incorrect and a repeat of the wind tunnel tests with properly calibrated pressure corrections would have to be made. Wind tunnel tests and calibration techniques will be discussed thoroughly in Chapter IV.

III. COMPUTATIONAL FLUID DYNAMICS (CFD)

A. INTRODUCTION

In an attempt to further compare the PMARC results, yet another powerful computational tool was used. The axisymmetric SAIP was modeled using inviscid, three-dimensional, Navier-Stokes computational fluid dynamics (CFD) methods.

The use of CFD in three dimensions is becoming more commonplace due to the power and availability of modern computers. Current software programs, GRIDGEN2D and HYPGEN, which generate computational grids, have been obtained at the Naval Postgraduate School. These programs allow for rapid generation of two and three dimensional grids on local NPS computers. These grids are then submitted to the OVERFLOW computational flow solver which is currently located on the CRAY2 computer at the NASA Ames Research Center.

B. METHODOLOGY

The first step was to generate the two-dimensional surface grid shown in Figures 18 and 19 using GRIDGEN2D. The GRIDGEN2D software package was developed by Steinbrenner and Chawner in order to generate a surface grid that would in turn be used to generate a three-dimensional grid [Ref. 9]. This 2-d grid served as the input for the HYPGEN grid generation program with the User Interface (UI) [Ref. 10]. HYPGEN uses

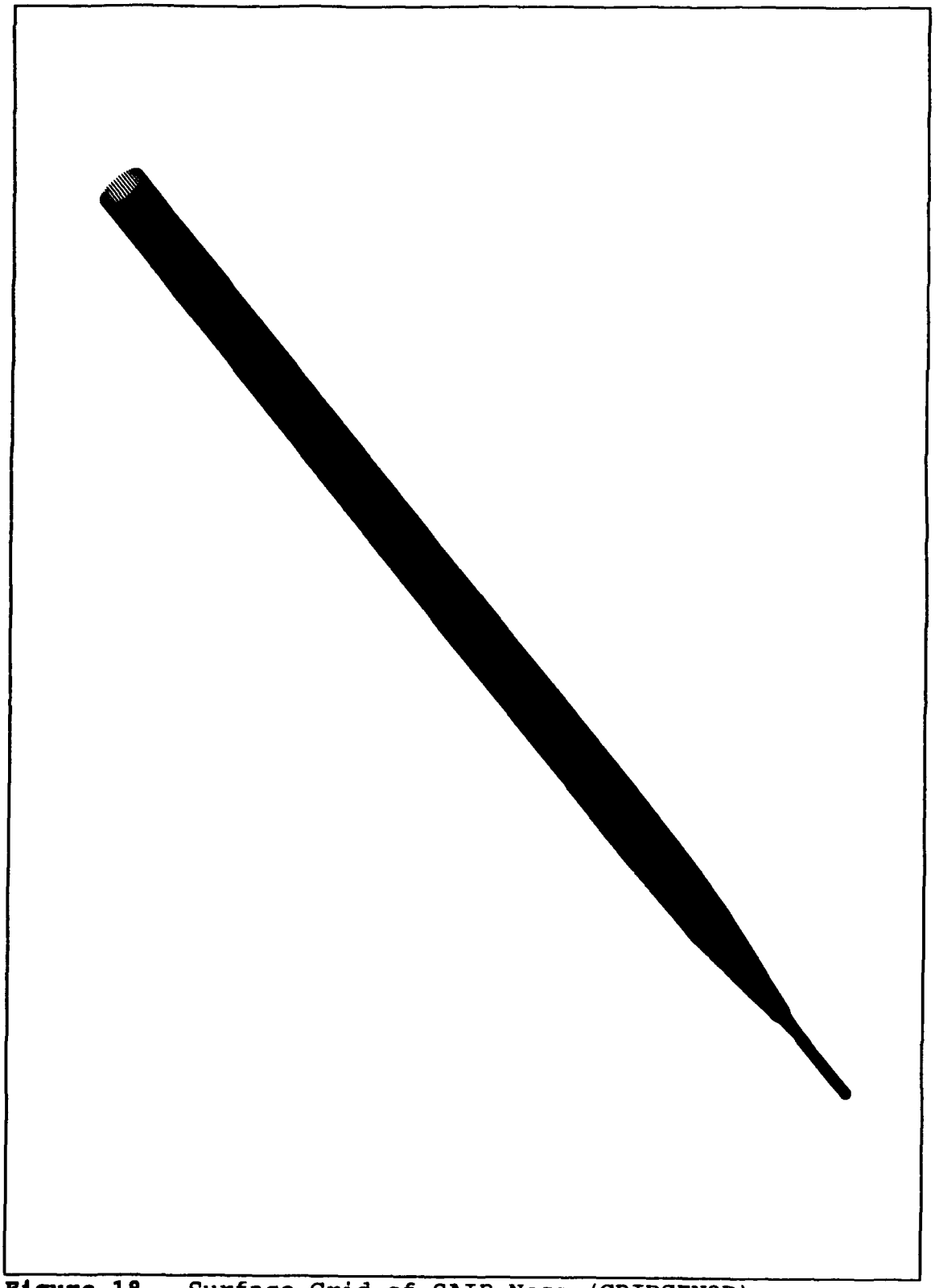

Figure 18. Surface Grid of SAIP Nose (GRIDGEN2D).

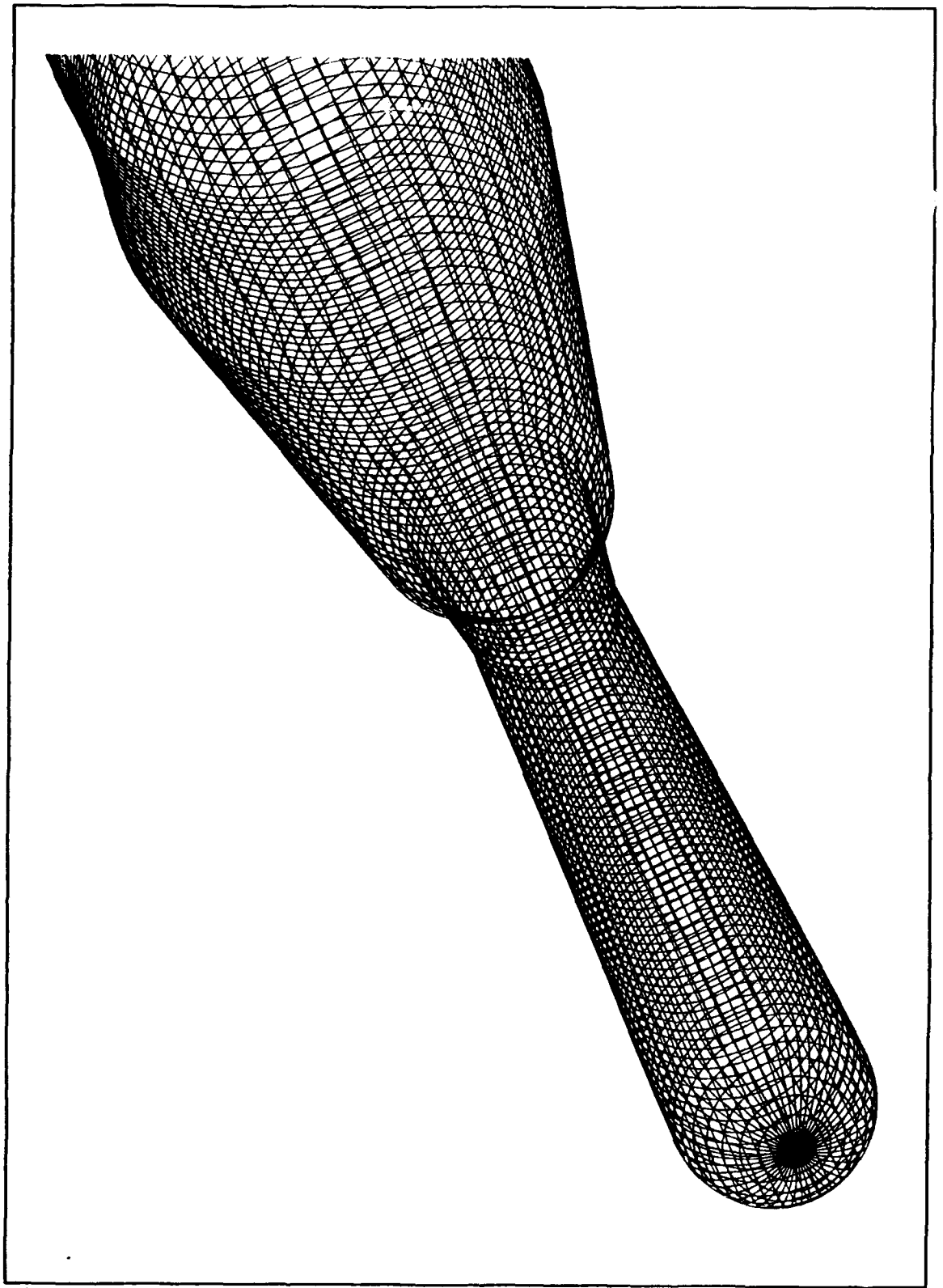

Figure 19. Axisymmetric SAIP (GRIDGEN2D).

hyperbolic partial differential equations to construct the volume grid shown in Figures 20 and 21. Figure 21 shows the initial grid spacing off the surface, away from the body. The purpose of this large initial spacing was to generate an inviscid solution (where boundary layer effects have been ignored). Both grids were generated on the NPS IRIS computer.

The volume grid was then submitted to the OVERFLOW program for each test case. OVERFLOW is a Navier-Stokes code developed by Pieter Buning at NASA Ames [Ref. 11] to calculate the flow-field around complex geometries. It solves the Reynolds-Averaged Navier-Stokes equations in Strong Conservative form. The first test case was computed at Mach 0.13, and zero degrees angle-of-attack (AOA). The second case was run a Mach 0.6, zero degrees AOA. Turbulence models and viscous terms were omitted in each case, which basically reduced the Navier-Stokes equations to Euler equations. Residuals were decreased at least two orders-of-magnitude to ensure pressure distribution convergence.

C. RESULTS

Data output from OVERFLOW were viewed using the PLOT3D graphics program developed by Buning [Ref. 12]. This highly capable graphics software creates a visual presentation of the flow-field characteristics. Figures 18 through 21 were generated with PLOT3D. The C_p distribution at Mach 0.13 and 0.6 generated with the Euler equations as compared to the

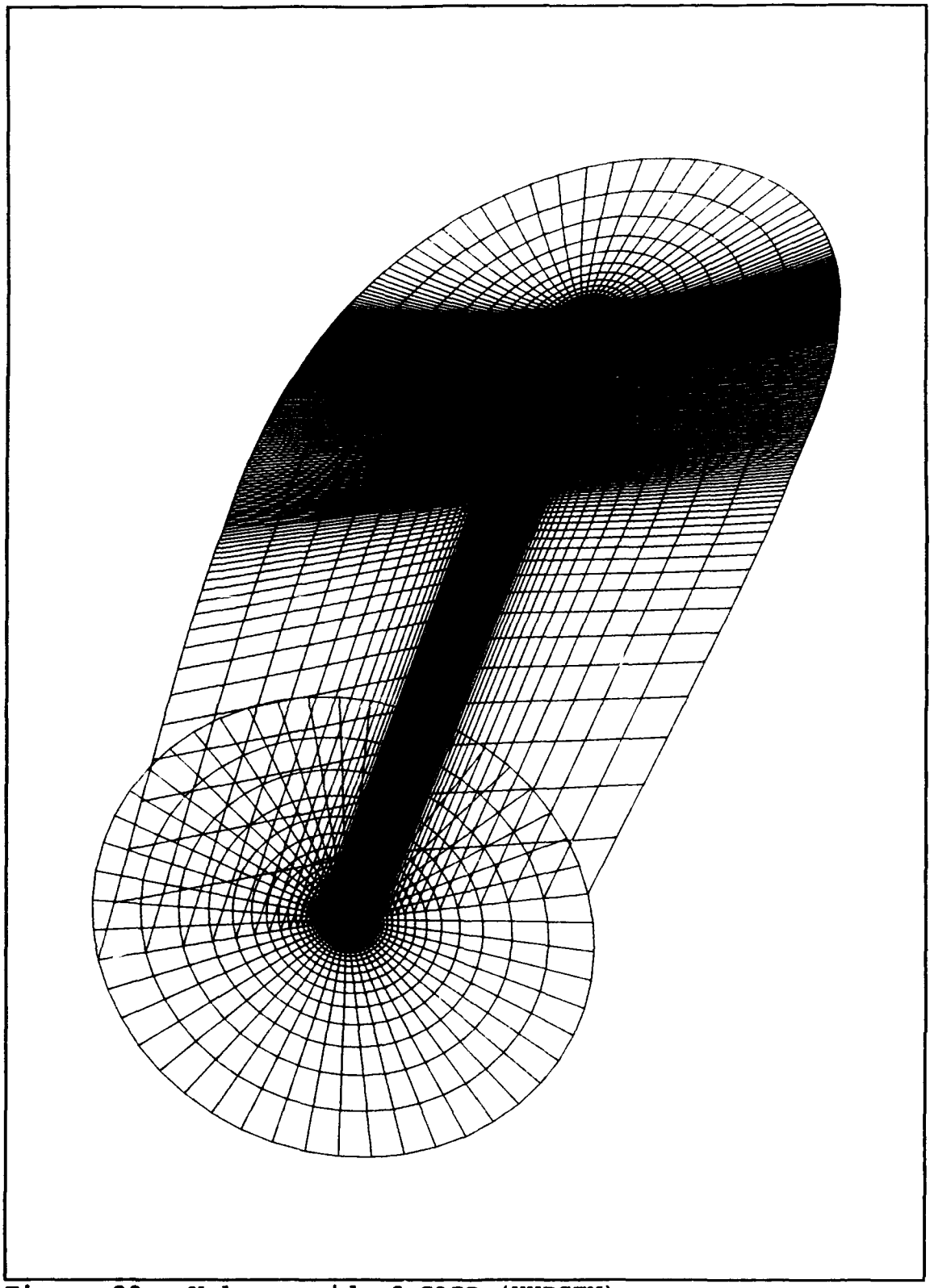

Figure 20. Volume grid of SAIP (HYPGEN).

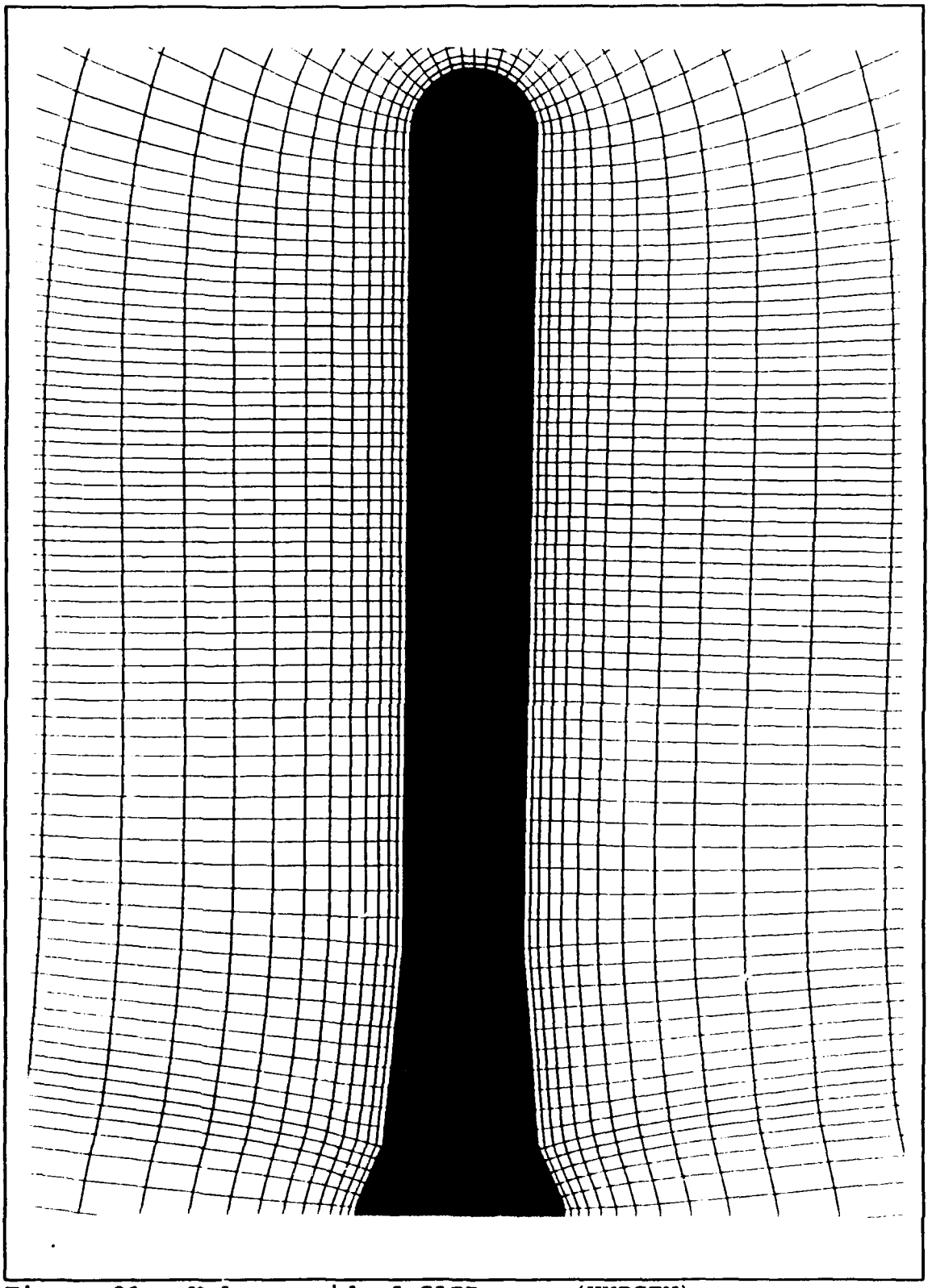

Figure 21. Volume grid of SAIP nose (HYPGEN).

PMARC solution is shown in Figures 22 through 25. These very similar and overlapping curves validate the earlier inviscid solutions. The Euler methods show higher spikes at the local maxima, but that may be due in part to the higher resolution of the CFD surface grid as compared to the panel surface grid. In any case, the C_p predicted near the static ports is very close to the PMARC values (Figs. 23 and 25).

Compressibility effects with the OVERFLOW solutions are shown in Figure 26. In comparison with Figure 7, the Prandtl-Glauert correction for the PMARC code is somewhat validated.

D. CFD SUMMARY

The first conclusion made from these results is method preference. If one wants to find inviscid solutions, panel methods is by far the easiest, fastest, and least expensive method for generating lift and pressure data. The PMARC solution takes about 20 minutes of CPU time on the VAX 3100 as opposed to about 1.5 hours of CRAY2 CPU time for CFD. However, using the Euler equations served their purpose in validating the panel method code solution and modeling techniques. These are also the initial computations which need to be done enroute to computing fully viscous flow.

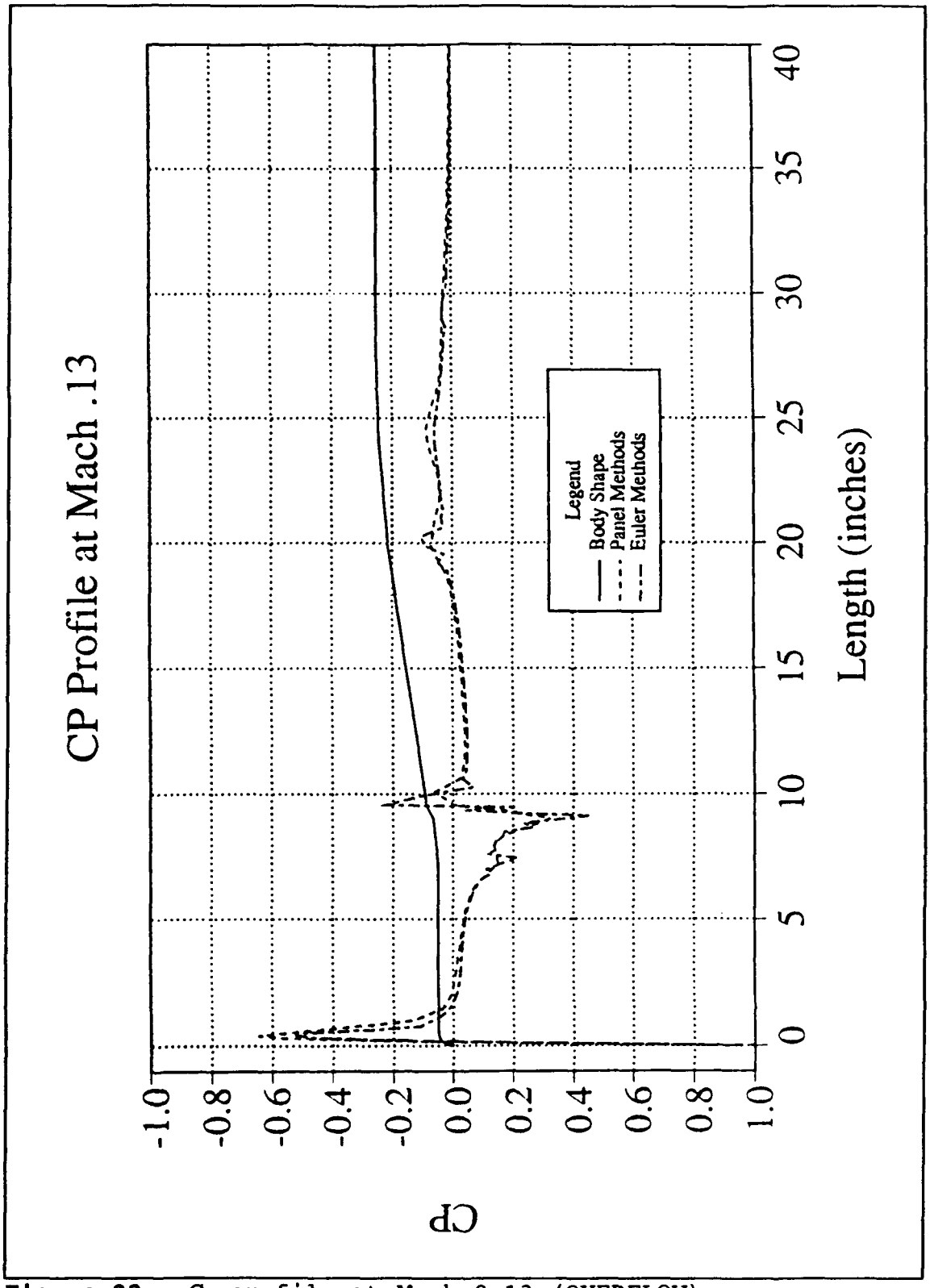

Figure 22. C_p profile at Mach 0.13 (OVERFLOW).

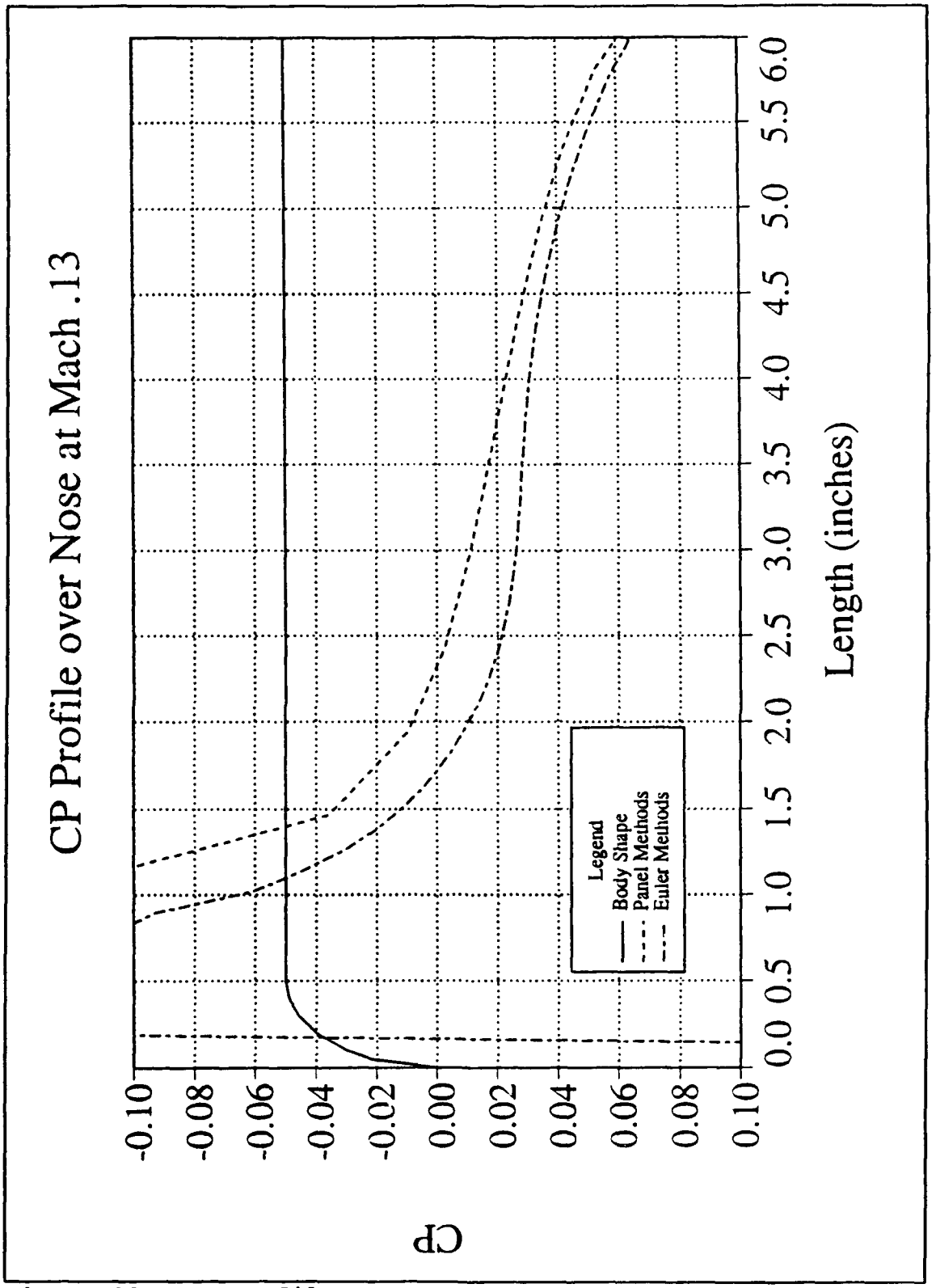

Figure 23. C_p profile over nose at Mach 0.13 (OVERFLOW).

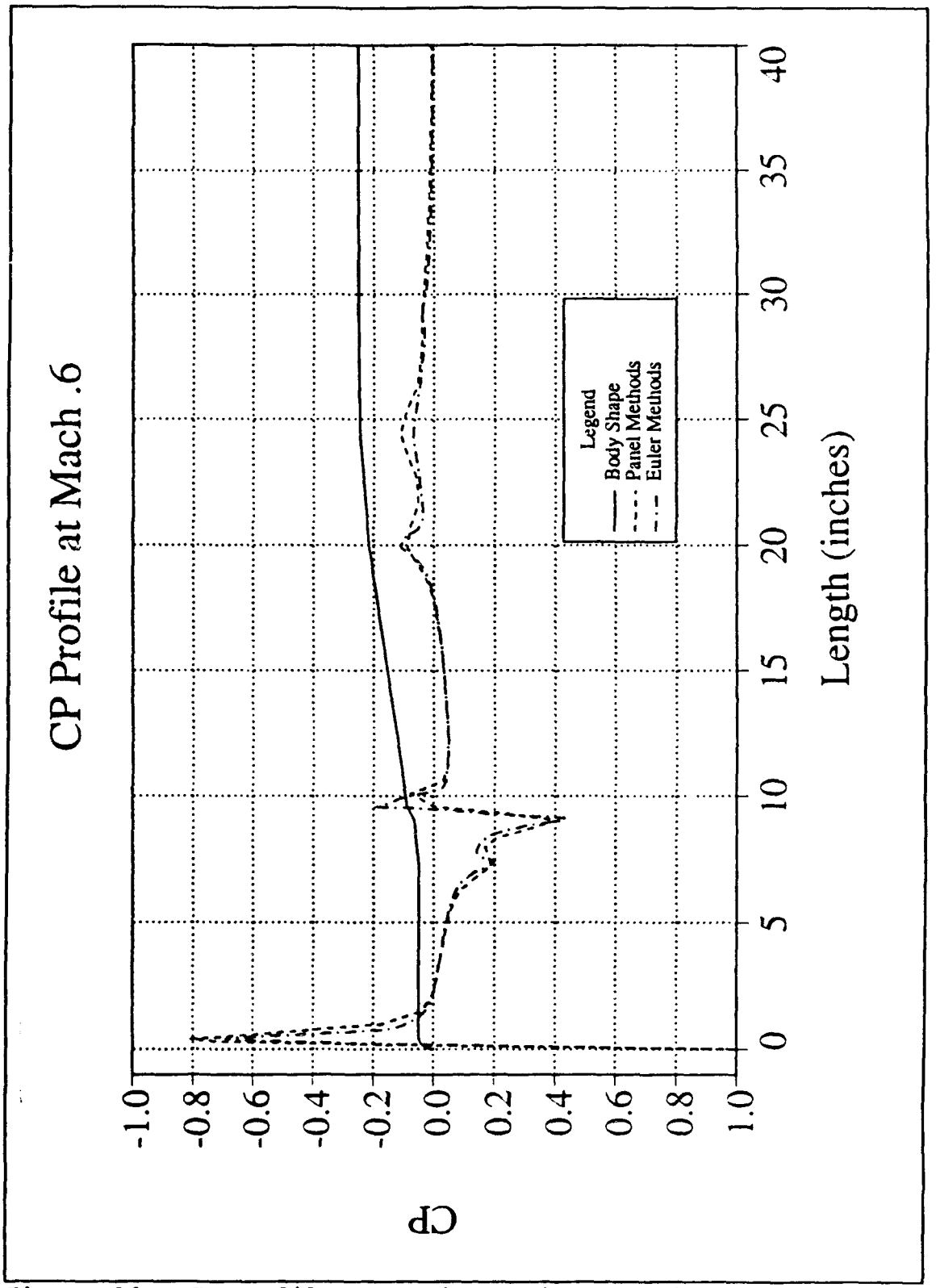

Figure 24. C_p profile at Mach 0.6 (OVERFLOW).

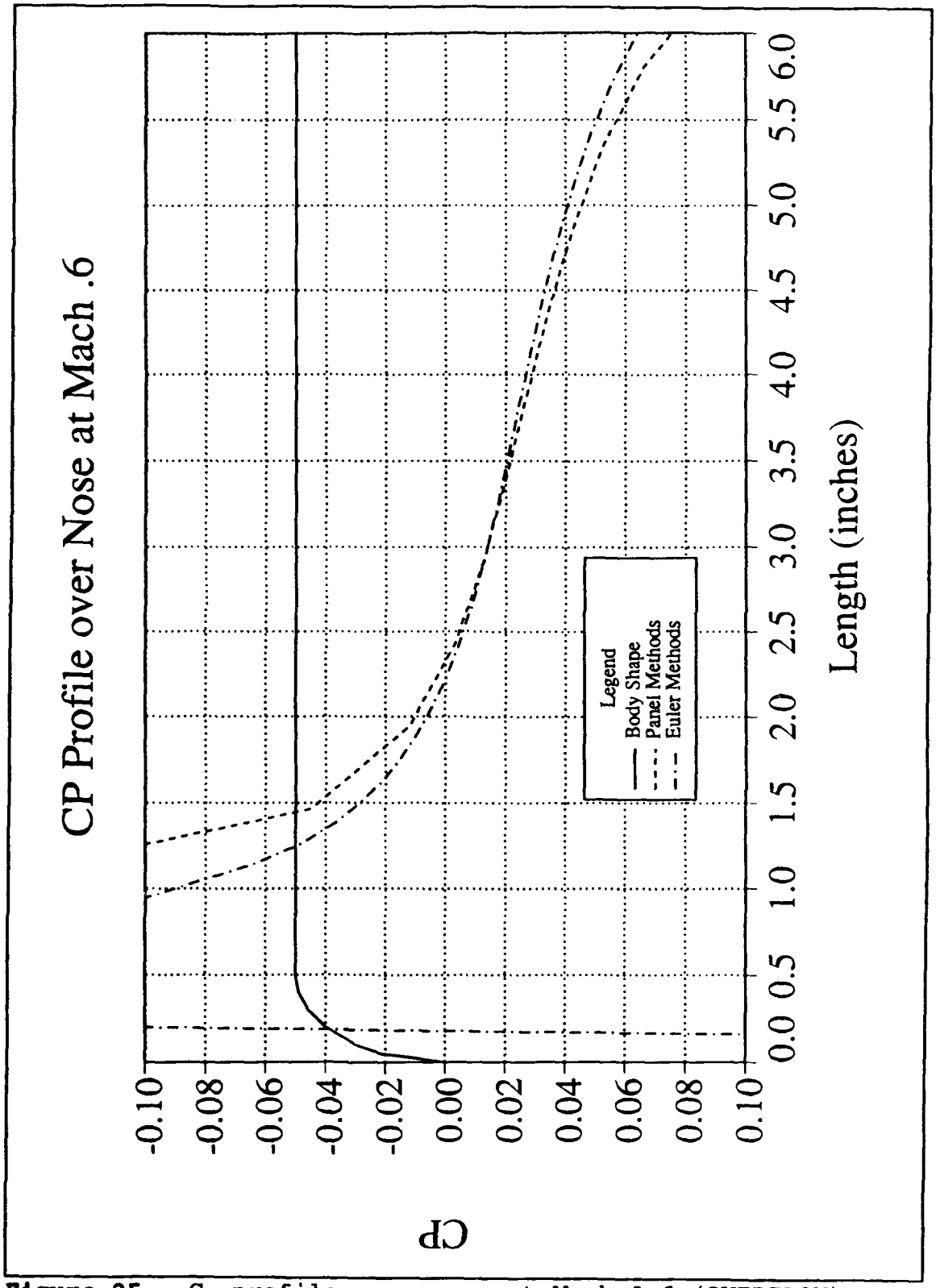

Figure 25. C_p profile over nose at Mach 0.6 (OVERFLOW).

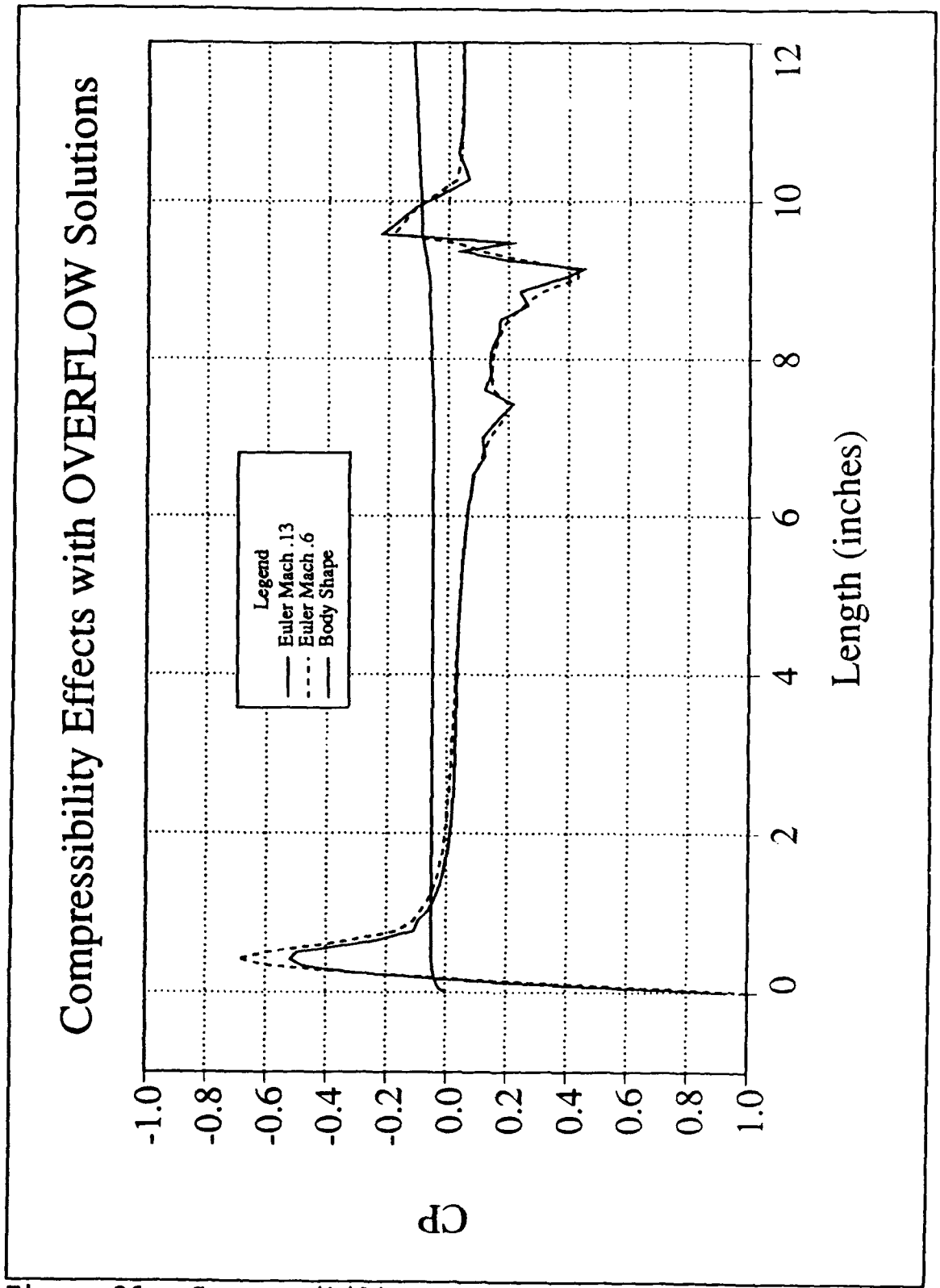

Figure 26. Compressibility effects with OVERFLOW solutions.

IV. Wind Tunnel Procedures and Data

A. Pressure Measurements

1. Wind Tunnel Apparatus

The SAIP Nose Cone Assembly (NCA) which served as the test article for the various engineering analysis performed to identify the source of SAIP altitude error was provided by the NAWCWPNS Range Development Department (Code 3143). Evaluation of NCA S/N 0040, P/N 2111940-001 was performed in the Naval Postgraduate School low-speed, horizontal-flow, wind tunnel illustrated in Figure 27. This single return tunnel is powered by a 100-horsepower electric motor coupled to a three-blade variable-pitch fan via a four-speed transmission. The tunnel is 64 feet long and ranges from 21.5 to 25.5 feet wide. To straighten the flow through the tunnel, a set of stator blades have been located aft of the fan blades. Additionally, turning vanes have been installed at all four corners of the tunnel, and two fine wire mesh screens have been positioned downstream of the settling chamber to reduce turbulence. [Ref. 13]

The dimensions of the wind tunnel's test section are 45 inches by 32 inches. A reflection plane installed above the base of the test section reduces the available height in this section to 28 inches. The tunnel contraction ratio, as

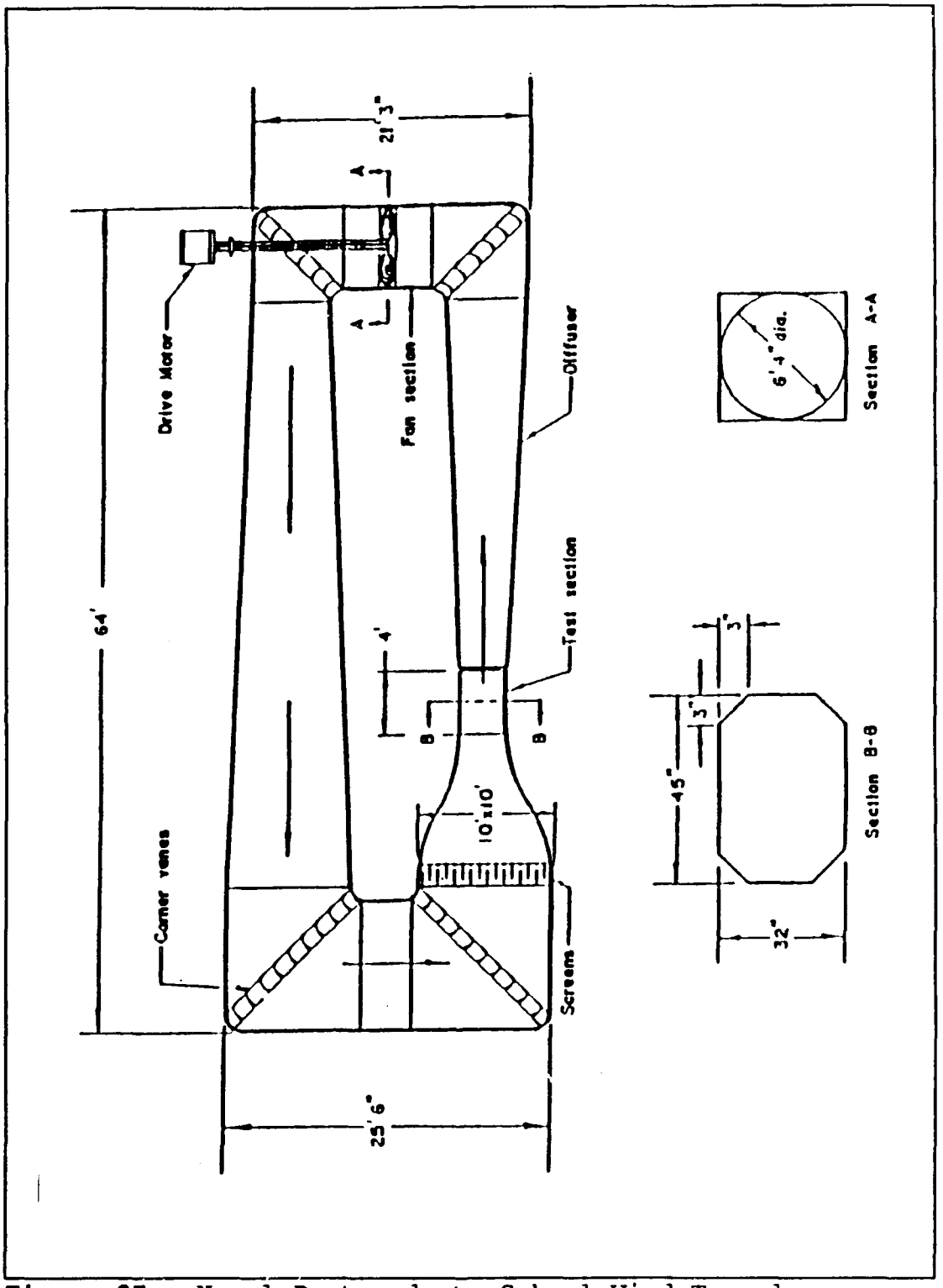

Figure 27. Naval Postgraduate School Wind Tunnel.

measured by the area of the settling chamber area divided by the test section area, is approximately 10:1. Corner fillets, which are located within the test section to provide covers over florescent lights, reduce the actual section cross-sectional area from 10 ft^2 to 8.75 ft^2. Similar fillets are installed at wall intersections throughout the tunnel to assist in the reduction of boundary layer effects. Prevention of the reduction in free stream pressure due to boundary layer growth within the test section is facilitated by a slight divergence of the walls in this area of the tunnel. [Ref. 13]

A turntable mounted flush with the reflection plane permits operator-controlled changes in the test article pitch angle or angle-of-attack (AOA) via a remotely controlled electric motor installed beneath the tunnel. The test section has been designed to operate at nearly atmospheric pressure, and to sustain this constant pressure, breather slots are installed around the circumference of the tunnel. The tunnel was designed to generate and maintain flow velocities of up to 290 ft/sec (Mach 0.26) [Ref. 13].

A dial thermometer extending into the settling chamber is used to measure internal tunnel temperature. Four pressure taps located upstream of the test section in the four adjoining walls are used to measure test-section reference static pressure. Additional pressure taps are located in the settling chamber section. The difference between the test section and the settling chamber pressures is used to

determine dynamic pressure. This is accomplished by manifolding the separate tap pressures at the two tunnel locations into two separate lines and then connecting these outputs to a water filled manometer. The reference change in pressure measured by this manometer is displayed in centimeters of water. Wind tunnel velocities are based on the measured value of ΔP [Ref. 13].

2. SAIP Wind Tunnel Tests

a. Nose Cone Assembly (NCA) Mounting Assembly

To facilitate secure mounting of the NCA in the wind tunnel's test section and to permit orientation of the probe in a variety of flow directions, the rigid mounting assembly shown in Figure 28 was used. The mechanism was secured to the rotatable disk situated at the base of the tunnel's test section, and was extended vertically into the flow field such that the probe was held in position in the center of the flow. Rotation of the NCA about the vertical axis was controlled by an electric motor which permitted operator-controlled positioning of the angle of attack. Constraints imposed by the width of the wind tunnel test section restricted the rotation of the NCA about the vertical axis to $\pm$ 37.5 degrees.

b. Instrumentation

The Air Data Unit (ADU) shown in Figure 29 was introduced in Chapter I consists of four capacitive pressure

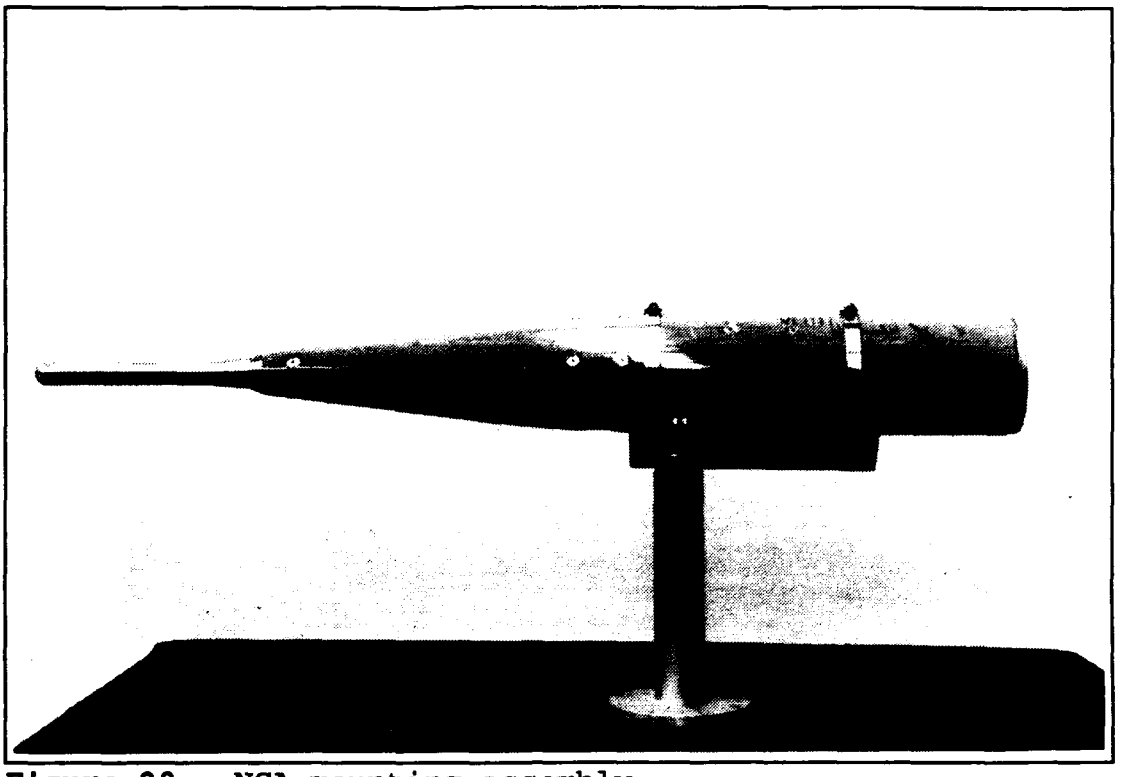

Figure 28. NCA mounting assembly.

transducers which are housed in a single assembly, as well as the associated electronic circuitry used for conditioning of the output signals from the transducers prior to their digitizing and formatting by the DPU/DIU [Ref. 3:p. 17]. Static pressure is measured by an absolute-type transducer which measures this pressure relative to a vacuum. A single static pressure line extends from the ASA into the static pressure coupler on the input side of the ADU. The remaining three transducers residing in the ADU, used to determine total angle-of-attack and angle-of-sideslip pressures, are differential capacitive transducers. These transducers convert pressures to voltages for subsequent output.

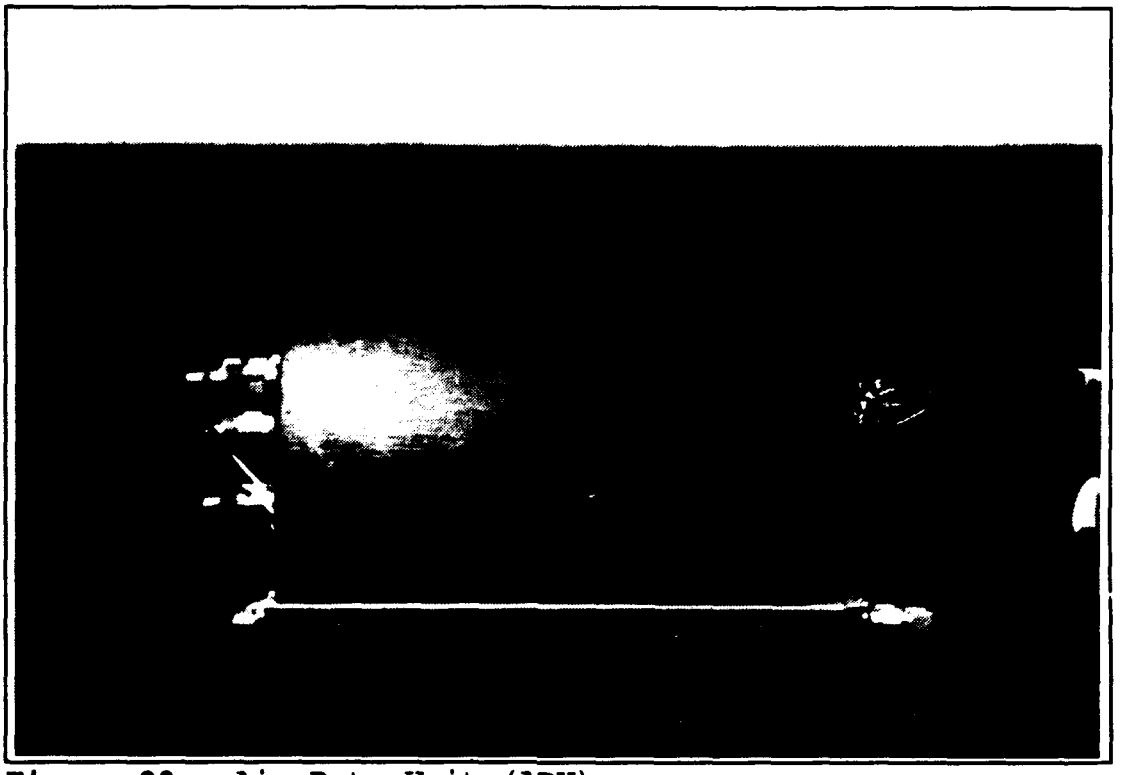

Figure 29. Air Data Unit (ADU).

The NCA was integrated with its instrumentation equipment by coupling the connector plug extending from the output side of the ADU on the test article with an external Fluke Model 8810A Digital Voltmeter (DVM) via a ± 15 volt power supply (Fig. 30). The module containing the power supply was designed to permit manual scanning of the four voltages output from the ADU corresponding to either static pressure, total pressure, angle-of-attack pressure or angle-of-sideslip pressure. The power supply housing also accommodated sampling of the voltage corresponding to the differential pressure existing between the tunnel section and ambient air outside of the tunnel.

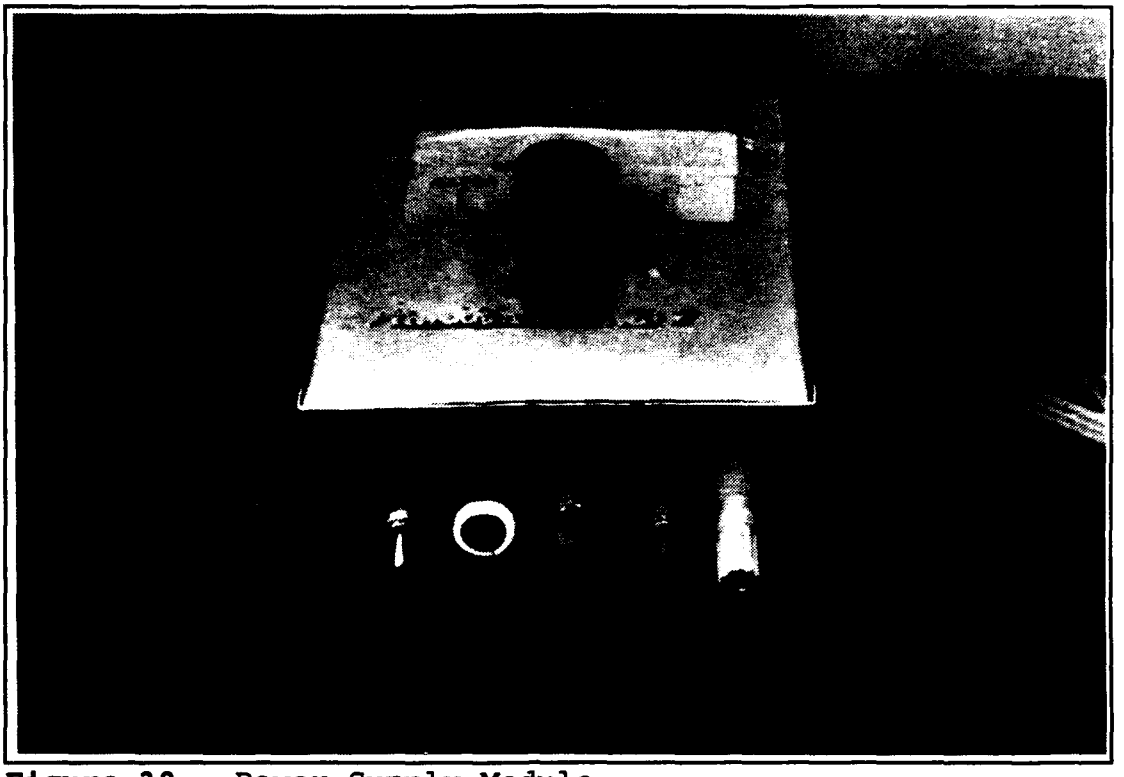

Figure 30. Power Supply Module.

c. SAIP Calibration

A plot of voltage versus pressure was needed to provide a conversion factor for converting Volts measured by the SAIP (ADU output) to ΔP. A U-tubed calibration manometer (Figure 31) with an attached adjustable diaphragm unit was used to apply known positive and negative pressures while subsequently measuring the resultant voltage output of the ADU on the digital voltmeter. The results of this calibration verified the 0.4 volts/psia conversion of Reference 2.

d. Test Section Pressure Corrections

The design of the wind tunnel is such that the test section is maintained at a nominal pressure of one

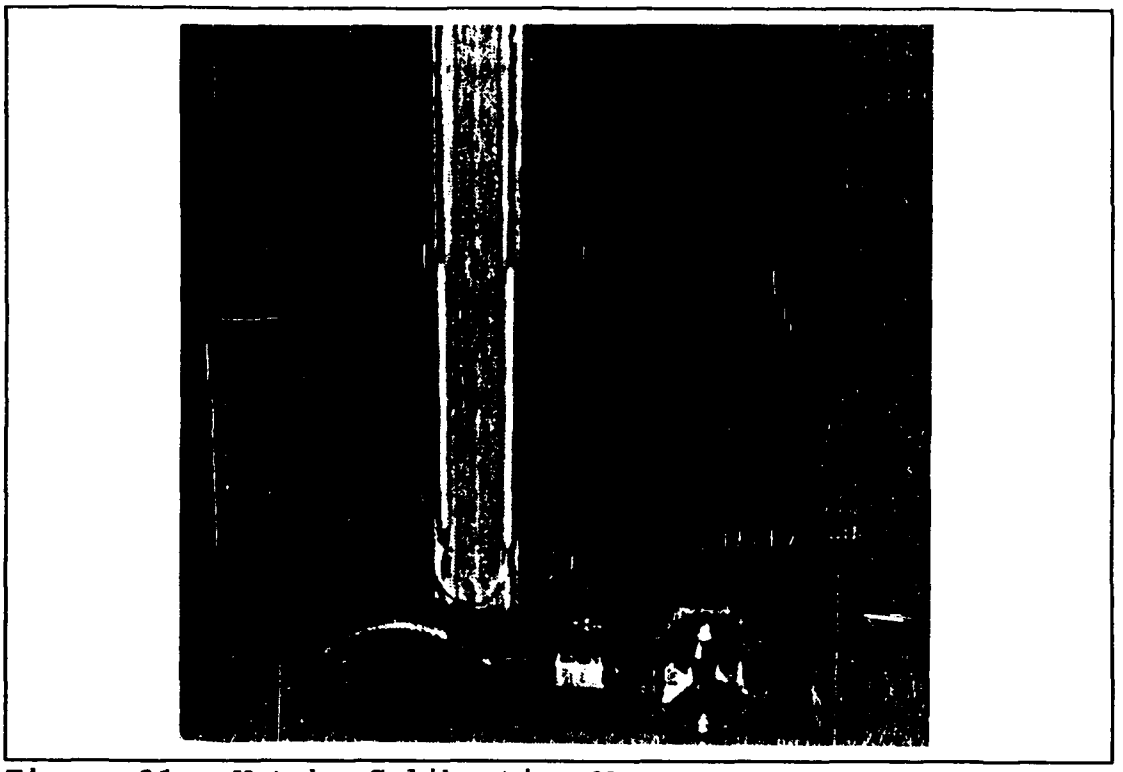

Figure 31. U-tube Calibration Manometer.

atmosphere, this pressure actually varies during wind tunnel testing. Russell measured this change in tunnel static pressure with an inclined manometer and calculated it to be 0.010 psia below atmospheric at V_∞ = 157.8 ft/sec [Ref. 11:p. 28]. He then applied this correction to all static pressures measured during wind tunnel tests. However, his measurements were made with an empty wind tunnel test section. To obtain an exact reading of the test section static pressure, a calibrated static probe was installed in the tunnel directly above the static port region of the NCA in the center of the test section. This stationary static probe facilitated recording of the differential static pressure existing between

the tunnel and surrounding ambient conditions, and provided a standard against which the static pressure reported by the SAIP could be compared. The tunnel static pressure sampled by the stationary static probe was fed into a MKS Baratron Type 223B differential pressure transducer (Fig. 32). The output end of the transducer was ported to the atmosphere. The MKS Baratron transducer was calibrated with the U-Tube Calibration Manometer resulting in a conversion factor of 52.73 volts/psia (Fig. 33).

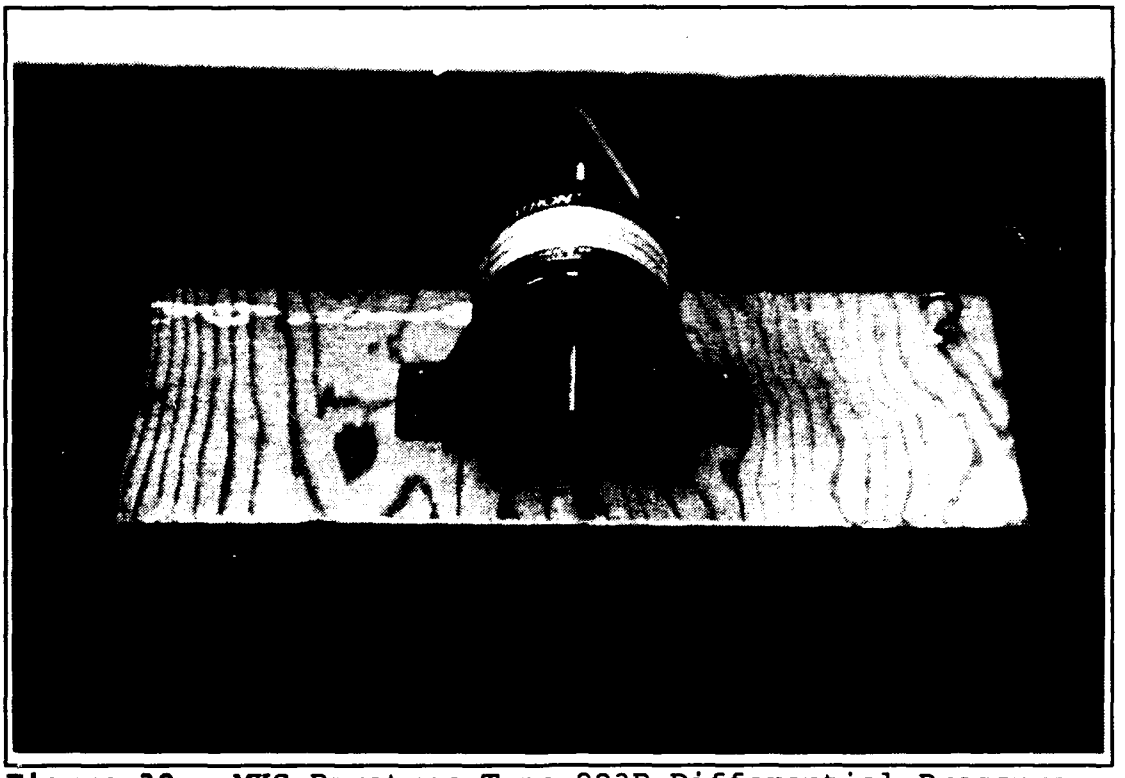

Figure 32. MKS Baratron Type 223B Differential Pressure Transducer.

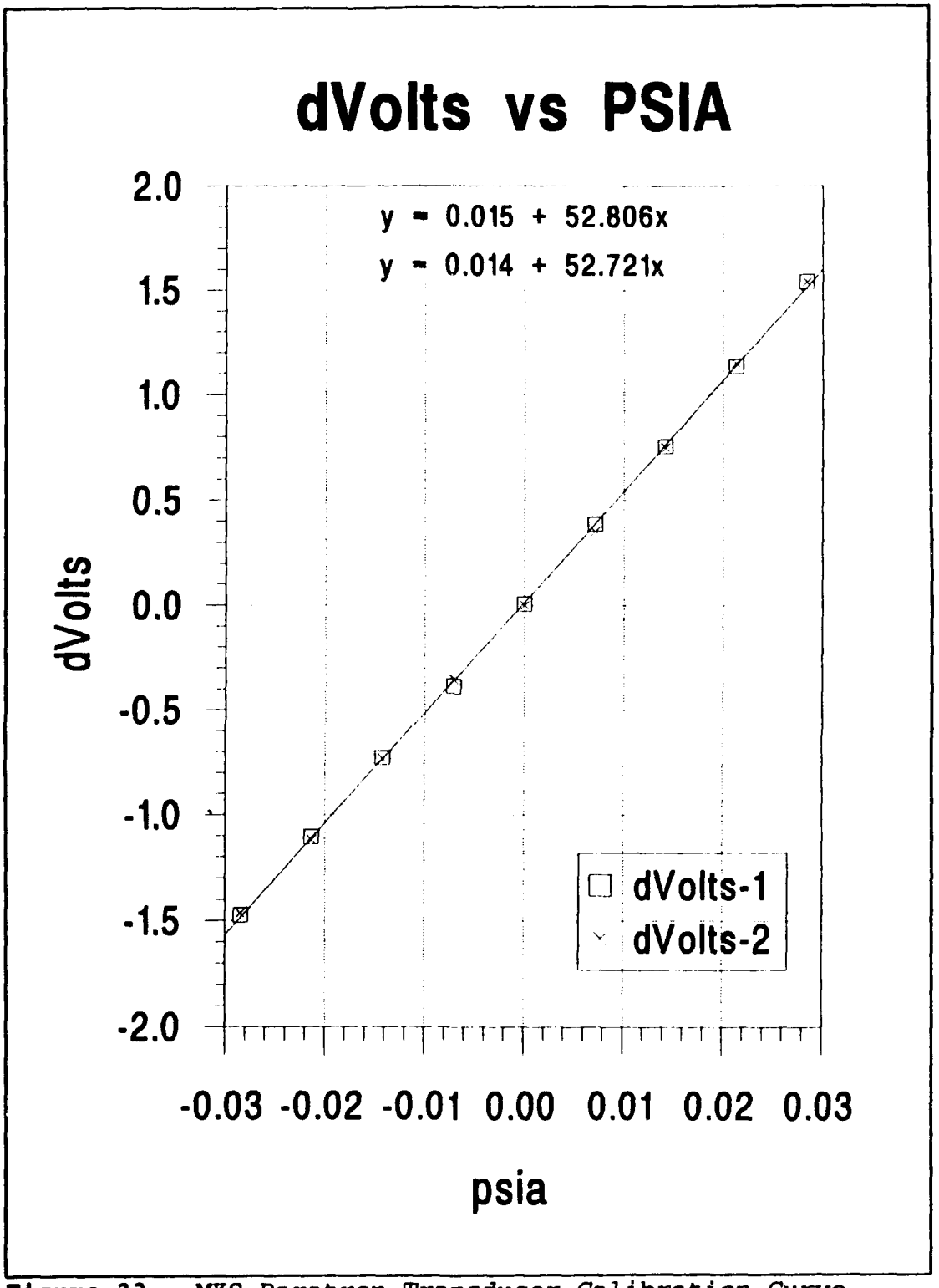

Figure 33. MKS Baratron Transducer Calibration Curve using a U-tube Calibration Manometer.

Three tests were conducted in order to quantify the pressure differentials associated with wind tunnel tests. The first was conducted with the tunnel empty, the second with the NCA mounting at various angle-of-attacks (AOA), and the third with the ASA mounting (Fig. 34) at various angle-of-attacks. Figure 35 is the result of these tests. The pressure differential associated with an empty wind tunnel was found to be 0.0063 psia below atmospheric as opposed to .01 psia below used in Reference 2. The ASA has a relatively small cross section compared to the test section, so it is reasonable that the results in Figure 35 show a slight flow

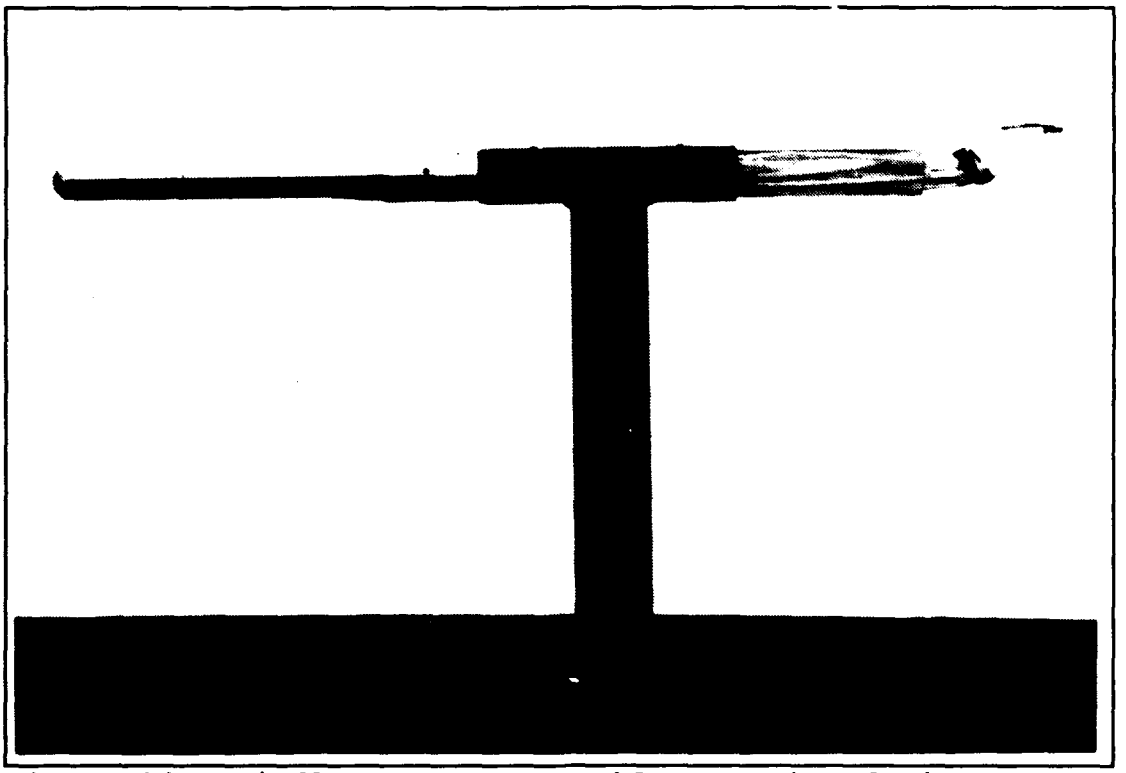

Figure 34. Airflow Sensor Assembly mounting device.

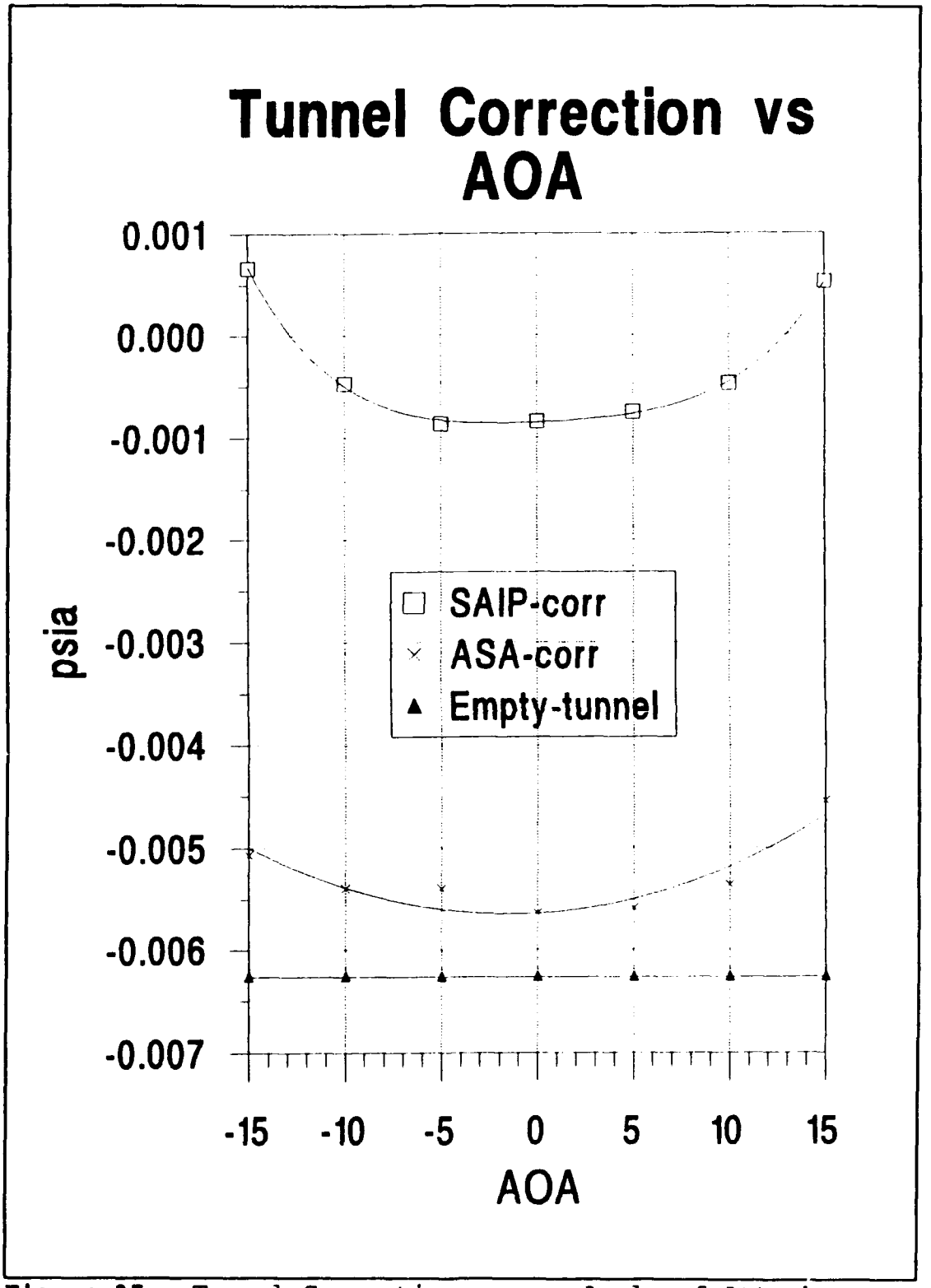

Figure 35. Tunnel Correction versus Angle-of-Attack.

blockage which increases with angle of attack. The most striking result of this test was the pressure differential associated with the NCA mounting. The flow blockage associated with the NCA is quite significant. In fact, only a minor correction for the NCA is necessary, for the atmospheric pressure in the test section is approached with the NCA body slightly choking the flow. If these more accurate corrections were added (as a function of AOA) to the static measurements in Reference 2, instead of the -0.01 psia correction, the C_p profile measured would be significantly lower. This new revelation necessitated repeating the wind tunnel tests in Reference 2.

e. Wind Tunnel Procedures

The NCA was placed in the wind tunnel and voltage measurements were taken at 13 cm-H_2O (157.8 ft/sec). The NCA was rotated through ± 15 degrees angle-of-attack. Voltages read directly from the voltmeter were compared to the voltage measured when tunnel velocity was not on and the ΔVolts converted to ΔP. A correction from Figure 35 was applied to the measured ΔP to correct the tunnel test section pressure to ambient pressure.

f. Wind Tunnel Results

The relationship between ΔP and C_p is based on the following equation

$$\frac{P_s - P_\infty}{P_\infty} = \frac{\gamma}{2} M_\infty^2 C_p \qquad (17)$$

Knowing M_∞ together with $P_s - P_\infty$ (ΔP) we can extract values of C_p from wind tunnel data [Ref. 2:p. 32]. Figure 36 is a plot of pressure coefficient versus AOA. At zero degrees angle-of-attack, the pressure coefficient is 0.056. This is much less than the value deduced in Reference 2 and much closer to the numerical solution of 0.02 to 0.025 (panel method and Euler equations respectively). The difference between inviscid computational methods and wind tunnel data remains significant. A C_p of 0.056 corresponds to an altitude error of 363 feet (Mach 0.6, 10,000 ft) which still places the SAIP's altitude measurements out of limits. Also, the magnitude of the C_p measured in the wind tunnel at low Mach numbers predicts errors much smaller than those found during flight test. Perhaps the inviscid assumption is not valid in this case and the C_p is Reynolds number dependent, and/or the pressure field of the aircraft wing/body/pylon cannot be ignored. These questions will be dealt with in Chapter V.

3. ASA Wind Tunnel Tests

For Airflow Sensor Assembly (ASA) acceptance tests, Rosemount mounted a calibrated aerodynamic standard of the applicable pitot static tube model in the Rosemount three-inch Free Jet Wind Tunnel with the axis of the tube aligned with the center of the free jet (Fig. 37). The nose tip was

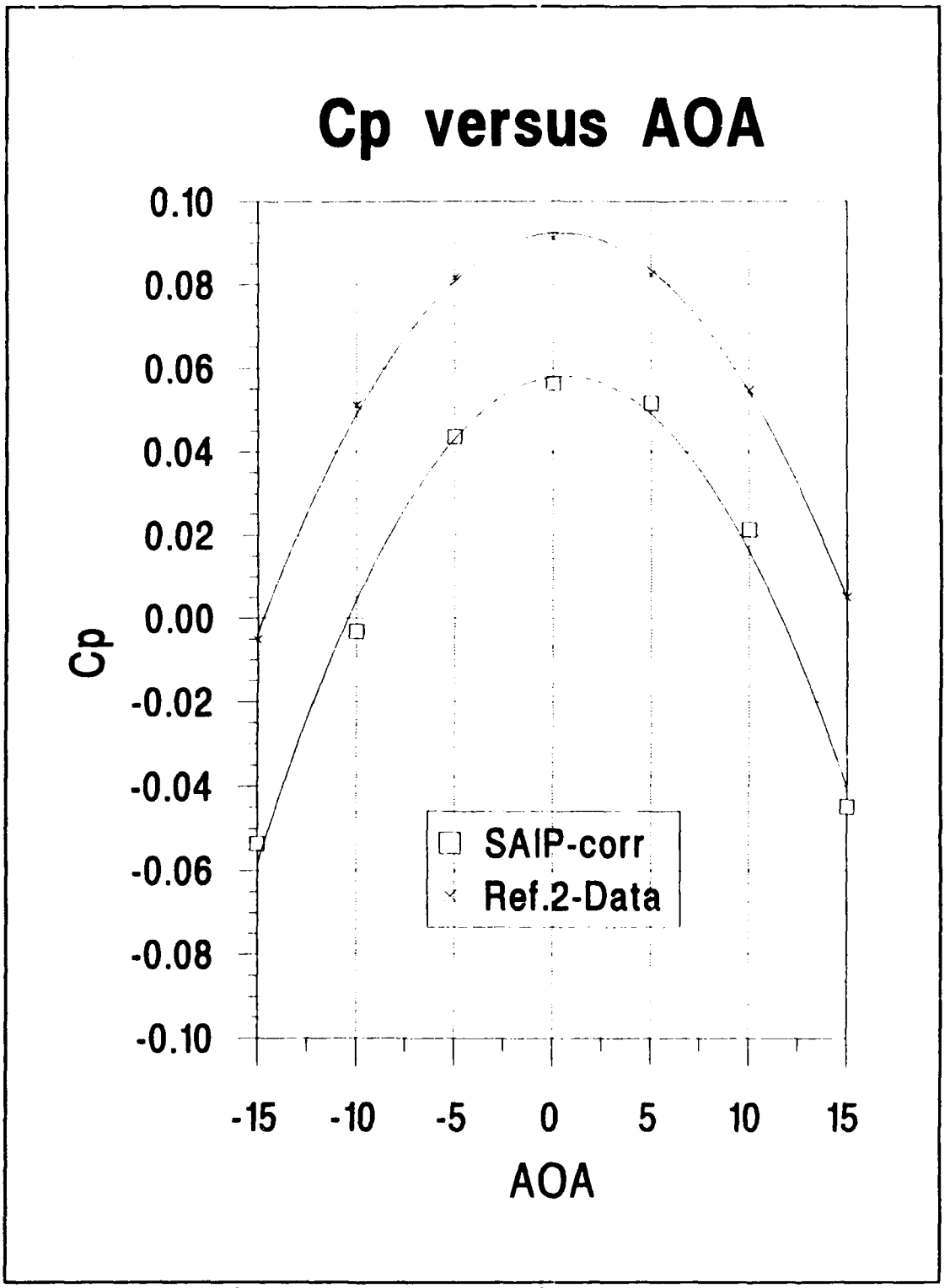

Figure 36. Saip Pressure Coefficient versus Angle-of-Attack.

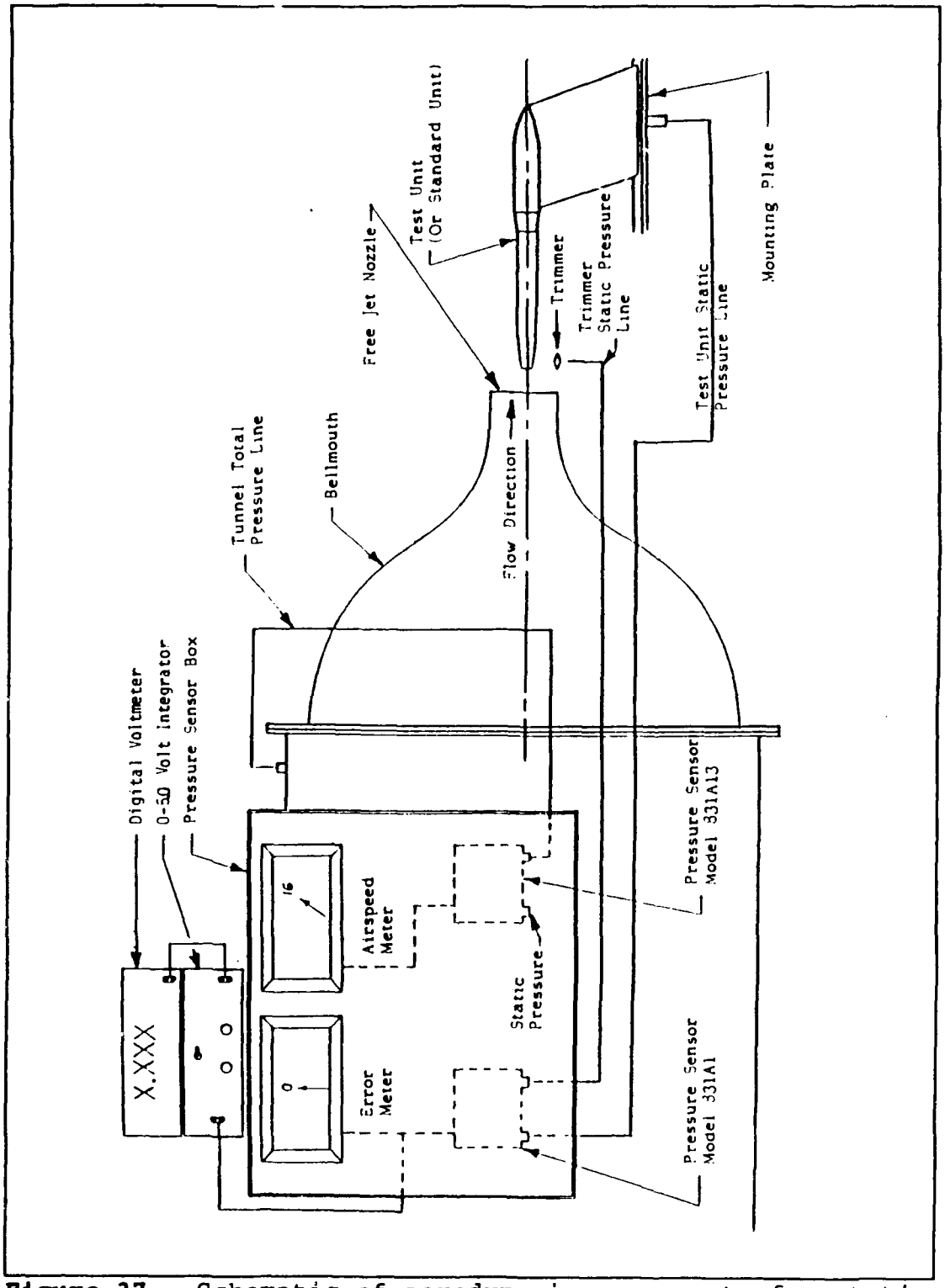

Figure 37. Schematic of aerodynamic components for static pressure reproducibility.

located three inches from the free jet nozzle. The Free jet was operated at 85 knots (approximately Mach 0.13). Differential pressure measurements between the static ports of the standard unit and the reference static tap in the trimmer located at the edge of the free jet were obtained. There is no indication of any static pressure measurements at different angle-of-attacks. Therefore, it can be conclude that the ASA was built specifically for very low speeds and small angle of attacks. Why General Dynamics decided to incorporate this nose design into the five inch diameter SAIP is still unknown to this author.

a. ASA Mounting Assembly

The second SAIP delivered to NPS was dismantled for ASA testing in order to verify Rosemount's acceptance results. A test stand was manufactured to hold the ASA as shown in Figure 34. Attention was paid to minimizing the test stand size to limit flow blockage. The ASA was rotated through ±15 degrees angle-of-attack in the same manner and speeds as the NCA.

b. Instrumentation

The static pressure line of the ASA was lengthened with tygon tubing and extended outside the wind tunnel where it was connected to the ADU. The output from the ADU was measured in the same manner as the NCA.

c. Wind Tunnel Results

The wind tunnel pressure correction factors found earlier for the ASA were added to the pressure differentials measured. Figure 38 is a plot of pressure coefficient versus AOA. At zero degrees AOA the C_p is measured at -0.0121. This value compares well with the PMARC solution. These wind tunnel results emphasize two points. First, the ASA by itself is a finely calibrated altitude measuring device. Second, the SAIP's five inch body has significant impact on the static pressure measurements.

4. Further Discussion of Flow Blockage

The precision of the pressures measured depend significantly on the pressure correction applied. Therefore, a thorough knowledge of wind tunnel flow characteristics is imperative. Efforts were made to carefully quantify those local pressure errors using a calibrated pitot static tube mounted above the NCA and ASA. It is known that the stream lines of the flow are at a slight angle with the centerline of the test section. This is due in part to the last turn in the wind tunnel prior to the test section. Zero degrees angle-of-attack is approximately three degrees to the right on the turn table. This off-center flow is evident in the C_p versus AOA curves. Also, the nominal free-stream turbulence level is 0.2%. This is not to say that data measured is invalid. On the contrary, the measured pressures provide significant

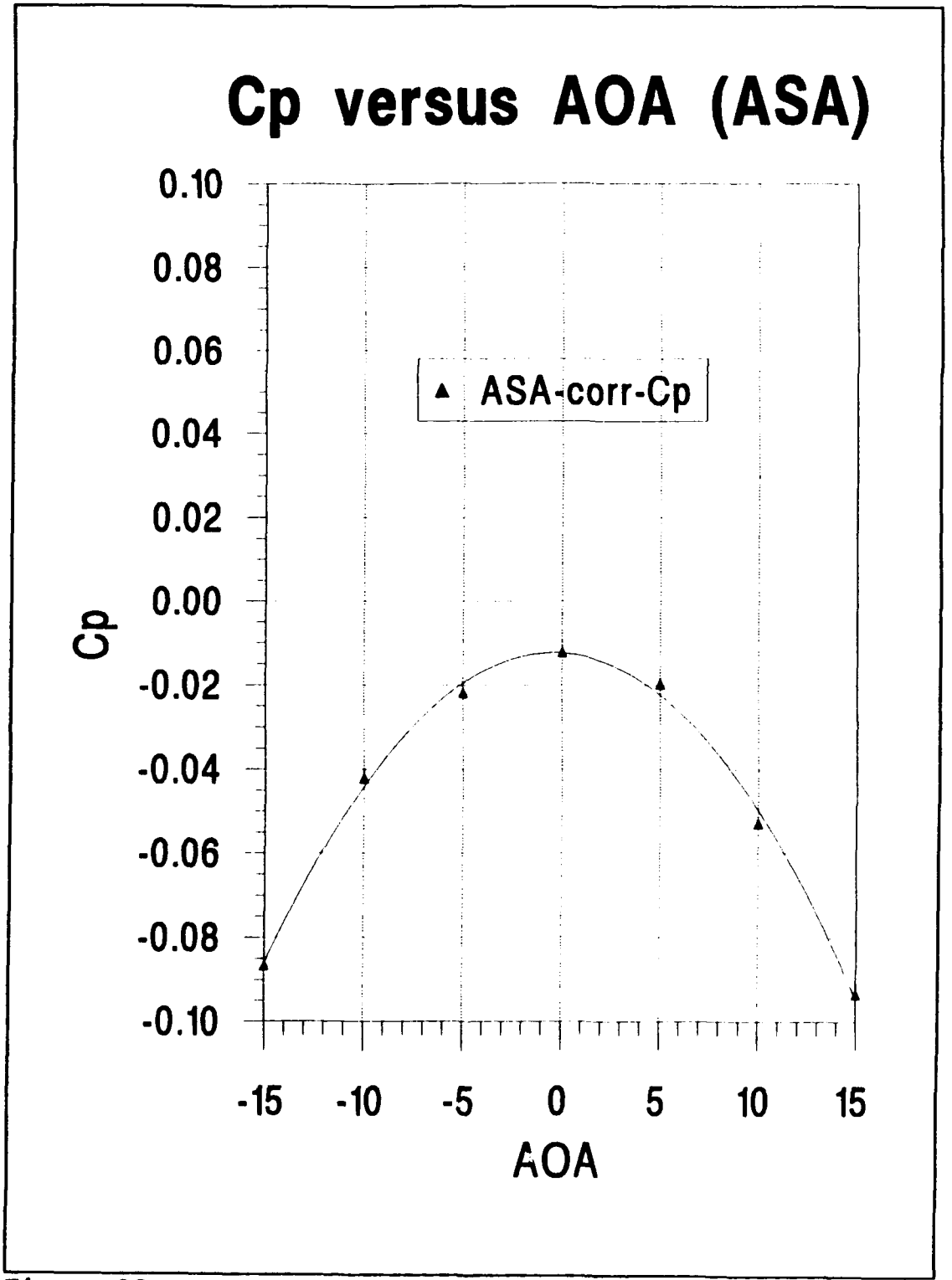

Figure 38. ASA Pressure Coefficient versus Angle-of-Attack.

trends and relatively accurate results. However, there will always be a small margin of error associated with the results.

B. FLOW VISUALIZATION

The discrepancy between the PMARC solution and wind tunnel data had to be quantified. This lead to the investigation of separated flow over the hemispherical nose and the effects it may have on the static pressure readings.

Anderson presents a section in Reference 7 that deals with flow over a sphere. Figure 39 illustrates laminar flow over a spherical surface. Here, the Reynolds number is 15,000, which is conducive for laminar flow, yet the flow separates from the surface. In fact it separates prior to the vertical equator of the sphere. Figure 40 shows another case of laminar flow over a sphere (Re = 30,000). However, in this case a trip wire induces turbulent flow prior to the original separation region, Because this flow is turbulent, separation takes place much further aft, resulting in a thinner wake.[Ref. 7:pp 387-388]

It was hypothesized that the flow over the SAIP was separating on the relatively blunt hemispherical nose and that the inviscid assumption may be invalid depending on the severity.

Russell performed flow separation studies just aft of the static pressure ports [Ref. 2]. However, The tufts used in his experiment were rather large and aft of the area of

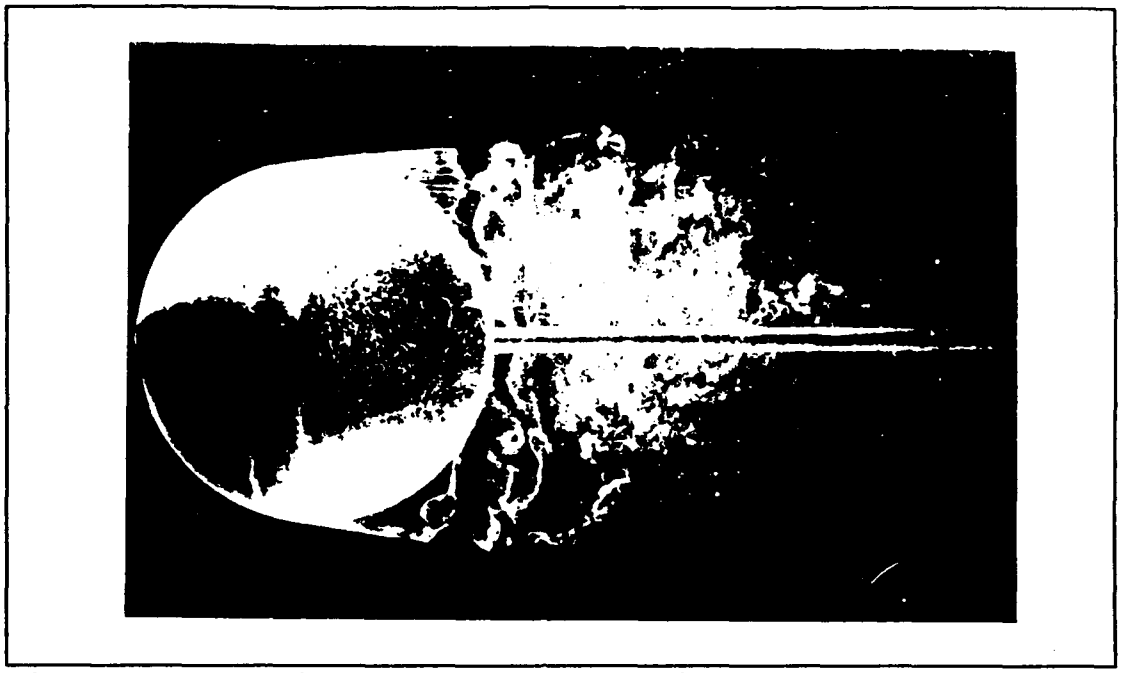

Figure 39. Laminar flow over spherical surface (RE = 15,000).

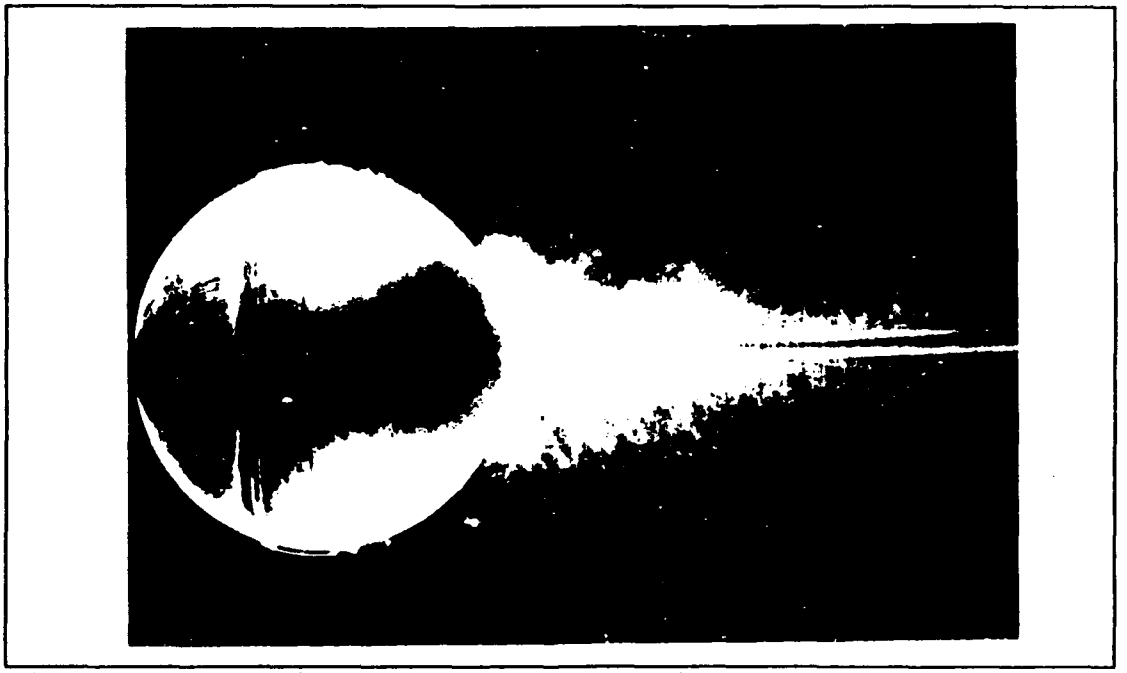

Figure 40. Laminar flow over spherical surface (RE = 30,000), where a trip wire induces turbulent flow.

interest. Therefore, more flow separation studies had to be performed using more precise techniques.

1. Separated Flow

Flow separation tests were performed with both the NCA and ASA. It was decided to use oil for flow visualization, due to its non-destructive effects. Initial concepts were to use a smoke generator and vent smoke through one of the angle-of-attack ports. However, the smoke would not be visible in the wind tunnel at significant velocities. Also, the smoke left a residue which would contaminate the ASA's tubing.

The oil utilized was made with nine parts 30 weight motor oil and one part toner (found in standard copiers) which was subsequently strained with a paint strainer. Thin, clear tape was placed over the pressure ports to avoid contamination. The oil was brushed on the nose of NCA from the equator of the hemispherical nose to the static pressure ports (Fig. 41). The NCA was centered at zero AOA and the tunnel was turned on and accelerated to 157 ft/sec (13.00" H_2O). A hand held video recorder captured the event as well as a 35 mm camera.

Figure 42 shows the instantaneous flow at 157 ft/sec (this photograph captures a definite separation bubble just aft of the hemispherical equator). It is approximately 3/8 inch thick, and distorts when rotated through various angle-of-attacks. The flow reattaches prior to the static ports.

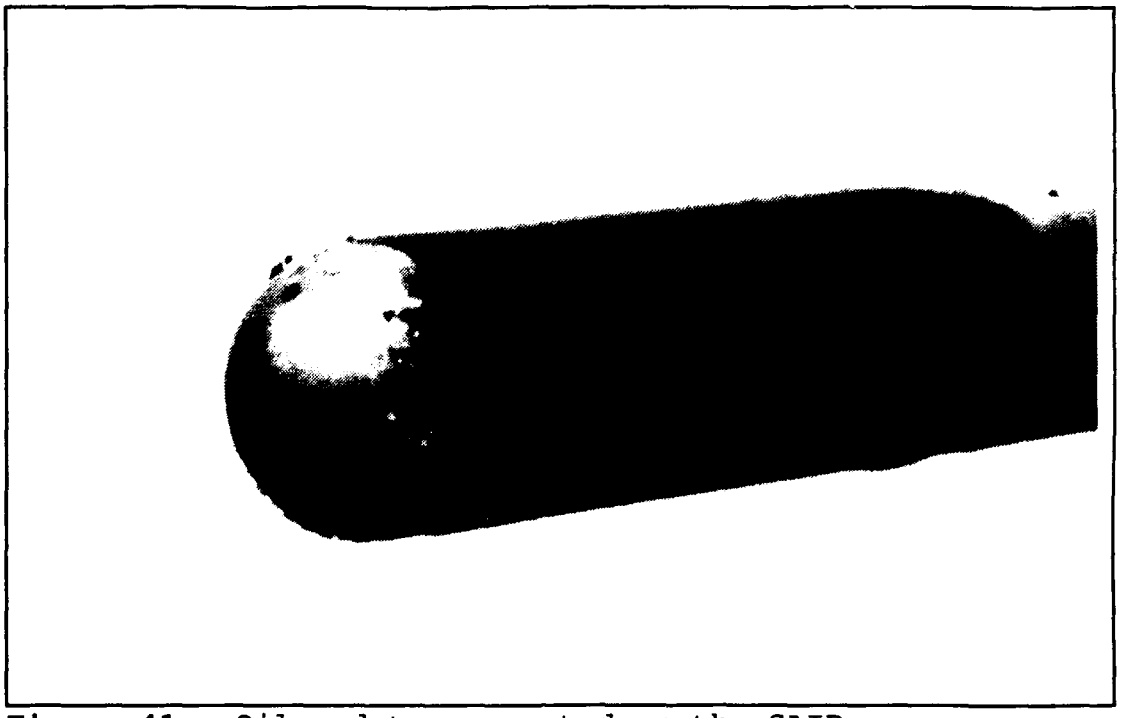

Figure 41. Oil and toner coated on the SAIP nose.

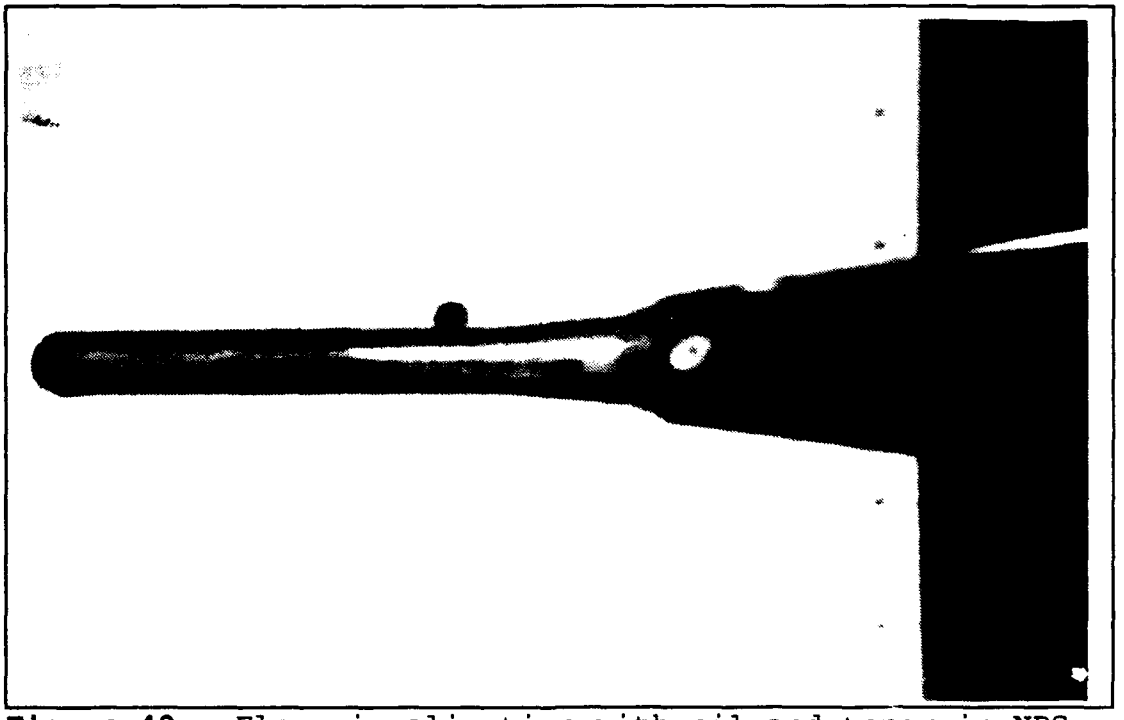

Figure 42. Flow visualization with oil and toner in NPS wind tunnel.

After a few minutes, the oil in the separation bubble would pool toward the bottom due to gravity effects.

These same procedures were repeated with the ASA. The separation region appeared smaller (1/4 inch), however the flow characteristics were the same.

2. Tripped Flow

In order to determine the effects of this separation region, the flow must be tripped similar to the method introduced by Prandtl (discussed by Anderson) to induce turbulent flow, and subsequent pressure measurements taken. Placing a trip wire on the hemispherical nose was not possible. However, the nose could be roughened in a non-destructive manner using contact cement and grains of sand, which is basically the same principle as placing dimples in a golf ball. Figure 41 shows the sand and contact cement tripping mechanism. This is a crude method of tripping the flow, and requires extreme patience in applying. However, this crude method was successful in eliminating the separation bubble completely. The tripping mechanisms had to be removed and reapplied every run due to the messy nature of the oil and sand.

Pressure measurements were made for the tripped flow. The Reynolds number was 83,000 based on standard sea level conditions and a reference length of one inch (diameter of

ASA). Figures 43 and 44 show the differences in the tripped flow compared to the non-tripped flow. The C_p dropped slightly in both cases indicating a measurable change. While the measured change may not be significant in this case, these C_p increments may be more pronounced at the higher velocities encountered during flight tests thus indicating the possible viscous dependence.

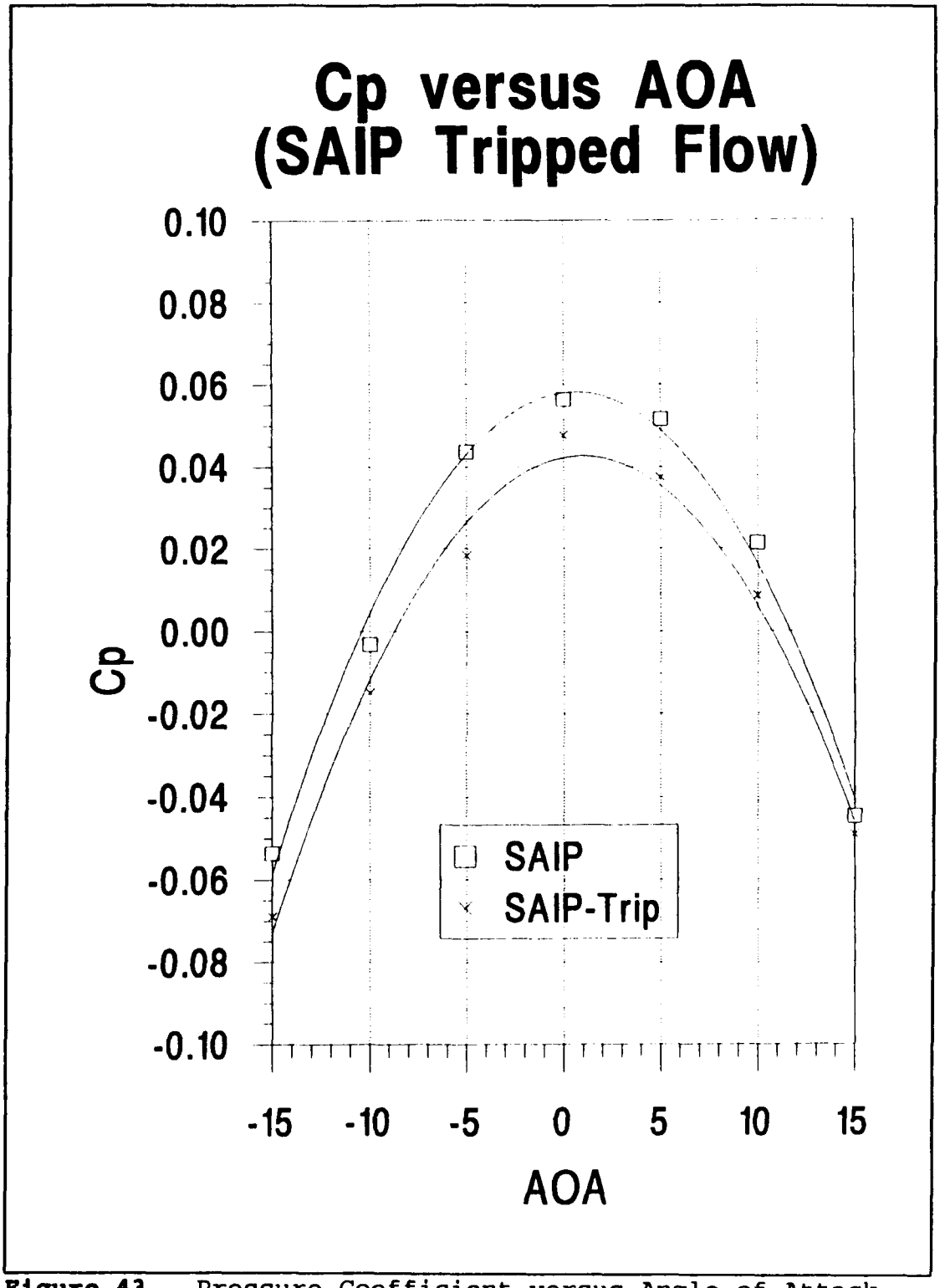

Figure 43. Pressure Coefficient versus Angle-of-Attack for SAIP with and without tripped flow.

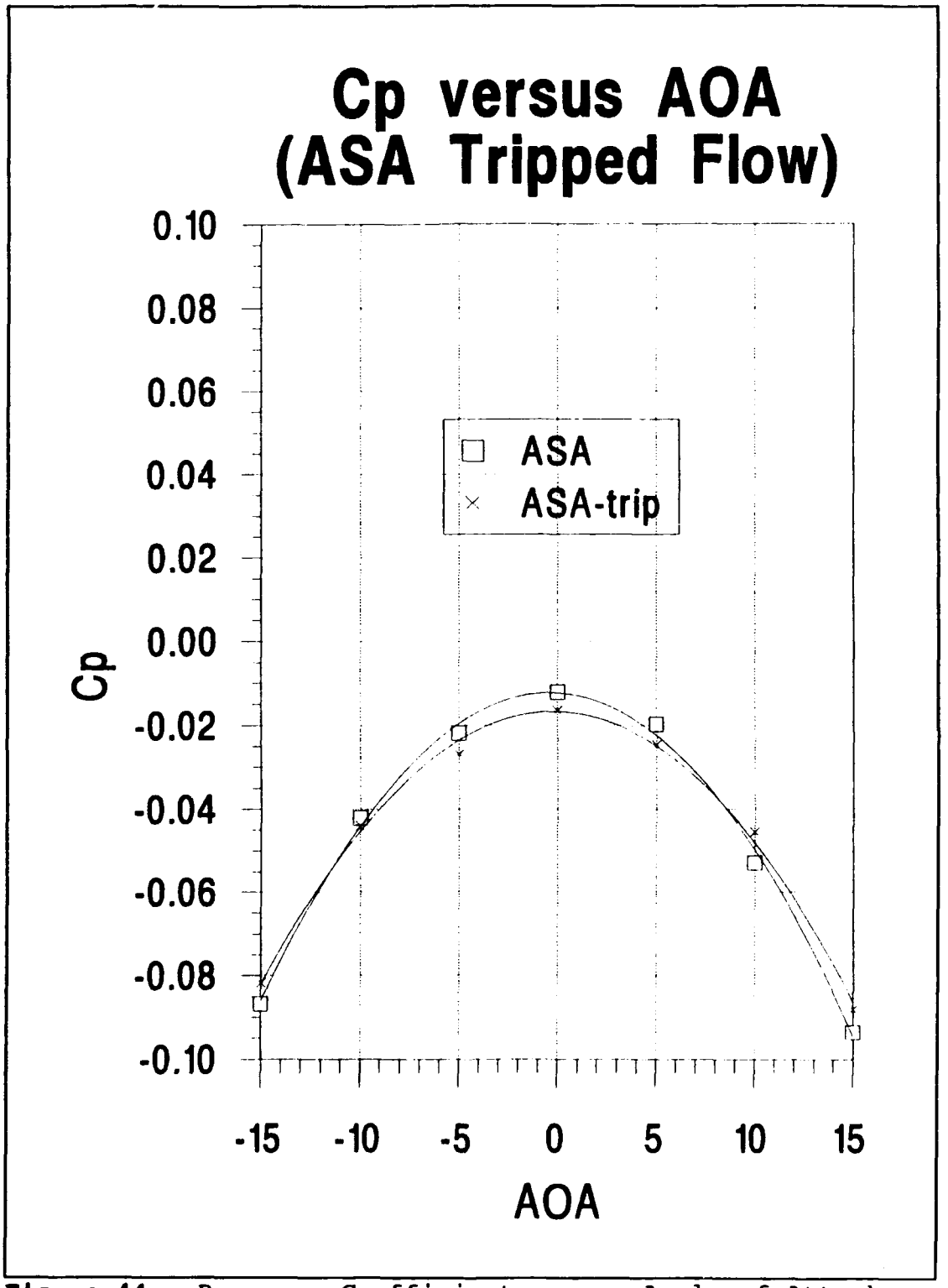

Figure 44. Pressure Coefficient versus Angle-of-Attack for ASA with and without tripped flow.

V. AIRCRAFT PRESSURE FIELDS

A. INTRODUCTION

Over-pressures induced by the five inch body of the SAIP were shown to create detrimental effects on static pressure readings. However, the magnitudes of the errors were much less than those observed during flight tests. Therefore, the effects of the aircraft had to be investigated. If the SAIP's five inch body degraded the static pressure measurement, the combination wing/body/pylon could degrade it even more. This chapter attempts to quantify the effects of aircraft pressure fields.

B. NACA INVESTIGATIONS

In 1951 the National Advisory Committee for Aeronautics (NACA) investigated the variation of static-pressure error of a static-pressure tube with distance ahead of a wing and a fuselage [Ref. 14]. Tests were conducted with the tube located 1/4 to 2 chords ahead of the wing of a fighter airplane (Fig. 45), 1/2 to 1.5 body diameters ahead of the fuselage nose and 1 chord ahead of the wing of a trainer airplane (Fig. 46). Speeds ranged from stall to 265 miles per hour (Mach 0.348). Some of the results are shown in Figures 47 through 49. Figures 47 and 48 plot the measured pressure coefficient versus the lift coefficient for static tube

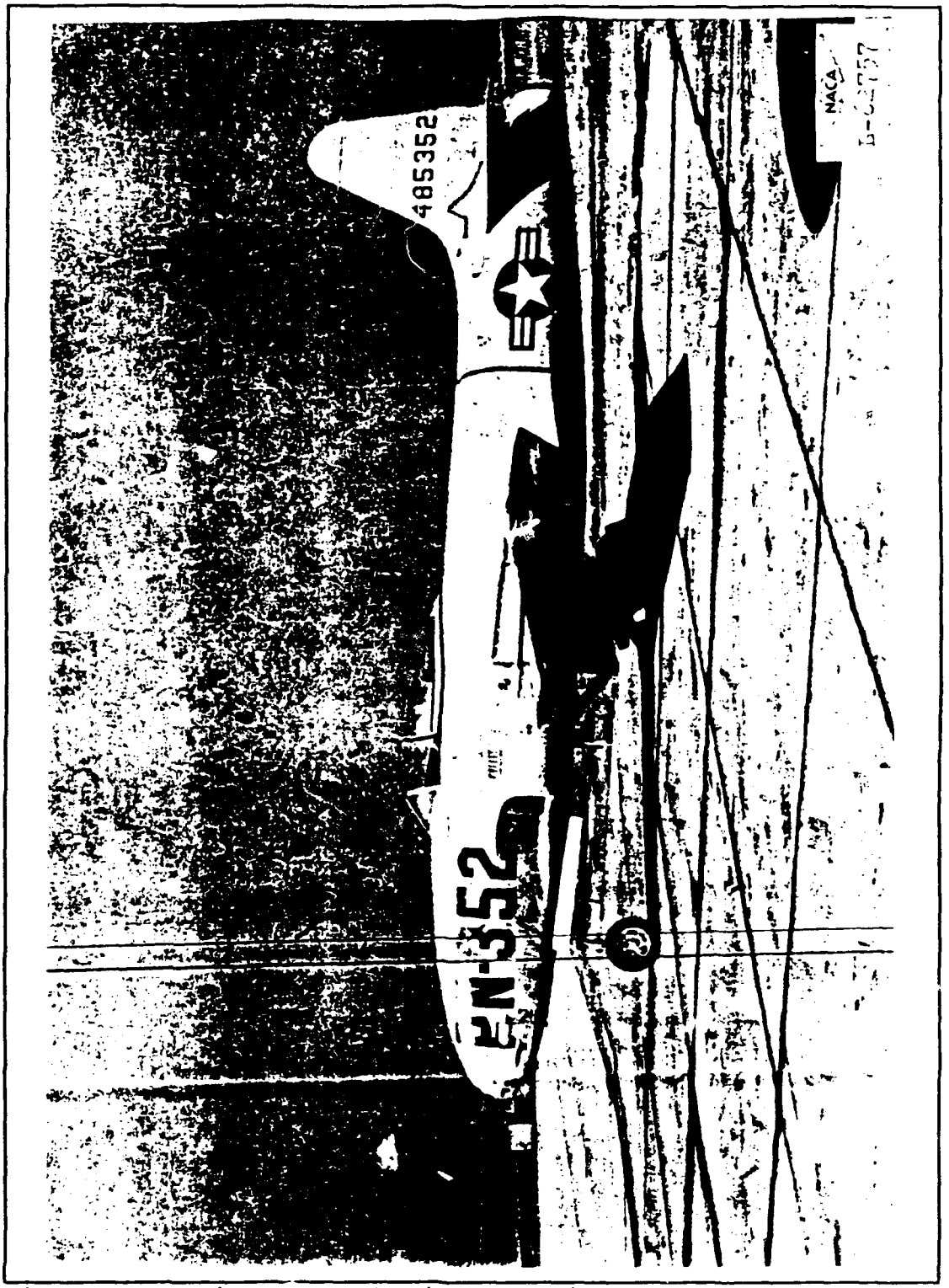

Figure 45. Airspeed-tube installations on fuselage nose and wing tip of fighter airplane [Ref. 14].

Figure 46. Airspeed-tube installations on wing of trainer airplane [Ref. 14].

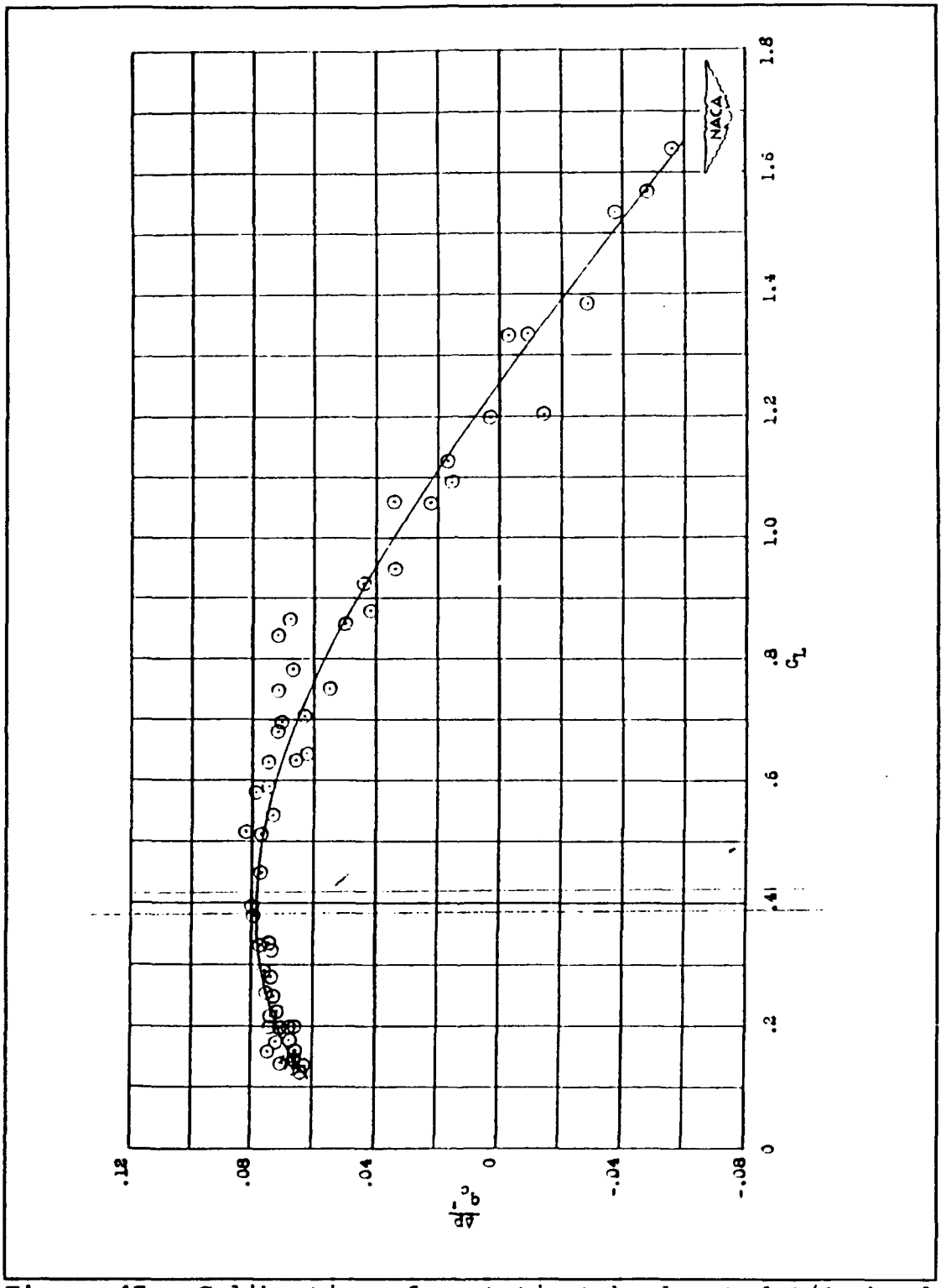

Figure 47. Calibration of a static tube located 1/4 chord ahead of the wing tip of the trainer airplane [Ref. 14].

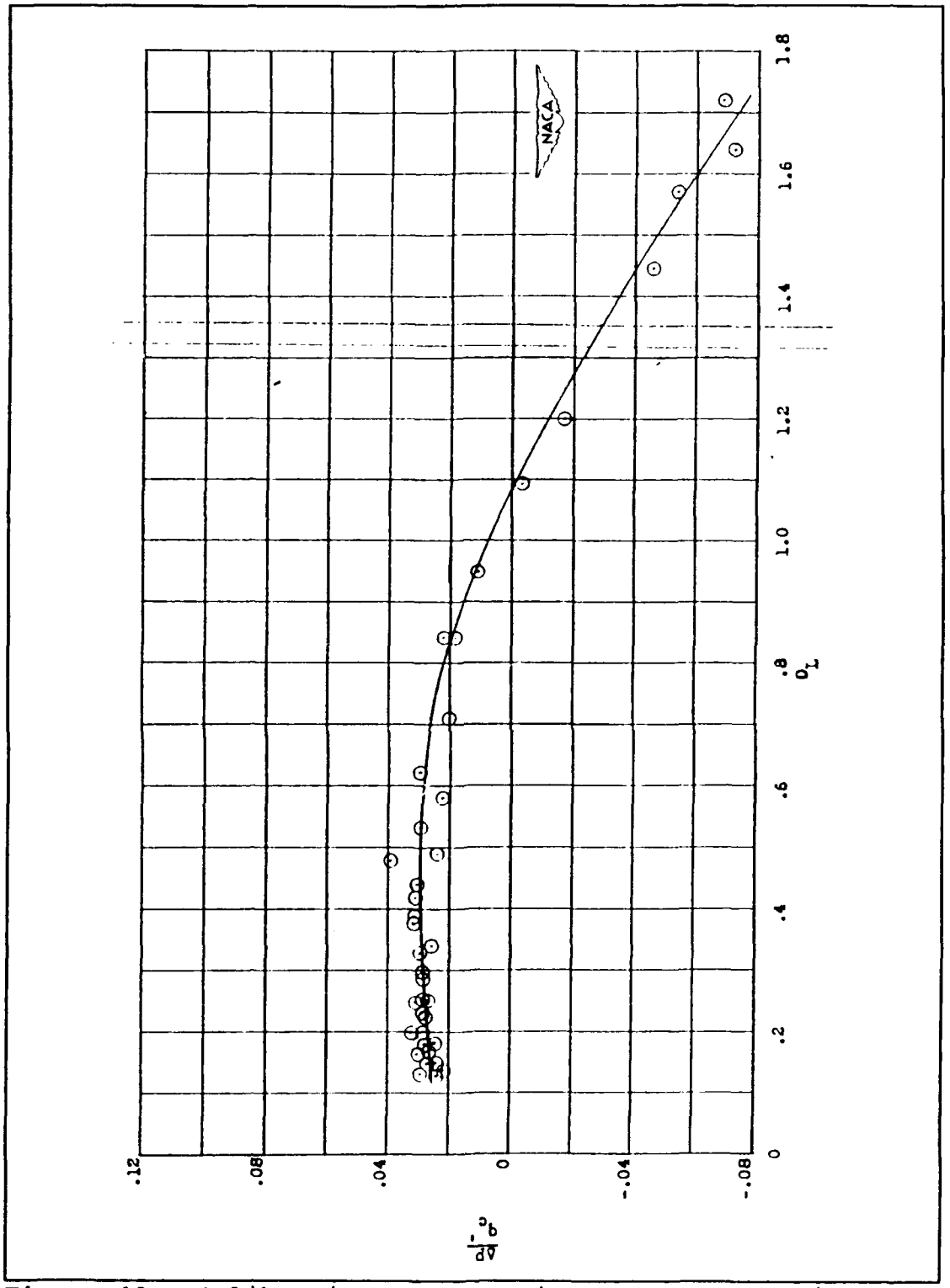

Figure 48. Calibration of a static tube located 1/2 chord ahead of the wing tip of the trainer airplane [Ref. 14].

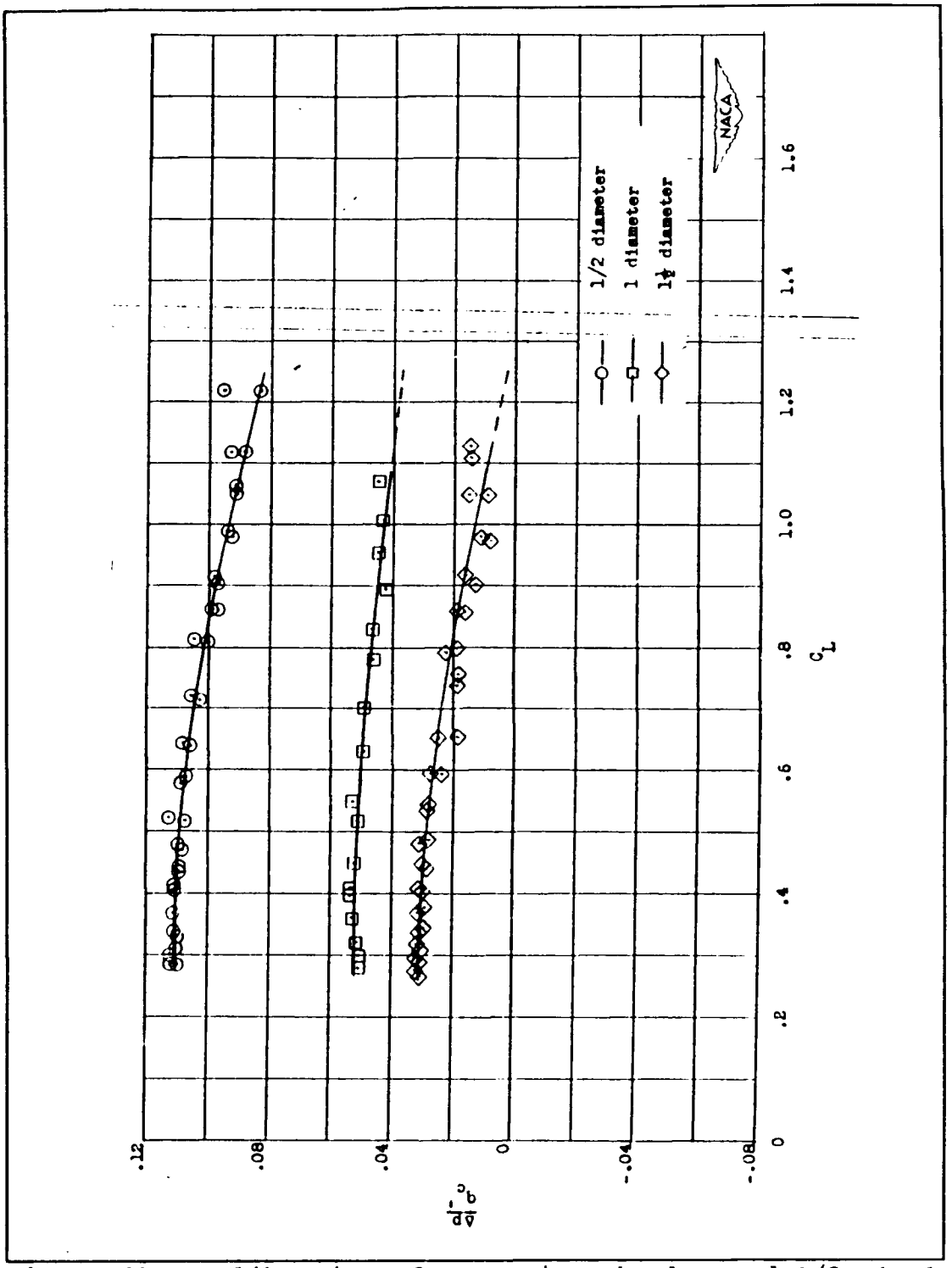

Figure 49. Calibration of a static tube located 1/2, 1, 1 1/2 body diameters ahead of the nose of the fighter airplane [Ref. 14].

locations 1/4 and 1/2 local chord lengths ahead of the wing tip of the trainer. Figure 49 shows plots of the measurements of the static tube located 0.5, 1, and 1.5 body diameters ahead of the fuselage nose of a fighter airplane.

While these results pertain to low subsonic airspeeds, they do illustrate the major effects of the aircraft pressure fields. Figure 50 is a sketch of the SAIP mounted on an A-6 aircraft outboard wing pylon. The static ports are located approximately 1/2 local chord distance from the wing tip. If one approximates the pylon and LAU-7 as a vertical wing, the static ports are located less than 1/4 chord from this mounting combination. It was concluded that the wing and pylon were responsible for the remaining discrepancy between wind tunnel data and flight test data. Computational methods in the following sections would be used to analyze those errors.

C. VSAERO CHINA LAKE

1. Background

To model the effects of the aircraft on the SAIP, a wing and fuselage shape would have to be incorporated in the axisymmetric SAIP model. This would obviously increase the complexity of the PMARC model, which in turn would demand a large amount of VAX CPU time. Fortunately, the engineers at China Lake provided an alternative method. These engineers have used the proprietary VSAERO code to model store

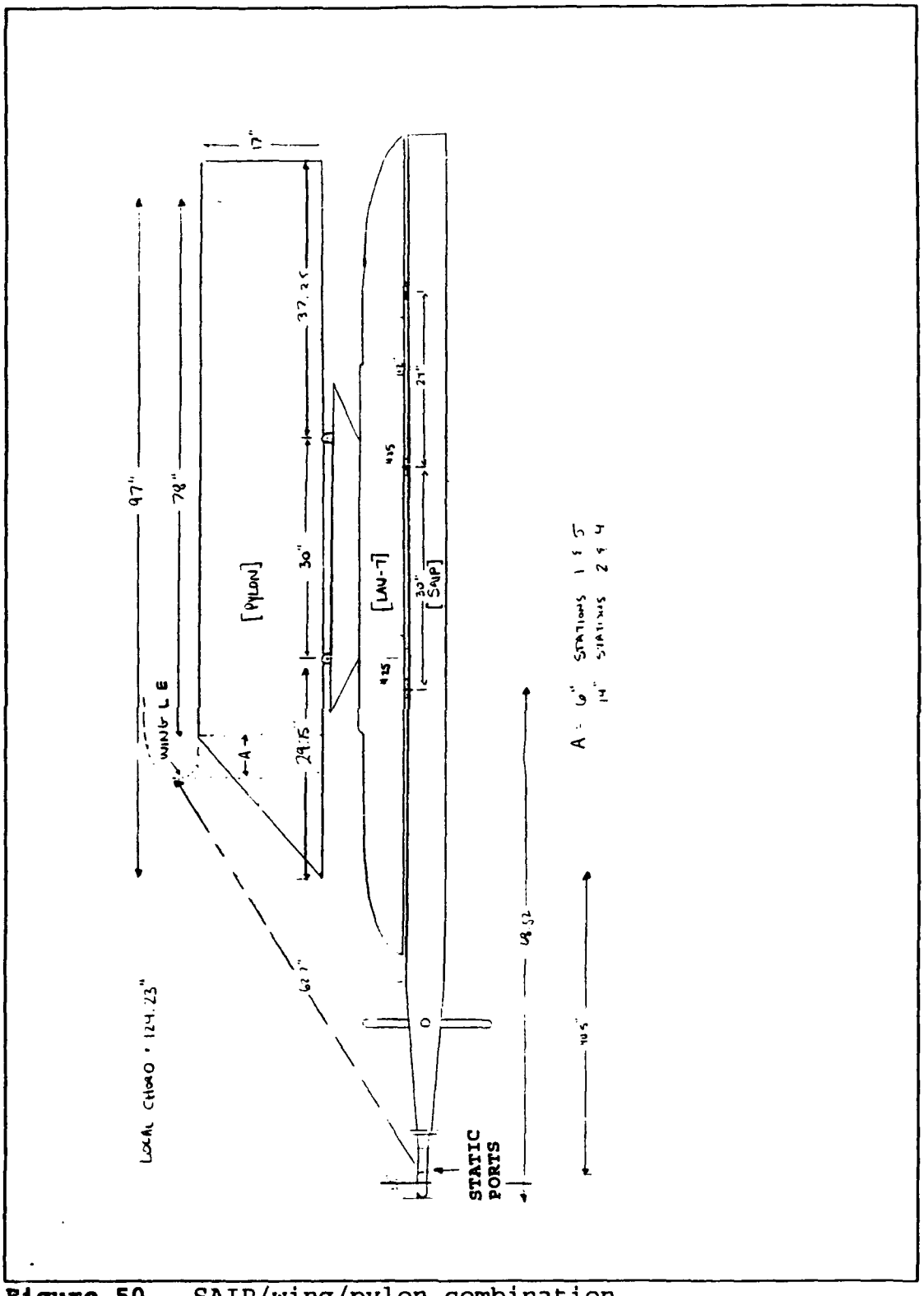

Figure 50. SAIP/wing/pylon combination.

separations from various Naval aircraft including the A-6. The powerful VSAERO code is compatible with the PMARC code. However, VSAERO is difficult to use, requires extensive knowledge and familiarity to generate shapes for analysis and is not available for use at the Naval Postgraduate School. Mr. Larry Gleason, one of the engineers at China Lake, provided that expertise for modeling the SAIP in the A-6 environment. Solutions were generated an a CRAY computer.

2. SAIP C_p Versus Aircraft Location

Initial computational runs were made at Mach 0.6, which represents a median flight test speed, and 10,000 feet altitude. Mach 0.6 also corresponds to the speed of the original axisymmetric SAIP in Chapter II. Appropriate angle-of-attack was assigned for the corresponding flight speed based on the A-6 aircraft's proper attitude. Five test cases were computed for different SAIP locations. Case I modeled the SAIP at the outboard pylon with no LAU-7 incorporated. Figures 51 through 53 show front, top, and side view of the A-6/SAIP as modeled with VSAERO. Over 3000 panels were used in modelling, 1200 of which were placed on the SAIP. Figure 54 shows the C_p distribution over the SAIP. Aircraft effects are evident due to the lack of overlap of the upper and lower curves. Case II (Figs. 55 and 56) modeled the SAIP at the outboard pylon with a LAU-7 "simulation". The LAU-7 was far too difficult to model for the time allotted, so the pylon was

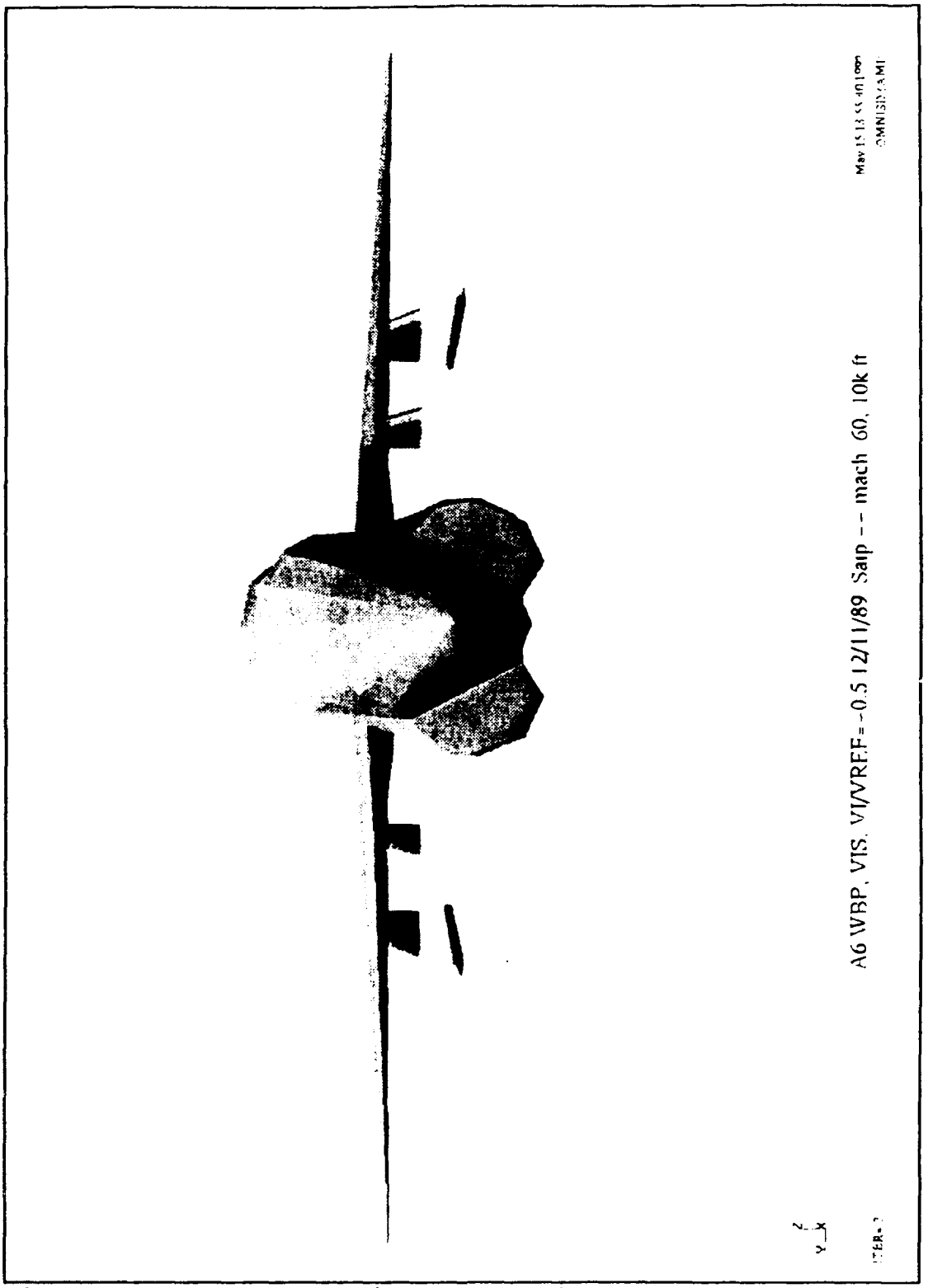

Figure 51. VSAERO SAIP/A-6 front view (Case I).

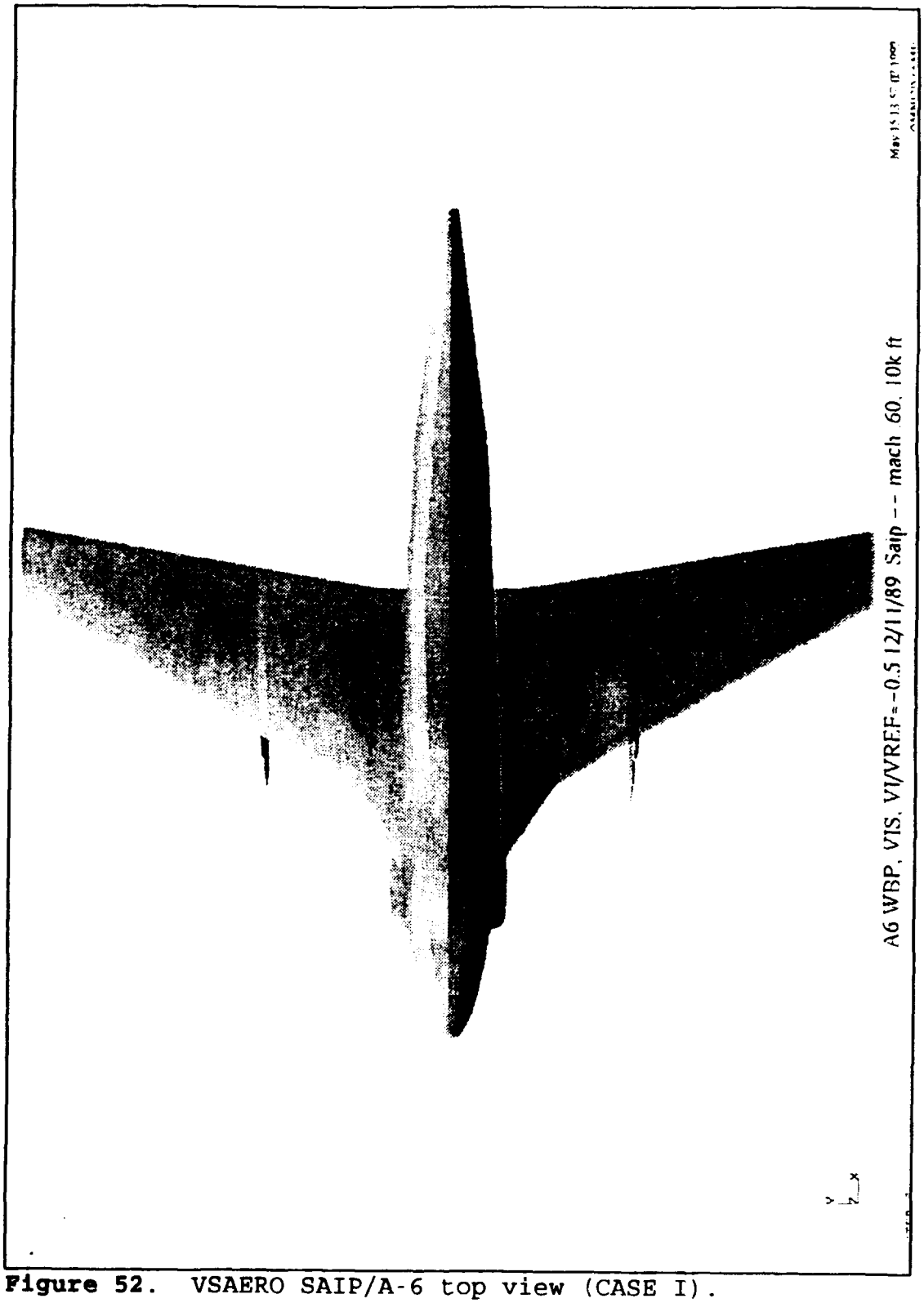

Figure 52. VSAERO SAIP/A-6 top view (CASE I).

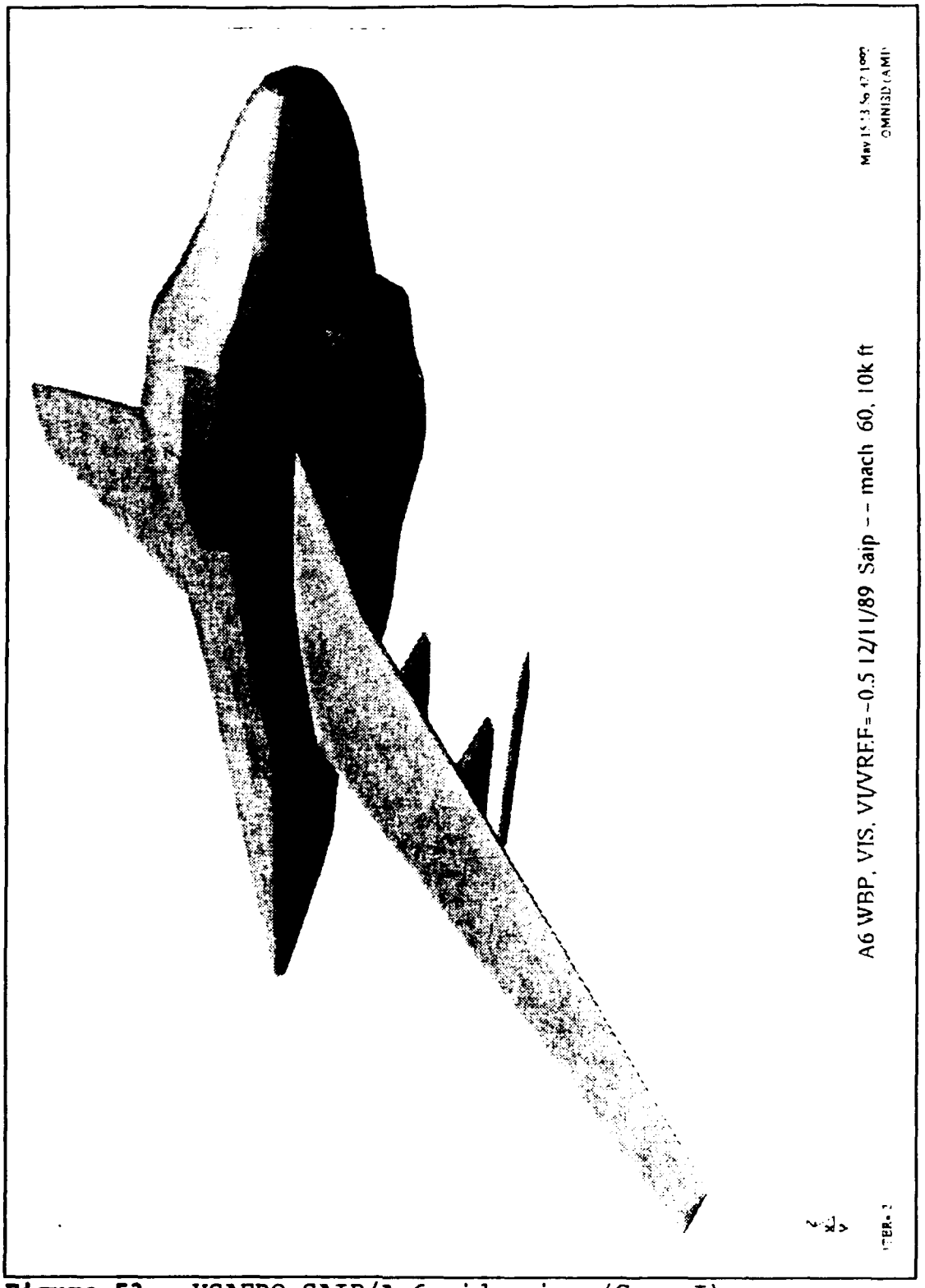

Figure 53. VSAERO SAIP/A-6 side view (Case I).

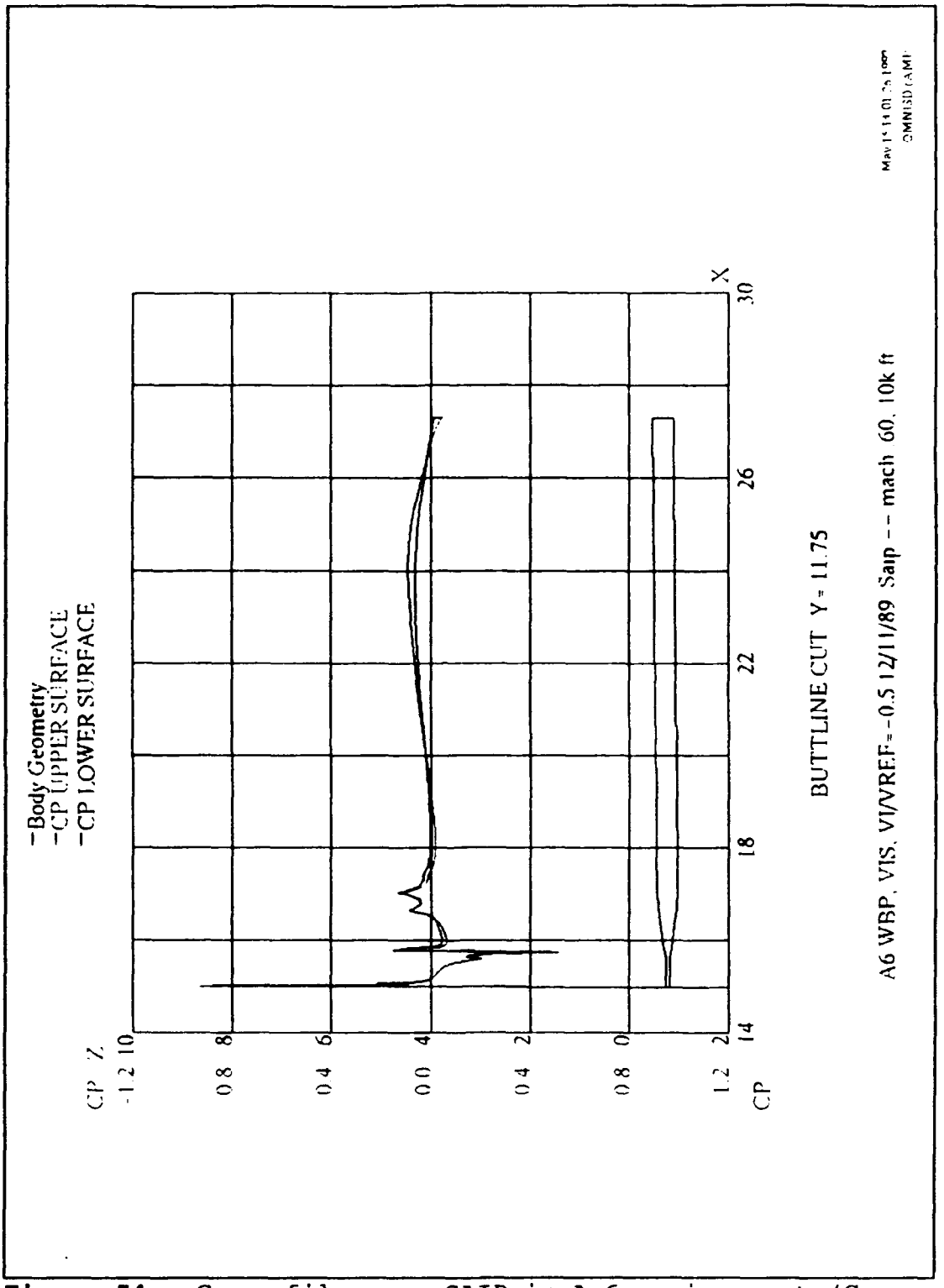

Figure 54. C_p profile over SAIP in A-6 environment (Case I).

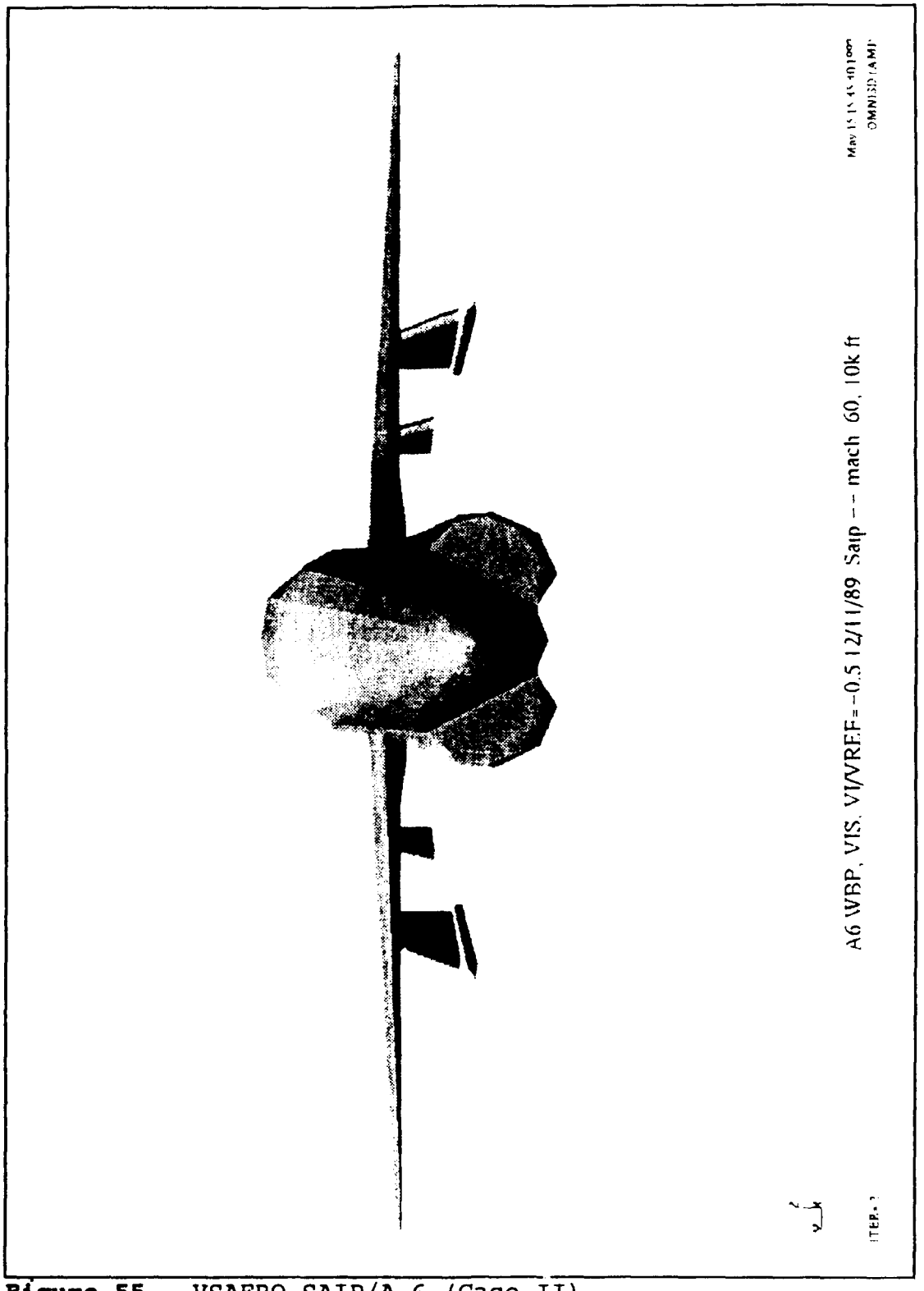

Figure 55. VSAERO SAIP/A-6 (Case II).

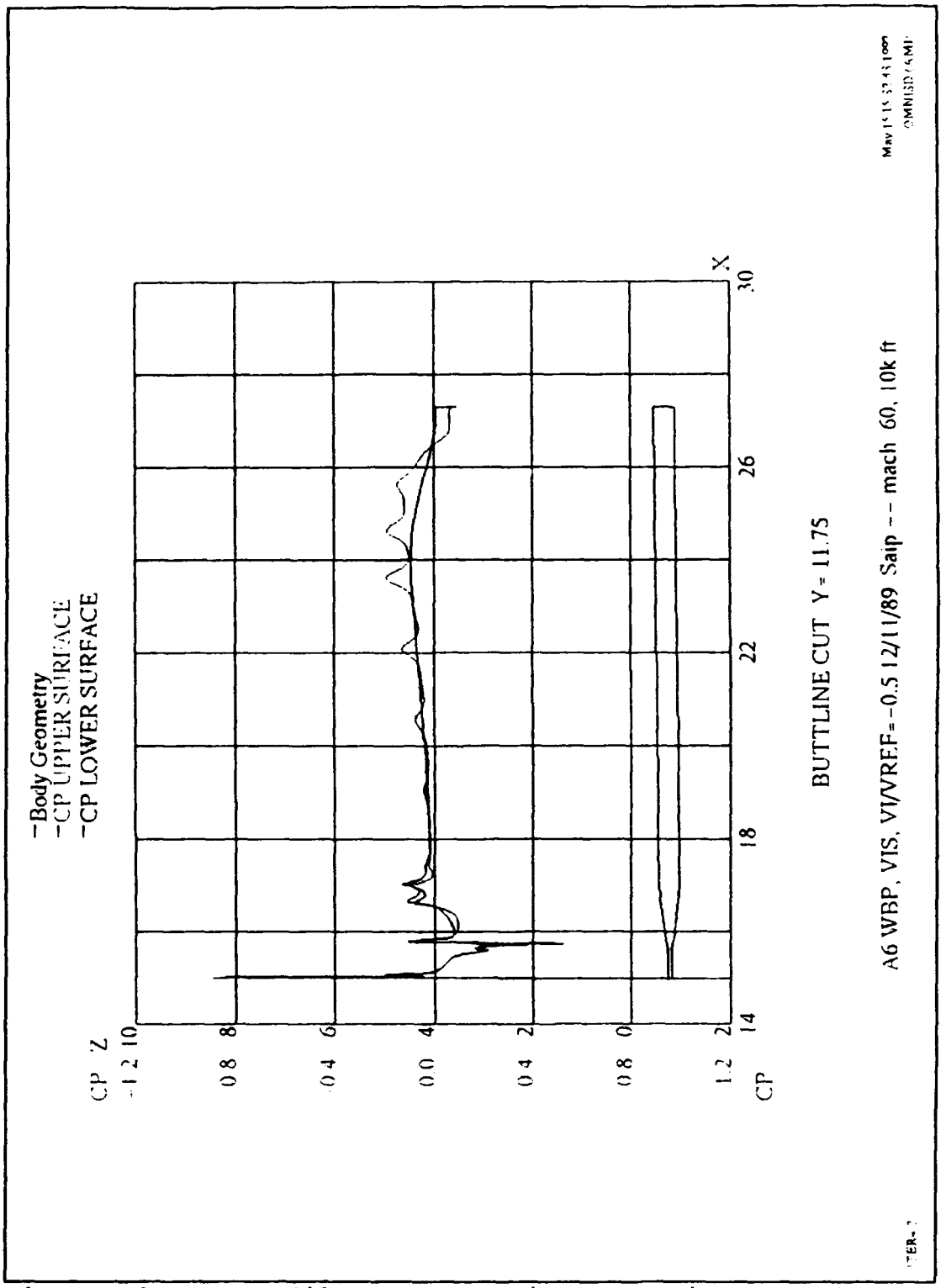

Figure 56. C_p profile over SAIP in A-6 environment (Case II).

extended to represent the LAU-7. This is a "worst case" scenario, because the pylon extension is larger than the LAU-7. Case III (Figs. 57 and 58) placed the SAIP at the inboard pylon with no LAU-7. Case IV was run with the SAIP in an imaginary position between the pylons near the bottom of the wing, and Case V with the SAIP between the pylons, near the bottom of the wing, with the static ports two feet closer to the wing tip as in Case IV. Figures 59 and 60 show the C_p curves for Case IV and V respectively.

A direct comparison of each case is shown is Figure 61. The curves represent the region between ± one inch from the static ports. At Mach 0.6 the effects of SAIP location are evident. Again, the magnitudes are much lower than predicted. This is why Case IV and Case V were generated. Initially, (Case I,II, and III) the aircraft pressure effects did not seem to be significant. However, after running Case IV and V, and after carefully analyzing the non-symmetric C_p profiles, it became obvious the aircraft effects were being felt, despite the low magnitudes. Case I show virtually no difference as compared to the SAIP (no aircraft) curve, indicating at Mach 0.6 the wing has no effect on the static port location. Case II offers some difference. However, the LAU-7 simulation is larger than the LAU-7 itself. This led to the conclusion that perhaps Mach 0.6 is too fast to analyze aircraft effects. The NACA report was conducted at Mach numbers below 0.35. It was surmised that the over-pressure of

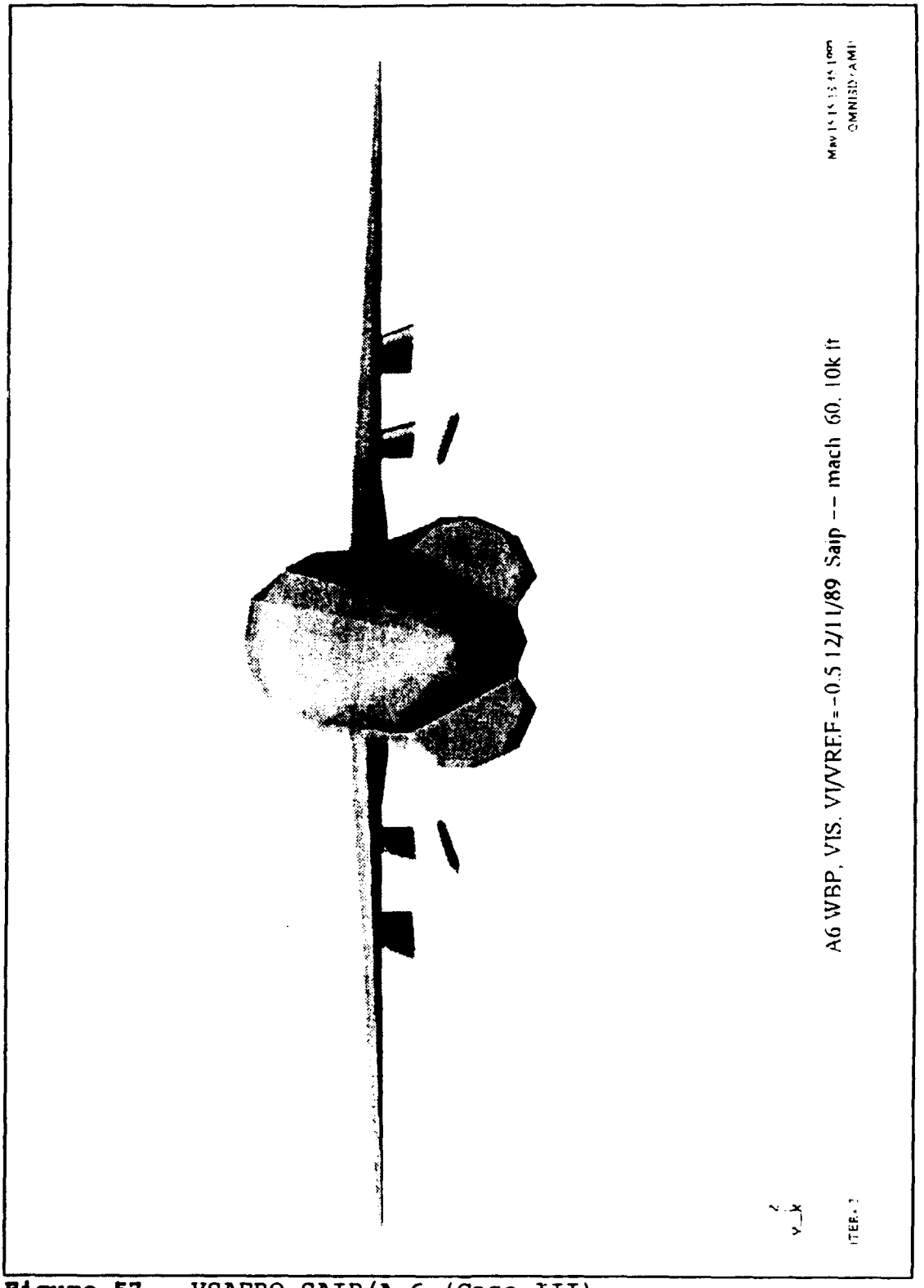

Figure 57. VSAERO SAIP/A-6 (Case III).

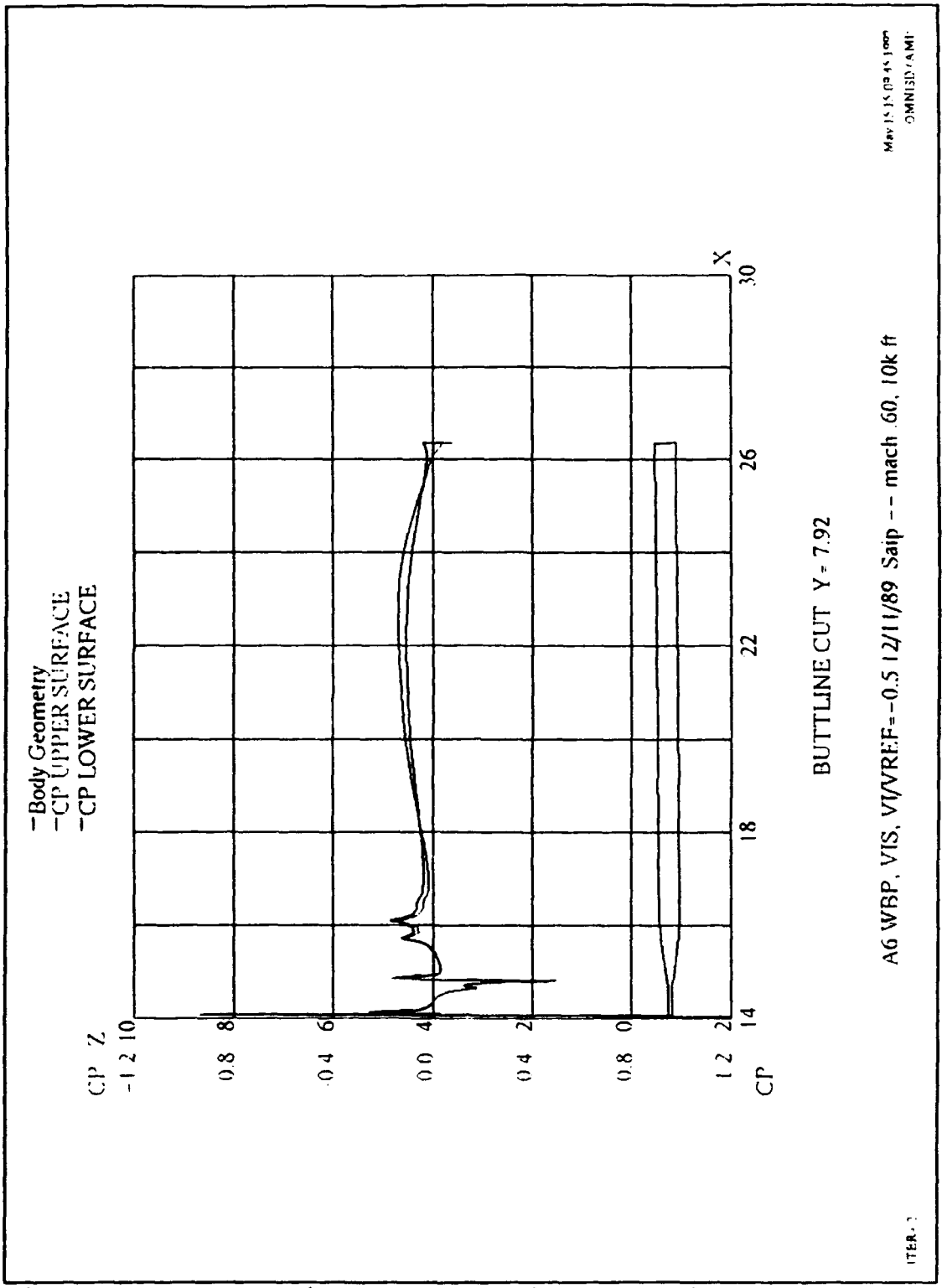

Figure 58. C_p profile over SAIP in A-6 environment (Case III).

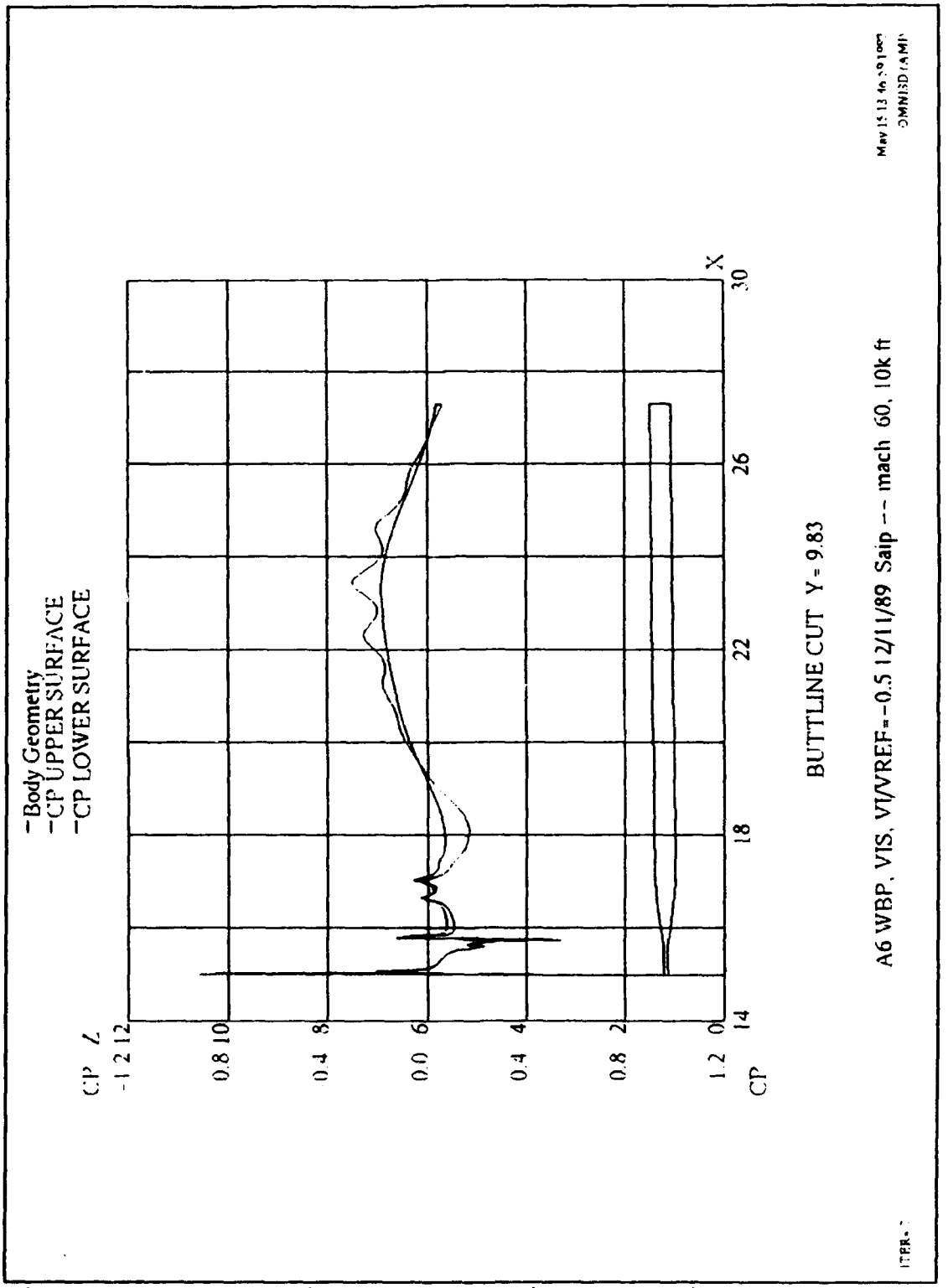

Figure 59. C_p profile over SAIP in A-6 environment (Case IV).

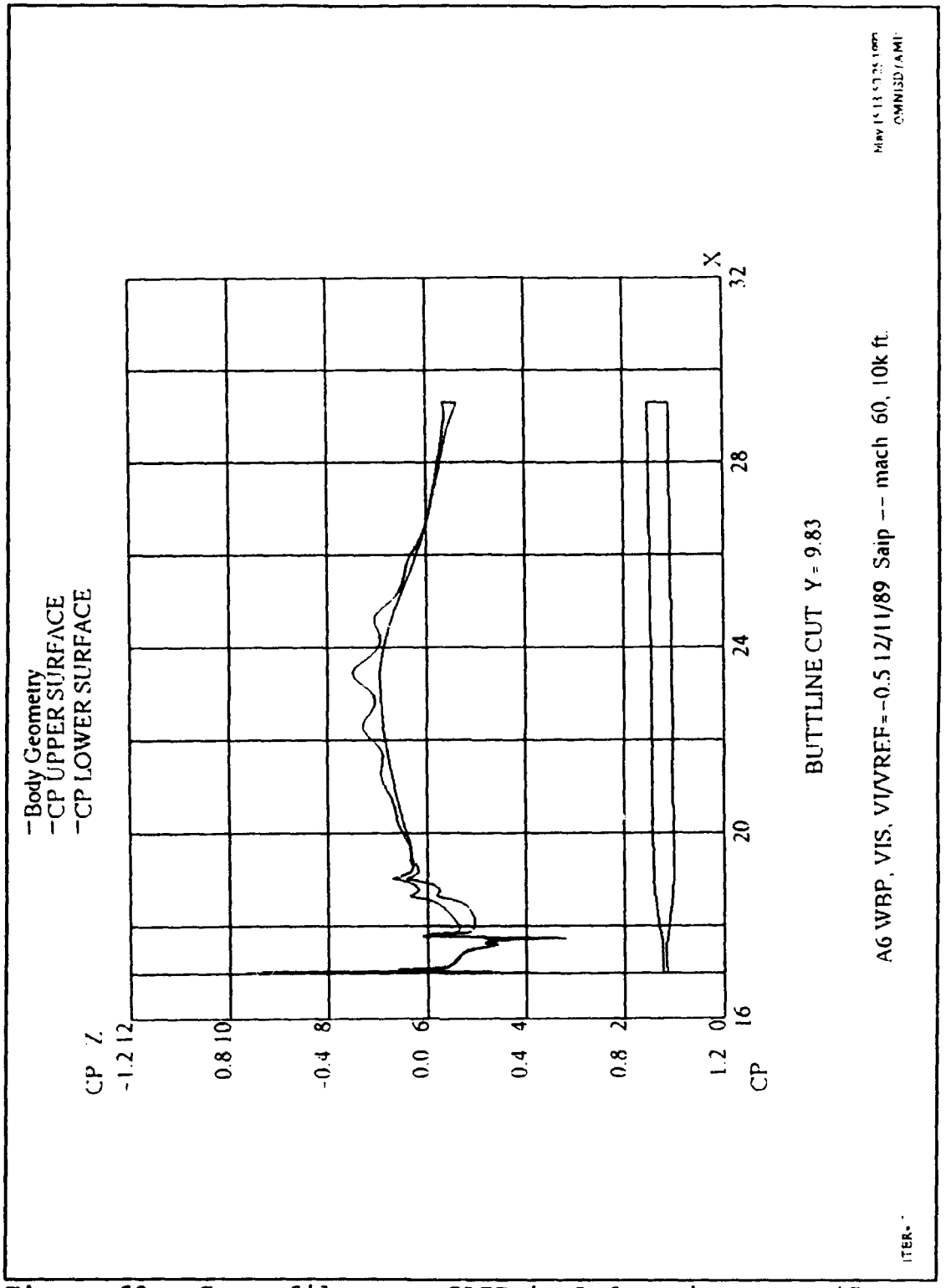

Figure 60. C_p profile over SAIP in A-6 environment (Case V).

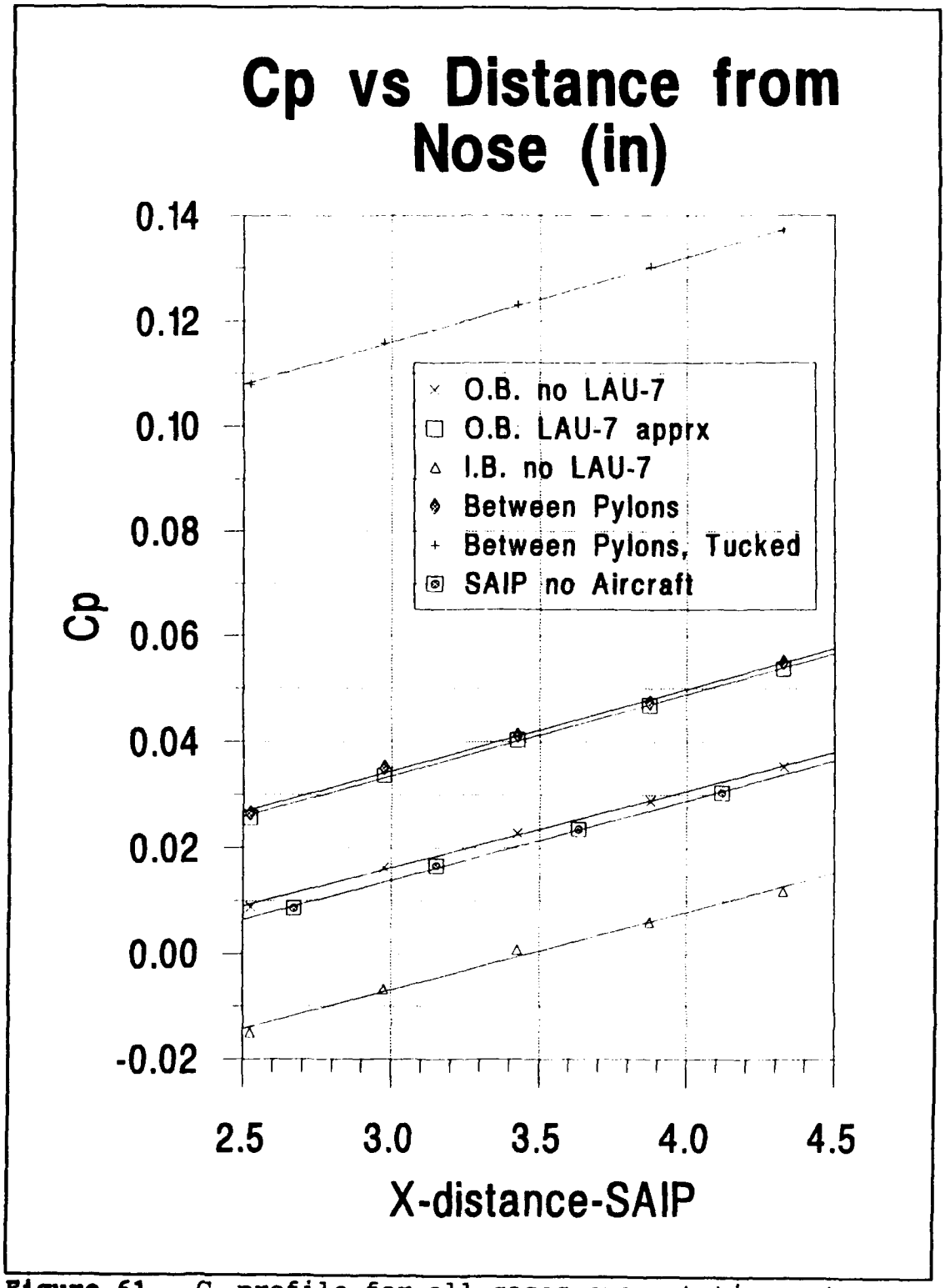

Figure 61. C_p profile for all cases over static port region of the SAIP.

the aircraft was not being propagated forward enough to have significant effects at Mach 0.6.

3. SAIP C_p Versus Aircraft Speed

The Case I model was run over a range of airspeed to analyze the aircraft effects over a range of flight speeds. Ten panels run circumferentially over the static port location (3.5 inches from the nose tip). The C_p calculated for each panel is plotted in polar coordinates as shown Figures 62a-d. The radius of the polar plot extends from a $C_p = 0$ to $C_p = 0.1$. Therefore, the closer the data points come to the edge of the circle, the closer the C_p value approaches 0.1 At Mach = 0.2, the over-pressures felt near the static ports are large. As the Mach number is increased, the over-pressures diminish in magnitude and become more symmetric, At Mach 0.8 the over-pressures due to the aircraft as well as the five inch body of the SAIP are no longer felt (assuming subsonic flow throughout). Of course the Mach 0.8 is unrealistic, due to transonic flight characteristics. Even though the magnitudes shown are still lower than the flight test data, the trend is clear; aircraft pressure effects are felt at the static port region and can be significant depending on the Mach number. As the aircraft accelerates, the pressure effects due to the aircraft drop off and eventually disappear.

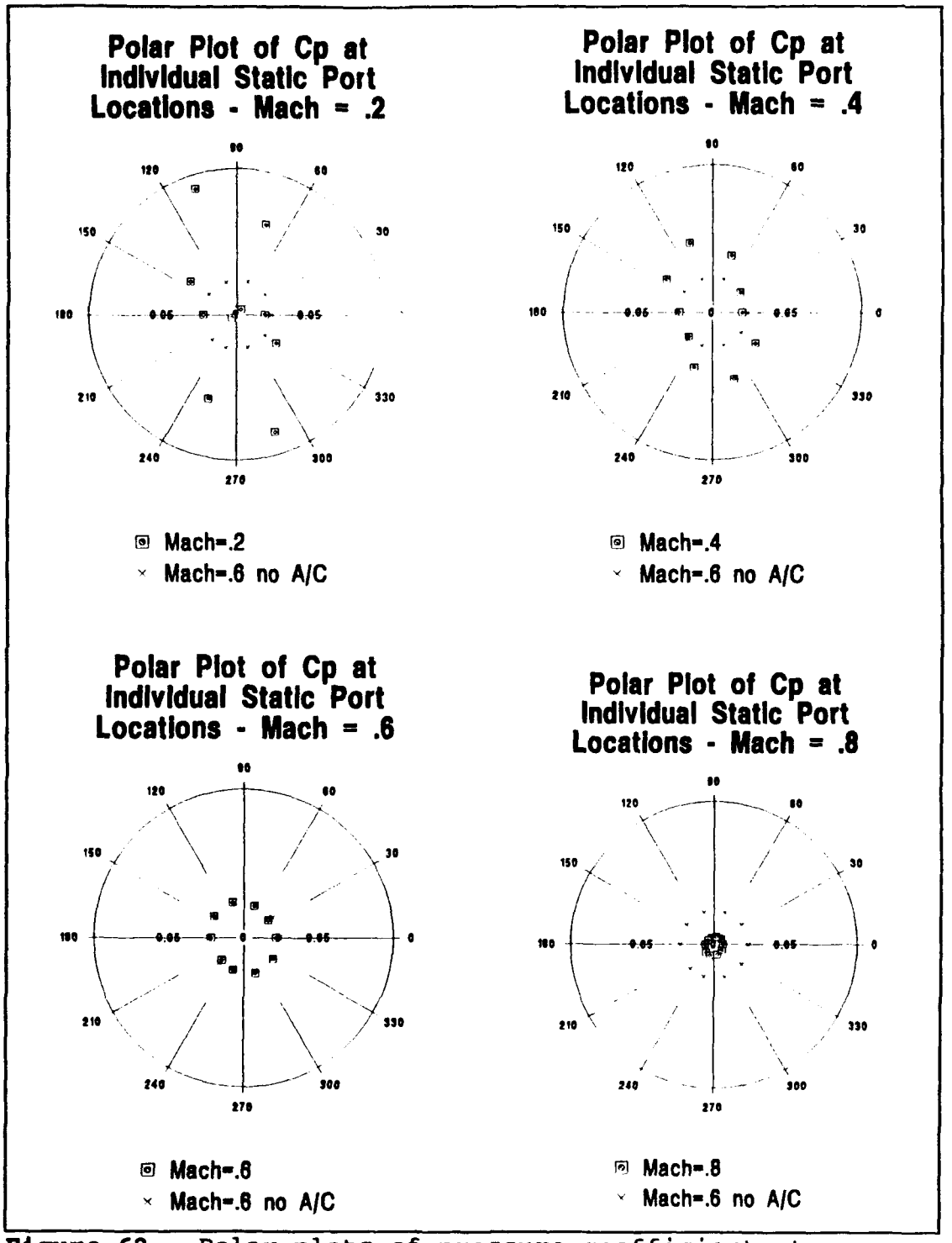

Figure 62. Polar plots of pressure coefficient at individual static ports (right to left, top to bottom)
a) Mach = 0.2 b) Mach = 0.4
c) Mach = 0.6 d) Mach = 0.8

D. FLIGHT TEST DATA

1. Angle-of-Attack (AOA) Corrections

Wind tunnel tests measured the C_p to be approximately 0.055 in magnitude at the static pressure ports at zero degrees AOA. However, as the A-6 aircraft accelerates the angle-of-attack decreases. Table 1 shows the AOA variation with true airspeed for 4,000 and 10,000 ft altitude [Ref. 15].

TABLE 1: AOA VERSUS TRUE AIRSPEED

AIRCRAFT TAS	AOA 4,000 FT	AOA 10,000 FT
385	7.95	9.56
440	4.73	5.85
495	3.38	4.16
550	2.62	3.03
605	2.08	2.42
660	1.63	1.86
715	1.24	1.41
770	1.01	1.10
825	0.73	0.90
880	0.56	0.73
935	0.48	0.65

Figure 35 demonstrates how the pressure coefficient varies with angle-of-attack. In particular, the C_p decreases in magnitude as the AOA is increased from zero degrees. Therefore, an approximate correction can be made to the pressure coefficient as a function of airspeed using Table 1 and Figure 36. Figure 63 shows how the C_p at static pressure ports varies for the SAIP as a function of airspeed (neglecting aircraft and compressibility effects). This trend is significant. If aircraft pressure effects and compressibility effects are ignored, the C_p increases with true airspeed. This correction approaches a limit as AOA varies very little with TAS at higher speeds.

2. Compressible Flow Corrections

Assuming that the SAIP pitot static probe can be approximated as a slender body of revolution, the Gothert Correction for a thin ellipsoid of revolution may be used [Ref. 16] to correct C_p for compressibility up to Mach numbers approaching the transonic region using

$$\frac{(-C_p)_{max}}{(-C_p)_{max}} = 1 + \frac{\ln\sqrt{1 - M_\infty^2}}{1 - \ln 2 + \ln\delta} \qquad (18)$$

where: δ = thickness ratio (t/l = 0.2), M_∞ = free stream Mach number, $C_{p\infty}$ = pressure coefficient for incompressible flow, and C_p = pressure coefficient for compressible flow. The value for $C_{p\infty}$ = 0.055 was chosen from wind tunnel tests. Figure 64 illustrates the effects of compressibility. Again, the trend

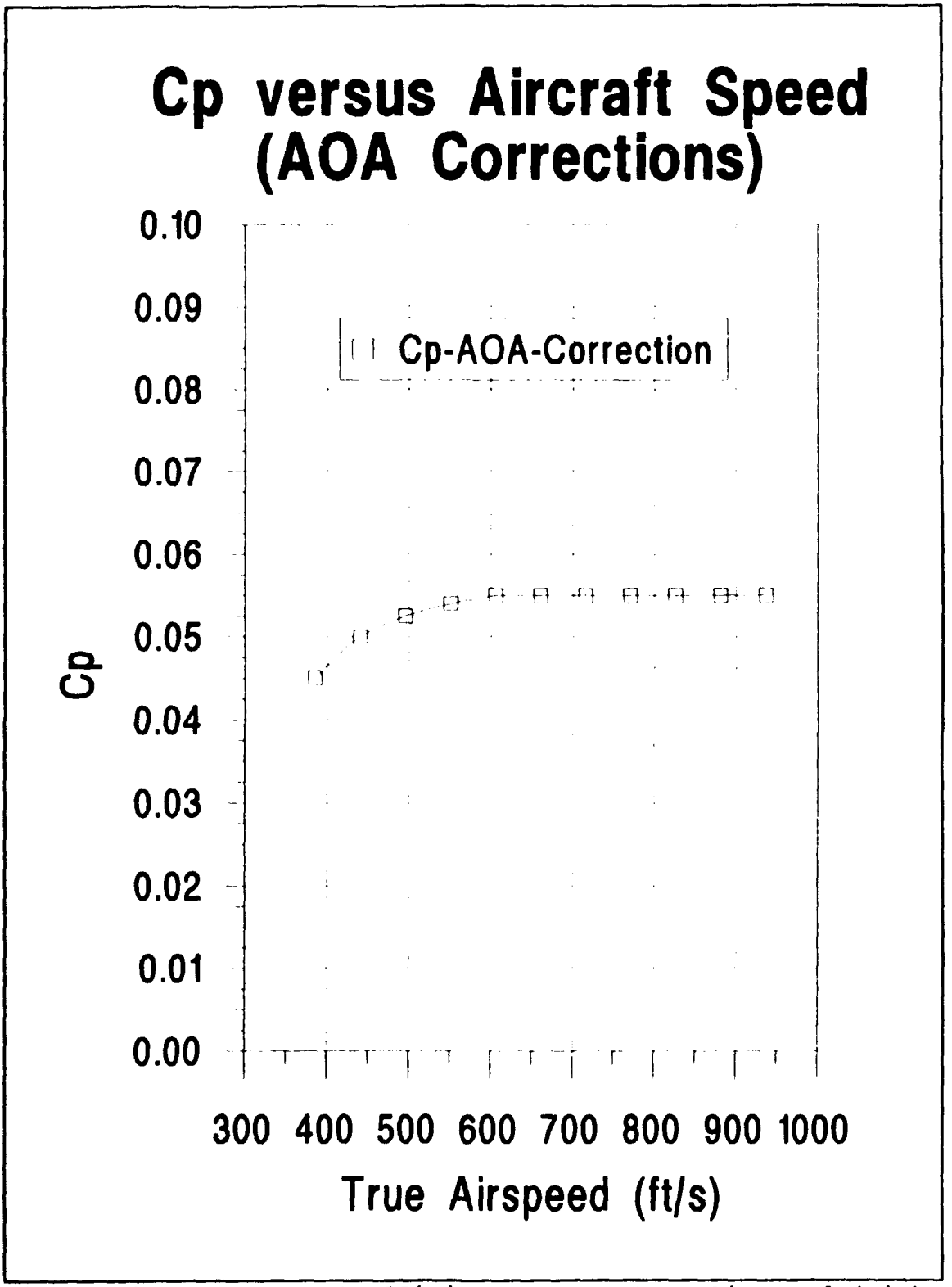

Figure 63. Pressure Coefficient versus True Airspeed (with angle-of-attack correction obtained from Figure 36).

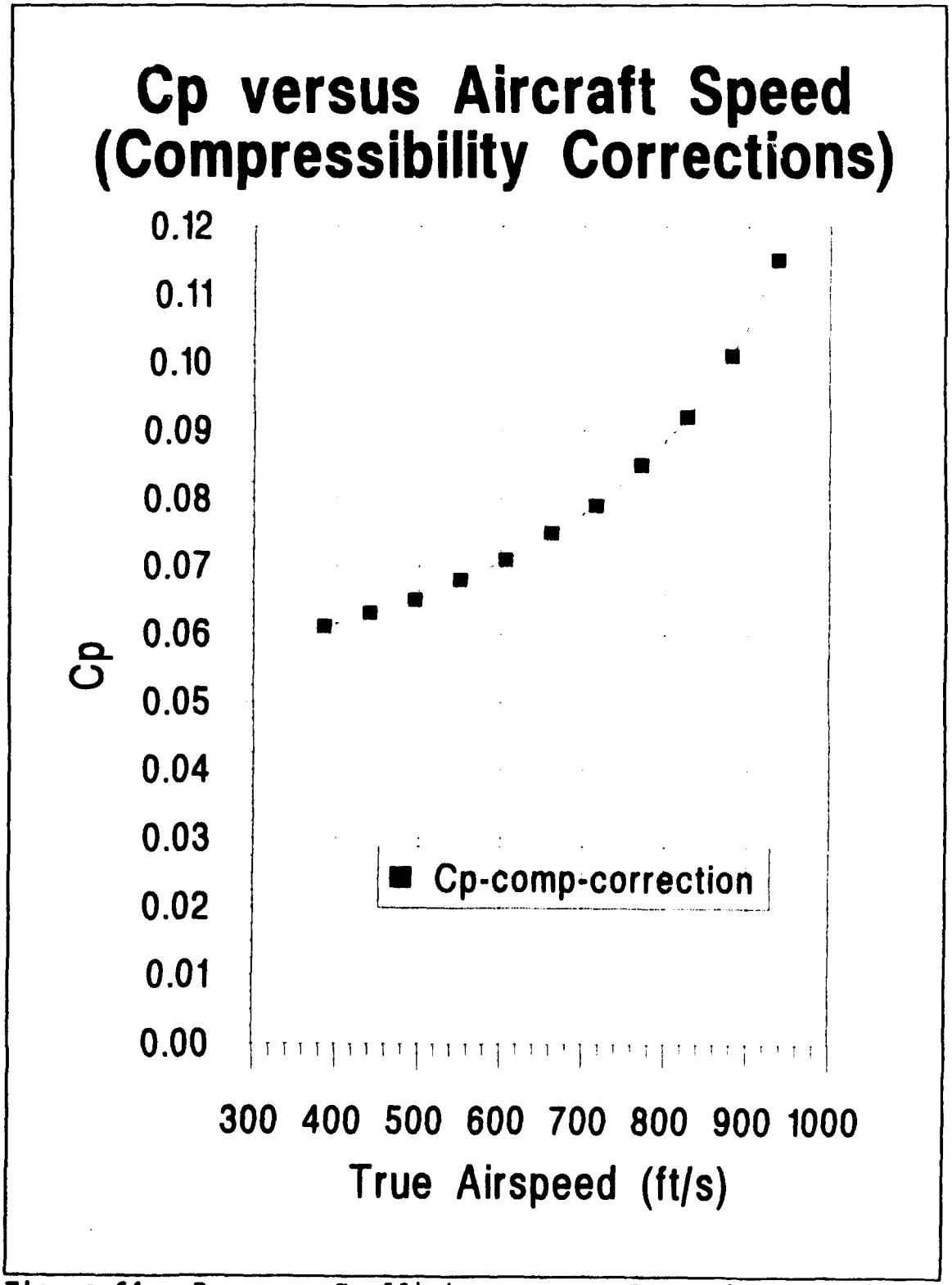

Figure 64. Pressure Coefficient versus True Airspeed with compressibility correction (Gothert correction).

is that C_p increases with true airspeed (ignoring AOA changes and aircraft pressure effects).

3. Aircraft Pressure Effects

Reference 1 investigated the altitude errors as a function of airspeed and altitude. Many plots were generated of ΔZ versus true airspeed and the data was analyzed in this manner. However, more information can be visualized if these errors are plotted as C_p versus true airspeed. Equation (15) was used to generate Figure 65. The data shown was for Run #2 at 4,000 ft altitude, and Run #3 at 10,000 ft altitude [Ref. 1:pp. 28-44]. Two trends are immediately apparent:

- First, the pressure coefficient at the static ports decreases as true airspeed increases.
- Second, there is an apparent altitude dependence on the C_p for a given true airspeed.

The first trend is caused by the aircraft pressure field as predicted by the VSAERO code. At low airspeeds and high angle-of-attack the pressure generated by the aircraft effects the static pressure ports of the SAIP. As airspeed increases, these effects are not propagated as far forward. At high subsonic speeds they are hardly felt at all. This decrease of C_p with TAS overcomes the upward trends of the AOA and compressibility effects of the SAIP alone.

The second trend may be a function of many factors. At a given true airspeed the C_p (and therefore altitude error)

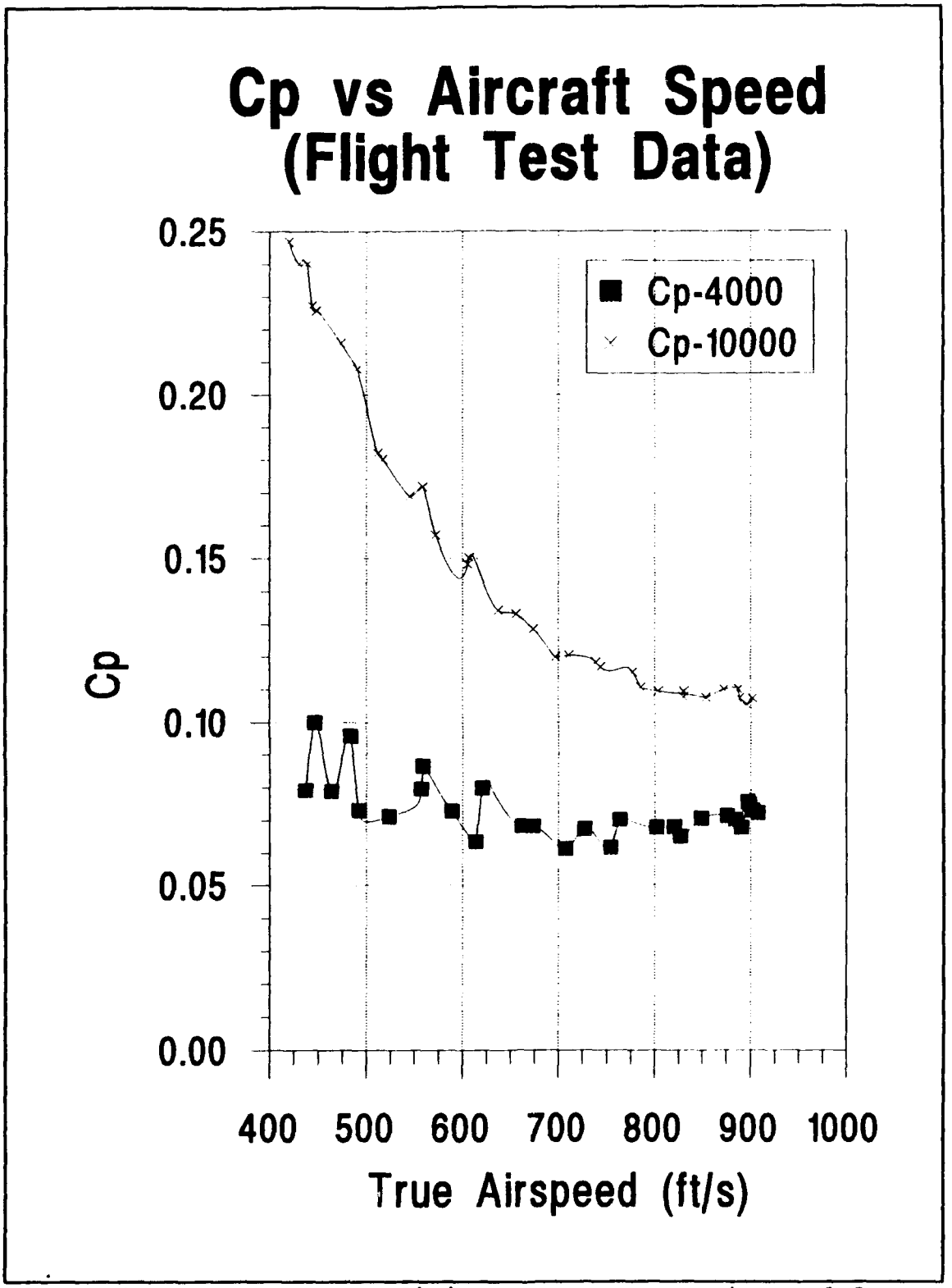

Figure 65. Pressure Coefficient versus True Airspeed for flight test data.

is higher at 10,000 ft than at 4,000 ft, especially in the low speed region. Inviscid theory holds C_p constant with altitude. However, the effects of the aircraft again become a factor. At higher altitudes at a given true airspeed, the angle-of-attack of the aircraft is higher (Table 1). Therefore, the flow field is altered, and higher pressures are propagated forward (note that the SAIP is located forward and under the wing). Also, the flow over the SAIP is not inviscid. Viscous effects, which can be altitude/Reynolds number dependent, could play a part. Regardless of the phenomenon, the altitude errors are a function of altitude as well as airspeed.

Both curves approach a common value. It is postulated that the curves would intersect in supersonic flight. Also, at low speeds, the errors will be severely aggravated at higher altitudes.

4. Flight Testing

The measurement of airspeed and altitude by most existing aircraft is performed using pressure transducers in the same manner as the SAIP. Pitot-static tubes mounted on various places of the aircraft, or pitot tubes with static ports drilled directly into the fuselage are used to extract the pressure data. Every single one of these systems suffers from a deficiency termed "position error". Position error

(Δp) is determined principally by the value of the pressure coefficient at the location of the static source where

$$\Delta p = p_s - p_\infty \qquad (19)$$

Its magnitude can be minimized depending upon the location of the static ports. Decisions on where to locate these regions are based on empirical, numerical, and/or intuitive knowledge. Once a decision is made on the proper location of the static ports flight tests are then performed to properly quantify these position errors.

The AGARD (Advisory Group for Aeronautical Research and Development North Atlantic Treaty Organization) Flight Test Manual describes in detail the techniques necessary for position error determination [Ref. 17]. It states

> The static pressure pickup may be located on the side of the fuselage or on a suitable probe. Unfortunately, it is seldom possible to find a location where true ambient pressure is sensed because the pressure field at all points in the vicinity of the airplane (at subsonic speeds) is generally a function of speed and altitude, and the secondary parameters, angle of attack and the Mach number M [Ref. 17:p. 1:16].

Flight tests are performed over a range of airspeeds as well as a range of altitudes.

Once these errors are quantified, charts are generated in order for the pilot to correct his altitude from that indicated. With the advent of on board computers, this manual tasks is no longer required, for algorithms are written to replace the charts, relieving the pilot of these duties as

well as relaxing the efforts of manufactures to properly locate the static ports. However, these charts are still used in event of computer failure.

The SAIP, which is to be located forward and under a variety of aircraft wings, at any pylon location, does not account for position error. In other words, the altitude measured by the SAIP is based strictly on the pressure measured at the static pressure ports.

VI. CONCLUSIONS AND RECOMMENDATIONS

A. CONCLUSIONS

The airflow sensor assembly (ASA) was designed and tested to measure static pressure in a low speed, unrealistic environment. Integrating the ASA into a five inch diameter after-body and mounting it at an arbitrary position on any aircraft, while neglecting to account for position error is a serious design flaw. Since their conception, the use of pitot-static systems to measure aircraft altitude and airspeed have been subject to position error which is recognized as the major deficiency in accurate static pressure measurements. This position error is the cause of altitude deficiencies of the SAIP. This error consists of aircraft pressure effects, SAIP body pressure effects, and the effects due to the static ports location or end effects (in close proximity to the nose tip).

Although our research focused primarily on subsonic flight, the literature suggests that the hemispherical nose is a poor choice for transonic static pressure readings [Ref. 19]. Also, for supersonic flight where aircraft effects are more restricted, recommendations are for static pressure ports to be located at least eight diameters aft of the nose tip. Therefore, in its current configuration, the SAIP will never

accurately measure static pressure in any flow regime without extensive calibrations.

B. RECOMMENDATIONS

The AGARD Flight Test Manual as well as the Naval Test Pilot School Flight Test Manual describe in detail procedures necessary for position error determination. This effort would require a multitude of flights over a range of airspeeds, a range of altitudes, and a range of aircraft to quantify these errors. After which, algorithms must be written and processed by a computer prior to down-link. This procedure is costly, for it not only requires extensive flight tests, but hardware and software changes as well.

In addition to these changes considerations must be made for extending the ASA nose by approximately six to 10 inches. This would alleviate end effects for both subsonic and supersonic flight. Vibration studies would have to be made in order to determine if any detrimental effects would be present due to a longer nose. The hemispherical nose can not be altered due to the necessity of measuring yaw and angle-of-attack.

Another entirely different option is to tap the altitude information from the host aircraft. This may be the most inexpensive fix but requires some hardware modifications and mission adjustment.

Finally, there are plans by NAWCWPNS to use a geopositional satellite system (GPS) to measure altitude in the distant future. Perhaps this system can be incorporated sooner. That way, the SAIP could retain its autonomous nature and become an effective self-contained airborne positioning pod.

LIST OF REFERENCES

1. Eastburg, S.R., *An Engineering Study of Altitude Determination Deficiencies of the Service Aircraft Instrumentation Package (SAIP)*, Master's Thesis, Naval Postgraduate School, Monterey, California, December 1991.

2. Russell R.J., *A Continuing Study of Altitude Determination Deficiencies of the Service Aircraft Instrument Package (SAIP)*, Master's Thesis, Naval Postgraduate School, Monterey, California, September 1991.

3. *Function Specification for the Service Instrumentation Package (SAIP)*, Pacific Missile Test Center Specification PMTC-CD-EL-697-76A, 31 March 1989.

4. NASA Technical Memorandum 102851, *Potential Flow Theory and Operation Guide for the Panel Code PMARC*, by Dale L. Ashby, Michael R. Dudley, Steve K. Iguchi, Lindsey Browne, and Joseph Katz, January 1991.

5. Margison, R.J., Kjelgaard, S.O., Sellers, W.L., Morris, C.E., Walkey, K.B., Shields, E.W., *Subsonic Panel Methods - A Comparison of Several Production Codes*, AIAA Paper 85-0280, January 1985.

6. Sterling Federal Systems, Inc. Project TN89-2000-205-100, *PMAPP User's Guide*, by Paula K. Lovely and Linnea J. Wigren, December 1989.

7. Anderson, John D., *Fundamentals of Aerodynamics*, 2nd ed., McGraw Hill, 1991.

8. Benedict, R.P., *Fundamentals of Temperature, Pressure, and Flow Measurements*, 3rd ed., John Wiley and Sons, 1984.

9. *GRIDGEN User's Manual*, William M. Chan, NASA Ames Research Center, 1991.

10. *HYPGEN User's Manual*, John Steinbrenner and John Chawner, General Dynamics Corporation, 1990.

11. *OVERFLOW User's Manual*, Pieter Buning, Ing-Tsau Chiu, William Chan, and Kevin Renze, NASA Ames Research Center, 1991.

12. *PLOT3D User's Manual*, P. Buning, P. Waiatka, L. Pierce, P. Elson, NASA Ames Research Center, March 1991.

13. Department of Aeronautics, *Laboratory Manual for Low-Speed Wind Tunnel Testing*, Naval Postgraduate School, Monterey, California, 1989.

14. NACA Technical Note 2311, *Flight Investigation of the Variation of Static-Pressure Error of a Static-Pressure Tube with Distance Ahead of Wing and a Fuselage*, by William Gracey and Elwood F. Scheithauer, March 1951.

15. *NATOPS Flight Manual*, A-6E/A-6E Tram/KA-6D Aircraft, NAVAIR 01-85ADF-1.

16. Shapiro, A.H., *The Dynamics and Thermodynamics of Compressible Fluid Flow*, Ronald Press Company, 1953.

17. *AGARD Flight Test Manual*, v. 1, Pergamon Press, 1959.

18. *Encyclopedia of Fluid Mechanics, Flow Phenomena and Measurements*, v. 1, Gulf Publishing Company, 1986.

INITIAL DISTRIBUTION LIST

		No. Copies
1.	Defense Technical Information Center Cameron Station Alexandria, VA 22304-6145	2
2.	Library, Code 52 Naval Postgraduate School Monterey, CA 93943-5002	2
3.	Chairman Department of Aeronautics, Code AA Naval Postgraduate School Monterey, CA 93943-5000	1
4.	Mr. Wayne Biesecker Naval Air Warfare Center, Weapons Division Code 3333 Point Mugu, CA 93042-5001	1
5.	Mr. Brian Frankhauser Naval Air Warfare Center, Weapons Division Code 3333 Point Mugu, CA 93042-5001	1
6.	Mr. Guy Cooper Naval Air Warfare Center, Weapons Division Code 9054 Point Mugu, CA 93042-5001	1
7.	Mr. William Harrington Naval Air Warfare Center, Weapons Division Code 3421.4 Point Mugu, CA 93042-5001	1
8.	Mr. Rick Navarro Naval Air Warfare Center, Weapons Division Code 3333 Point Mugu, CA 93042-5001	1
9.	Mr Francis Richason NASA Ames Research Center Mail Stop 247-2 Moffett Field, CA 94035	1

10. Mr Larry Gleason 1
Naval Air Warfare Center, Weapon Division
Code 3592
China Lake, CA 93555

11. Prof. Oscar Biblarz 1
Department of Aeronautics, Code AA/Bi
Naval Postgraduate School
Monterey, CA 93943-5000

12. Prof. Garth Hobson 1
Department of Aeronautics, Code AA/
Naval Postgraduate School
Monterey, CA 93943-5000

13. LT Joseph W. Rixey 1
212 G Ave
Coronado, CA